Supplementary Information: The Effect of Structural Heterogeneity upon the Microviscosity of Ionic Liquids

Ryan Clark, Mohd A. Nawawi, Ana Dobre, David Pugh, Qingshan Liu, Aleksander P.Ivanov, Andrew White, Joshua B. Edel, Marina K. Kuimova, Alastair J.S. McIntosh, and Tom Welton

Contents

S1: Syntheses of Ionic Liquids

Solvents used in all synthetic procedures were AcroSeal™ solvents of the highest quality purchasable (>99.5 %). They were all stored over molecular sieves in a dry nitrogen atmosphere and were only used for a maximum of three months after first puncture of the seal.
All purifications and synthetic procedures were performed under a dry nitrogen atmosphere.

Purification of alkyl halides

Before use, all haloalkanes were purified by washing with concentrated sulphuric acid (95-98 %) until the acid layer remained colourless. The organic layer was then neutralised with a saturated solution of sodium bicarbonate in distilled water, and washed with distilled water until the aqueous washing had a pH of approximately 6. The organic layer was then dried with magnesium sulphate overnight. After removal of the magnesium sulphate by filtration the filtrate was dried with phosphorous pentoxide overnight and followed by a further distillation.

Purification of 1-methylimidazole

Before use, 1-methylimidazole was purified by stirring with KOH pellets overnight, followed by distillation. The distillate was then treated with freshly cut sodium overnight, followed by a further distillation.

Cleaning of glassware

All glassware used in these synthetic procedures (including purification) were cleaned by washing with ethanol, followed by decon® 90 and distilled water. The glassware was then washed with piranha solution (3:1 mixture of 95-98 % sulphuric acid and 30% hydrogen peroxide) until effervescence from organic residues ceased. Then at least four washes with distilled water were performed to remove the piranha solution, and then the glassware was dried overnight in a clean oven at 120 °C.

All glass joints were joined with thick walled PTFE sleeves that had also been rinsed in piranha solution and distilled water.

Synthesis of 1-ethyl-3-methylimidazolium bromide [C_2C_1im]Br

1-bromoethane (150 mL, 2.01 mol, 1.1 eq) was added dropwise to a cooled solution of 1-methylimidazole (146 mL, 1.82 mol, 1 eq) in 250 mL dry ethyl acetate under constant stirring. The reaction mixture was stirred overnight at room temperature affording white crystals. Excess solvent was decanted, the crystals were washed with extra dry ethyl acetate (3 × 100 mL) and then dried under vacuum at room temperature. The white crystal was then dissolved in 200 ml acetonitrile at 35 °C, precipitated at -20 °C overnight, and excess solvent removed by cannula filtration, and this was repeated twice more. The white crystals were dried under vacuum at room temperature for two days (273 g, 78% yield).

^{1}H NMR (400 MHz, DMSO-d_6) δ 9.37 (1H, s, NC*H*N), 7.88 (1H, s, NC*H*CHN), 7.78 (1H, s, NCHC*H*N), 4.22 (2H, t, $^3J_{HH}$ = 7.3 Hz, N$C\mathit{H}_2CH_3$), 3.88 (3H, s, N$C\mathit{H}_3$), 1.40 (3H, t, $^3J_{HH}$ = 7.3 Hz, $NCH_2C\mathit{H}_3$).

^{13}C NMR (101 MHz, DMSO-d_6) δ 136.76 (s, N*C*HN), 123.97 (s, N*C*HCHN), 122.44 (s, NCH*C*HN), 44.57 (s, N$\mathit{C}H_2CH_3$), 36.23 (s, N$\mathit{C}H_3$), 15.66 (s, $NCH_2\mathit{C}H_3$).

Synthesis of 1-ethyl-3-methylimidazolium bis(trifluoromethylsulfonyl)imide [C_2C_1im][NTf_2]

Solid lithium bis(trifluoromethylsulfonyl)imide (50.00 g, 0.17 mol, 1 eq) was added to a solution of 1-ethyl-3-methylimidazolium bromide (33.28 g, 0.17 mol, 1 eq) in 250 mL dichloromethane and stirred overnight at room temperature. The lithium bromide precipitate was remove by filtration and the filtrate washed with distilled water (6 × 50 mL) until the aqueous phase was halide free, tested by the silver nitrate test. Excess solvent was removed by rotary evaporation and the crude liquid was washed with 100 mL n-hexane before removal of excess solvent *in vacuo*. The resulted colourless oily liquid was stirred with activated charcoal overnight and then filtered through filter paper and a sterile 0.2 µm PTFE membrane filter. The resulting liquid was dried *in vacuo* at 55 °C for 2 days to give clear viscous liquid (58.67 g, 86% yield).

^{1}H NMR (500 MHz, DMSO-d$_6$) δ 7.92 (1H, s, NCHN), 6.86 (1H, s, NC*H*CHN), 6.78 (1H, s, NCHC*H*N), 3.61 (2H, q, $^3J_{HH}$ = 7.3 Hz, NC*H$_2$*CH$_3$), 3.28 (3H, s, NC*H$_3$*), 0.88 (3H, t, $^3J_{HH}$ = 7.4 Hz, NCH$_2$C*H$_3$*).

^{13}C NMR (101 MHz, DMSO-d$_6$) δ 135.15 (s, N*C*HN), 124.05 (s, N*C*HCHN), 121.21 (s, NCH*C*HN), 119.28 (q, $^1J_{CF}$ = 320.6 Hz, *C*F$_3$), 44.20 (s, N*C*H$_2$CH$_3$), 34.92 (s, N*C*H$_3$), 13.54 (s, NCH$_2$*C*H$_3$).

m/z (M$^+$) 111.1 ([C$_2$C$_1$im]$^+$, 100%); (M$^-$) 279.8 ([NTf$_2$]$^-$, 100%)

Found: C, 25.0; H, 2.9; N, 10.4. Calc. for $C_8H_{11}F_6N_3O_4S_2$: C, 24.5; H, 2.8; N, 10.7%

Synthesis of 1-propyl-3-methylimidazolium bromide [C$_3$C$_1$im]Br

1-bromopropane (150 mL, 1.65 mol, 1.1 eq) was added dropwise to a cooled solution of 1-methylimidazole (120 mL, 1.50 mol, 1 eq) in 200 mL dry ethyl acetate under constant stirring. The resulting solution was left to stir overnight affording a white crystal. Excess solvent was removed by cannula filtration. The resulting crystals were washed with dry ethyl acetate (3 × 100 mL) and then dried under vacuum at room temperature. The white crystal was then dissolved in 200 ml acetonitrile at 35 °C, precipitated at -20 °C overnight, and excess solvent removed by cannula filtration, and this was repeated twice more. The solvent was then removed by cannula filter and the resulting white crystals were dried under vacuum for 2 days (72.8 g, 88% yield).

^{1}H NMR (400 MHz, DMSO-d$_6$) δ 9.30 (1H, s, NCHN), 7.84 (1H, s, NC*H*CHN), 7.77 (1H, s, NCHC*H*N), 4.16 (2H, t, $^3J_{HH}$ = 7.3 Hz, NC*H$_2$*CH$_2$CH$_3$), 3.88 (3H, s, NC*H$_3$*), 1.80 (2H, t, NCH$_2$C*H$_2$*CH$_3$), 0.85 (3H, t, $^3J_{HH}$ = 7.4 Hz, NCH$_2$CH$_2$C*H$_3$*).

^{13}C NMR (101 MHz, DMSO-d$_6$) δ 137.02 (s, N*C*HN), 124.06 (s, N*C*HCHN), 122.74 (s, NCH*C*HN), 50.68 (s, N*C*H$_2$CH$_2$CH$_3$), 36.26 (s, N*C*H$_3$), 36.26 (s, NCH$_2$*C*H$_2$CH$_3$), 15.66 (s, NCH$_2$CH$_2$*C*H$_3$).

Synthesis of 1-propyl-3-methylimidazolium bis(trifluoromethylsulfonyl)imide [C$_3$C$_1$im][NTf$_2$]

Solid lithium bis(trifluoromethylsulfonyl)imide (45.00 g, 0.16 mol, 1 eq) was added to a solution of 1-propyl-3-methylimidazolium bromide (32.15 g, 0.16 mol, 1 eq) in 150 mL of dichloromethane with constant stirring and left overnight. The lithium bromide precipitate was filtered off and the filtrate was washed with distilled water (8 × 50 mL) until the aqueous phase was halide free, tested by the silver nitrate test. The dichloromethane was removed *in vacuo* and the resulting liquid treated with activated charcoal at room temperature overnight. The charcoal filtered off using filter paper followed by a sterile 0.2 µm PTFE filter. The ionic liquid was then dried overnight at 55 **°**C to yield a clear, colourless liquid (55.91 g, 88% yield).

^{1}H NMR (500 MHz, DMSO-d$_6$) δ 7.96 (1H, s, NCHN), 6.87 (1H, s, NC*H*CHN), 6.81 (1H, s, NCHC*H*N), 3.54 (2H, t, $^3J_{HH}$ = 7.3 Hz, NC*H$_2$*CH$_2$CH$_3$), 3.31 (3H, s, NC*H$_3$*), 1.29 (2H, t, $^3J_{HH}$ = 7.3 Hz, NCH$_2$C*H$_2$*CH$_3$), 0.31 (3H, t, $^3J_{HH}$ = 7.5 Hz, NCH$_2$CH$_2$C*H$_3$*).

^{13}C NMR (101 MHz, DMSO-d$_6$) δ 135.39 (s, N*C*HN), 124.02 (s, N*C*HCHN), 122.88 (s, NCH*C*HN), 119.24 (q, $^1J_{CF}$ = 320.6 Hz, *C*F$_3$), 50.45 (s, N*C*H$_2$CH$_2$CH$_3$), 34.92 (s, N*C*H$_3$), 22.37 (s, NCH$_2$*C*H$_2$CH$_3$), 8.92 (s, NCH$_2$CH$_2$*C*H$_3$).

m/z (M$^+$) 125.1 ([C$_2$C$_1$im]$^+$, 100%); (M$^-$) 279.8 ([NTf$_2$]$^-$, 100%)

Found: C, 26.8; H, 3.0; N, 10.2. Calc. for $C_9H_{13}F_6N_3O_4S_2$: C, 26.7; H, 3.2; N, 10.4%

Synthesis of 1-butyl-3-methylimidazolium chloride [C$_4$C$_1$im]Cl

1-chlorobutane (340 mL, 3.26 mol, 1.1 eq) was added dropwise to a cooled solution of 1-methylimidazole (235 ml, 2.96 mol, 1 eq) in 200 mL extra dry ethyl acetate under constant stirring. The reaction mixture was stirred for 1 week at room temperature. The temperature was increased by 10 °C every 4 days until the reaction reached 60 °C and was held at 60 °C for 3 weeks. The reaction mixture was cooled to -20 °C for 2 days affording white crystals. Excess solvent was decanted, and the crystals washed with extra dry ethyl acetate (2 × 150 mL) then recrystallised twice from acetonitrile:ethyl acetate (1:5) and then dried *in vacuo* yielding white crystals. (295.41 g, 57% yield).

$^{1}\mathrm{H}$ NMR (400 MHz, DMSO-d_6) δ 9.22 (1H, s, $\mathrm{N}C\mathrm{HN}$), 7.80 (1H, s, $\mathrm{NC}H\mathrm{CHN}$), 7.73 (1H, s, $\mathrm{NCHC}H\mathrm{N}$), 4.18 (2H, t, $^{3}J_{\mathrm{HH}}$ = 7.2 Hz, $\mathrm{NC}H_2\mathrm{(CH_2)_2CH_3}$), 3.86 (3H, s, $\mathrm{NC}H_3$), 1.77 (2H, p, $^{3}J_{\mathrm{HH}}$ = 7.4 Hz, $\mathrm{NCH_2C}H_2\mathrm{CH_2CH_3}$), 1.27 (2H, h, $^{3}J_{\mathrm{HH}}$ = 7.4 Hz, $\mathrm{N(CH_2)_2C}H_2\mathrm{CH_3}$), 0.91 (3H, t, $^{3}J_{\mathrm{HH}}$ = 7.4 Hz, $\mathrm{N(CH_2)_3C}H_3$).

$^{13}\mathrm{C}$ NMR (101 MHz, DMSO-d_6) δ 137.16 (s, $\mathrm{N}C\mathrm{HN}$), 124.09 (s, $\mathrm{N}C\mathrm{HCHN}$), 122.75 (s, $\mathrm{NCH}C\mathrm{HN}$), 48.94 (s, $\mathrm{N}C\mathrm{H_2(CH_2)_2CH_3}$), 36.21 (s, $\mathrm{N}C\mathrm{H_3}$), 31.83 (s, $\mathrm{NCH_2CH_2CH_2CH_3}$), 19.24 (s, $\mathrm{N(CH_2)_2}C\mathrm{H_2CH_3}$), 13.75 (s, $\mathrm{N(CH_2)_3}C\mathrm{H_3}$).

Synthesis of 1-butyl-3-methylimidazolium bis(trifluoromethylsulfonyl)imide [$\mathrm{C_4C_1im}$][$\mathrm{NTf_2}$]

Solid lithium bis(trifluoromethylsulfonyl)imide (71.15 g, 0.25 mol, 1 eq) was added to a stirred solution of 1-butyl-3-methylimidazolium chloride (43.29 g, 0.25 mol, 1 eq) in 300 mL dichloromethane. The mixture was stirred for 24 hours at room temperature then filtered to remove the lithium bromide precipitate. The filtrate was washed with distilled water (8 × 50 mL) until the aqueous phase was halide free, tested by the silver nitrate test. Excess solvent was removed on the rotary evaporator and the resulting liquid was washed with 150 mL n-hexane before removing excess solvent *in vacuo*. The oily liquid crude was stirred with activated charcoal overnight and filtered through filter paper followed by a sterile 0.2 µm PTFE membrane filter. The resulting liquid was dried *in vacuo* at 55 °C for 2 days to give clear viscous liquid (60.77 g, 58% yield).

$^{1}\mathrm{H}$ NMR (400 MHz, DMSO-d_6 capillary) δ 8.01 (1H, s, $\mathrm{NC}H\mathrm{N}$), 6.92 (1H, s, $\mathrm{NC}H\mathrm{CHN}$), 6.85 (1H, s, $\mathrm{NCHC}H\mathrm{N}$), 3.62 (2H, t, $^{3}J_{\mathrm{HH}}$ = 7.4 Hz, $\mathrm{NC}H_2\mathrm{(CH_2)_2CH_3}$), 3.35 (3H, s, $\mathrm{NC}H_3$), 1.30 (2H, p, $^{3}J_{\mathrm{HH}}$ =7.6 Hz, $\mathrm{NCH_2C}H_2\mathrm{CH_2CH_3}$), 0.78 (2H, h, $^{3}J_{\mathrm{HH}}$ = 7.4 Hz, $\mathrm{N(CH_2)_2C}H_2\mathrm{CH_3}$), 0.35 (3H, t, $^{3}J_{\mathrm{HH}}$ = 7.4 Hz, $\mathrm{N(CH_2)_3C}H_3$).

$^{13}\mathrm{C}$ NMR (101 MHz, DMSO-d_6 capillary) δ 135.42 (s, $\mathrm{N}C\mathrm{HN}$), 122.89 (s, $\mathrm{N}C\mathrm{HCHN}$), 121.63 (s, $\mathrm{NCH}C\mathrm{HN}$), 119.30 (q, $^{1}J_{\mathrm{CF}}$ = 320.7 Hz, $C\mathrm{F_3}$), 48.85 (s, $\mathrm{N}C\mathrm{H_2(CH_2)_2CH_3}$), 34.96 (s, $\mathrm{N}C\mathrm{H_3}$), 30.99 (s, $\mathrm{NCH_2}C\mathrm{H_2CH_2CH_3}$), 18.34 (s, $\mathrm{N(CH_2)_2}C\mathrm{H_2CH_3}$), 11.85 (s, $\mathrm{N(CH_2)_3}C\mathrm{H_3}$).

m/z ($\mathrm{M^+}$) 139 ([$\mathrm{C_4C_1im}$]$^+$, 100%); ($\mathrm{M^-}$) 281 ([$\mathrm{NTf_2}$]$^-$, 100%)

Found: C, 28.8; H, 3.7; N, 10.2. Calc. for $\mathrm{C_{10}H_{15}F_6N_3O_4S_2}$: C, 28.6; H, 3.6; N, 10.0%

Synthesis of 1-hexyl-3-methylimidazolium chloride [$\mathrm{C_6C_1im}$]Cl

1-chlorohexane (227 ml, 1.66 mol, 1.1 eq) was added dropwise to a cooled, stirring solution of 1-methylimidazole (120 ml, 1.51 mol, 1 eq) in 200ml of dry acetonitrile and stirred at room temperature for 1 week. The temperature was increased by 10 °C every 4 days until the reaction reached 60 °C and was held at 60 °C for 3 weeks. The reaction mixture was cooled to -20 °C for 2 days affording white crystals. Excess solvent was decanted, and the crystals washed with extra dry ethyl acetate (2 × 150 mL) then recrystallised twice from acetonitrile:ethyl acetate (1:5) and then dried *in vacuo* yielding a slightly pale yellow, viscous liquid (229.58 g, 75% yield).

$^{1}\mathrm{H}$ NMR (400 MHz, DMSO-d_6) δ 9.80 (1H, s, $\mathrm{N}C\mathrm{HN}$), 8.02 (1H, s, $\mathrm{NC}H\mathrm{CHN}$), 7.93 (1H, s, $\mathrm{NCHC}H\mathrm{N}$), 4.22 (2H, t, $^{3}J_{\mathrm{HH}}$ = 7.2 Hz, $\mathrm{NC}H_2\mathrm{(CH_2)_4CH_3}$), 3.90 (3H, s, $\mathrm{NC}H_3$), 1.80 - 1.72 (2H, m, $\mathrm{NCH_2C}H_2\mathrm{(CH_2)_3CH_3}$), 1.23 - 1.13 (6H, m, $\mathrm{N(CH_2)_2(C}H_2\mathrm{)_3CH_3}$), 0.84 - 0.76 (3H, m , $\mathrm{N(CH_2)_5C}H_3$).

$^{13}\mathrm{C}$ NMR (101 MHz, DMSO-d_6) δ 137.30 (s, $\mathrm{N}C\mathrm{HN}$), 123.99 (s, $\mathrm{N}C\mathrm{HCHN}$), 122.75 (s, $\mathrm{NCH}C\mathrm{HN}$), 49.02 (s, $\mathrm{N}C\mathrm{H_2(CH_2)_4CH_3}$), 36.11 (s, $\mathrm{N}C\mathrm{H_3}$), 31.02 (s, $\mathrm{NCH_2}C\mathrm{H_2(CH_2)_3CH_3}$), 29.90 (s, $\mathrm{N(CH_2)_2}C\mathrm{H_2(CH_2)_2CH_3}$), 25.59 (s, $\mathrm{N(CH_2)_3}C\mathrm{H_2CH_2CH_3}$), 22.34 (s, $\mathrm{N(CH_2)_4}C\mathrm{H_2CH_3}$), 14.24 (s, $\mathrm{N(CH_2)_5}C\mathrm{H_3}$).

Synthesis of 1-hexyl-3-methylimidazolium bis(trifluoromethylsulfonyl)imide [$\mathrm{C_6C_1im}$][$\mathrm{NTf_2}$]

Solid lithium bis(trifluoromethylsulfonyl)imide (50.00 g, 0.17 mol, 1 eq) was added to a cooled and stirred solution of 1-hexyl-3-methylimidazolium chloride (35.30 g, 0.17mol, 1 eq) in 200 mL dichloromethane and left stirring overnight at room temperature. The solid lithium bromide was filtered off and the filtrate was washed with distilled water (7 × 50 mL) until the aqueous phase was halide free, which was confirmed by the silver nitrate test. The solvent was removed *in vacuo* and the liquid was washed with 150 mL n-hexane before removing excess solvent *in vacuo*. The crude oily liquid was stirred with activated charcoal overnight filtered through filter paper and a sterile 0.2 µm PTFE membrane filter, then dried *in vacuo* at 55 °C for 2 days giving a clear viscous liquid (48.31 g, 62% yield).

^{1}H NMR (400 MHz, DMSO-d$_6$ capillary) δ 8.06 (1H, s, $\mathrm{NC}\mathit{H}\mathrm{N}$), 6.94 (1H, s, $\mathrm{NC}\mathit{H}\mathrm{CHN}$), 6.86 (1H, s, $\mathrm{NCHC}\mathit{H}\mathrm{N}$), 3.64 (2H, t, $^{3}J_{HH}$ = 7.4 Hz, $\mathrm{NC}\mathit{H_2}\mathrm{(CH_2)CH_3}$), 3.36 (3H, s, $\mathrm{NC}\mathit{H_3}$), 1.47 - 1.22 (2H, m, $\mathrm{NCH_2C}\mathit{H_2}\mathrm{(CH_2)_3CH_3}$), 0.98 - 0.61 (6H, m, $\mathrm{N(CH_2)_2(C}\mathit{H_2}\mathrm{)_2CH_3}$), 0.31 (3H, t, $\mathrm{N(CH_2)_5C}\mathbf{H_3}$).

^{13}C NMR (101 MHz, DMSO-d$_6$ capillary) δ 135.43 (s, $\mathrm{N}\mathit{C}\mathrm{HN}$), 122.92 (s, $\mathrm{N}\mathit{C}\mathrm{HCHN}$), 121.66 (s, $\mathrm{NCH}\mathit{C}\mathrm{HN}$), 116.13 (q, $^{1}J_{CF}$ = 320.7 Hz, $\mathit{C}\mathrm{F_3}$), 49.13 (s, $\mathrm{N}\mathit{C}\mathrm{H_2(CH_2)_4CH_3}$), 35.00 (s, $\mathrm{N}\mathit{C}\mathrm{H_3}$), 30.19 (s, $\mathrm{NCH_2}\mathit{C}\mathrm{H_2(CH_2)_3CH_3}$), 29.14 (s, $\mathrm{N(CH_2)_2}\mathbf{C}\mathrm{H_2(CH_2)_2CH_3}$), 24.84 (s, $\mathrm{N(CH_2)_3}\mathit{C}\mathrm{H_2CH_2CH_3}$), 21.41 (s, $\mathrm{N(CH_2)_4}\mathit{C}\mathrm{H_2CH_3}$), 12.55 (s, $\mathrm{N(CH_2)_5}\mathit{C}\mathrm{H_3}$).

m/z (M$^+$) 167.1 ([C$_6$C$_1$im]$^+$, 100%); (M$^-$) 279.8 ([NTf$_2$]$^-$, 100%)

Found: C, 32.1; H, 4.2; N, 9.3. Calc. for $\mathrm{C_{12}H_{19}F_6N_3O_4S_2}$: C, 32.2; H, 4.3; N, 9.4%

Synthesis of 1-octyl-3-methylimidazolium chloride [C$_8$C$_1$im]Cl

1-chlorooctane (410.3 g, 2.76 mol) was added drop-wise to a solution of 1-methylimidazole (206.0 g, 2.51 mol) in toluene (200 mL) at room temperature with stirring. The temperature was increased to 40 °C and the mixture was left to stir for 50 days, after which the temperature was decreased to 30 °C for a further 14 days. The reaction mixture was washed with ethyl acetate (6 x 50 mL) affording a clear, colourless oil. The crude was then dissolved in acetonitrile (40 mL) and precipitated with ethyl acetate (200 mL) five times, followed by a final wash with ethyl acetate. The resulting liquid was dried *in vacuo* overnight at 30 °C to give a clear, slightly yellow oil (383.68 g, 66% yield).

^{1}H NMR (400 MHz, DMSO-d6) δ 9.38 (s, 1H, $\mathrm{NC}\mathit{H}\mathrm{N}$), 7.83 (t, $^{3}J_{HH}$ = 1.7 Hz, 1H, $\mathrm{NC}\mathit{H}\mathrm{CHN}$), 7.76 (t, J = 1.7 Hz, 1H, $\mathrm{NCHC}\mathit{H}\mathrm{N}$), 4.17 (t, J = 7.2 Hz, 2H, $\mathrm{NC}\mathit{H_2}\mathrm{CH_2(CH_2)_5CH_3}$), 3.86 (s, 3H, $\mathrm{NC}\mathit{H_3}$), 1.77 (q, J = 7.4 Hz, 2H, $\mathrm{NCH_2C}\mathit{H_2}\mathrm{(CH_2)_5CH_3}$), 1.35 – 1.14 (m, 10H, $\mathrm{NCH_2CH_2(C}\mathit{H_2}\mathrm{)_5CH_3}$), 0.85 (t, J = 6.9 Hz, 3H, $\mathrm{NCH_2CH_2(CH_2)_5C}\mathit{H_3}$).

^{13}C NMR (101 MHz, DMSO-d6) δ 136.62 (s, $\mathrm{N}\mathit{C}\mathrm{HN}$), 123.54 (s, $\mathrm{N}\mathit{C}\mathrm{HCHN}$), 122.23 (s, $\mathrm{NCH}\mathit{C}\mathrm{HN}$), 48.68 (s, $\mathrm{N}\mathit{C}\mathrm{H_2(CH_2)_6CH_3}$), 35.69 (s, $\mathrm{N}\mathit{C}\mathrm{H_3}$), 31.13 (s, $\mathrm{NCH_2}\mathit{C}\mathrm{H_2(CH_2)_5CH_3}$), 29.38 (s, $\mathrm{N(CH_2)_2}\mathit{C}\mathrm{H_2(CH_2)_4CH_3}$), 28.45 (s, $\mathrm{N(CH_2)_3}\mathit{C}\mathrm{H_2(CH_2)_3CH_3}$), 28.32 (s, $\mathrm{N(CH_2)_4}\mathit{C}\mathrm{H_2(CH_2)_2CH_3}$), 25.47 (s, $\mathrm{N(CH_2)_5}\mathit{C}\mathrm{H_2(CH_2)_1CH_3}$), 22.02 (s, $\mathrm{N(CH_2)_6}\mathit{C}\mathrm{H_2CH_3}$), 13.91 (s, $\mathrm{N(CH_2)_7}\mathit{C}\mathrm{H_3}$).

Synthesis of 1-octyl-3-methylimidazolium bis(trifluoromethylsulfonyl)imide [C$_8$C$_1$im][NTf$_2$]

A solution of lithium bis(trifluoromethylsulfonyl)imide (72.11 g, 0.251 mol, 1.2 eq) in water was added drop-wise to a solution of 1-octyl-3-methylimidazolium chloride (49.27 g, 0.213 mol, 1.2 eq) in water at room temperature with stirring. The resulting solution was left stirring at room temperature for 5 days. The ionic liquid layer was isolated and washed with water (10 × 20 ml), until the aqueous washing were halide free, tested using the silver nitrate test. The ionic liquid was then stirred with activated charcoal in acetonitrile for 7 days and filtered through filter paper and a sterile 0.2 µm PTFE filter. The filtrate was collected and dried *in vacuo* overnight at room temperature to give a clear liquid (65.94 g, 66% yield).

^{1}H NMR (400 MHz, DMSO-d$_6$ capillary) δ 8.10 (1H, s, $\mathrm{NC}\mathit{H}\mathrm{N}$), 6.97 (1H, s, $\mathrm{NC}\mathit{H}\mathrm{CHN}$), 6.89 (1H, s, $\mathrm{NCHC}\mathit{H}\mathrm{N}$), 3.67 (2H, t, $^{3}J_{HH}$ = 7.3Hz, $\mathrm{NC}\mathit{H_2}\mathrm{(CH_2)_6CH_3}$), 3.39 (3H, s, $\mathrm{NC}\mathit{H_3}$), 1.38 (2H, q, $^{3}J_{HH}$ = 7.3Hz, $\mathrm{NCH_2C}\mathit{H_2}\mathrm{(CH_2)_5CH_3}$), 0.97 - 0.57 (10H, m, $\mathrm{N(CH_2)_2(C}\mathit{H_2}\mathrm{)_5CH_3}$), 0.35 (3H, t, $^{3}J_{HH}$ = 7.3Hz, $\mathrm{N(CH_2)_7C}\mathit{H_3}$).

^{13}C NMR (101 MHz, DMSO-d$_6$ capillary) δ 135.47 (s, $\mathrm{N}\mathit{C}\mathrm{HN}$), 122.97 (s, $\mathrm{N}\mathit{C}\mathrm{HCHN}$), 121.70 (s, $\mathrm{NCH}\mathit{C}\mathrm{HN}$), 116.16 (q, $^{1}J_{CF}$ = 320.8Hz, $\mathit{C}\mathrm{F_3}$), 49.19 (s, $\mathrm{N}\mathit{C}\mathrm{H_2(CH_2)_6CH_3}$), 35.05 (s, $\mathrm{N}\mathit{C}\mathrm{H_3}$), 30.97 (s, $\mathrm{NCH_2}\mathit{C}\mathrm{H_2(CH_2)_5CH_3}$), 29.29 (s, N $\mathrm{N(CH_2)_2}\mathit{C}\mathrm{H_2(CH_2)_4CH_3}$), 28.23 (s, $\mathrm{N(CH_2)_3}\mathit{C}\mathrm{H_2(CH_2)_3CH_3}$), 28.13 (s, $\mathrm{N(CH_2)_4}\mathit{C}\mathrm{H_2(CH_2)_2CH_3}$), 25.30 (s, $\mathrm{N(CH_2)_5}\mathit{C}\mathrm{H_2CH_2CH_3}$), 21.79 (s, $\mathrm{N(CH_2)_6}\mathit{C}\mathrm{H_2CH_3}$), 12.85 (s, $\mathrm{N(CH_2)_7}\mathit{C}\mathrm{H_3}$).

m/z (M$^+$) 195.2 ([C$_8$C$_1$im]$^+$, 100%); (M$^-$) 279.9 ([NTf$_2$]$^-$, 100%)

Found: C, 35.6; H, 4.8; N, 9.0. Calc. for $\mathrm{C_{14}H_{23}F_6N_3O_4S_2}$: C, 35.4; H, 4.9; N, 8.8%

Synthesis of 1-dodecyl-3-methylimidazolium chloride [C$_{12}$C$_1$im]Cl

1-chlorododecane (200 mL, 0.85 mol, 1.1 eq) was added dropwise to a cooled and stirred solution of 1-methylimidazole (61 mL, 0.77 mol, 1 eq) in 150 mL of dry ethyl acetate and left stirring at room temperature for three days. The temperature was increased by 10 °C every three days until the reaction reached 55 °C where it was held for three weeks.

The reaction mixture was then cooled to room temperature, and the solvent was removed *in vacuo* to yield a yellowish greasy solid. The solid was washed three times with 100 mL of dry ethyl acetate and acetonitrile (5:1) then dissolved in acetonitrile at 35 °C and precipitated by cooling in a dry ice. Excess solvent was removed by cannula filtration, and the solid was dried at 35 °C for two days *in vacuo* (160 g, 72% yield).

^{1}H NMR (400 MHz, DMSO-d_6) δ 9.44 (1H, s, $\mathrm{N}\mathit{C}\mathrm{HN}$), 7.86 (1H, s, $\mathrm{NC}\mathit{H}\mathrm{CHN}$), 7.79 (1H, s, $\mathrm{NCHC}\mathit{H}\mathrm{N}$), 4.21 (2H, t, $^3J_{HH}$ = 8.0Hz, $\mathrm{NC}\mathit{H_2}\mathrm{(CH_2)_{10}CH_3}$), 3.88 (3H, s, $\mathrm{NC}\mathit{H_3}$), 1.76 (2H, q, $^3J_{HH}$ = 6.6Hz, $\mathrm{NCH_2C}\mathit{H_2}\mathrm{(CH_2)_9CH_3}$), 1.24 (18H, s, $\mathrm{NCH_2CH_2(C}\mathit{H_2}\mathrm{)_9CH_3}$), 0.85 (3H, t, $^3J_{HH}$ = 6.6 Hz $\mathrm{N(CH_2)_{11}C}\mathit{H_3}$).

^{13}C NMR (101 MHz, DMSO-d_6) δ 137.15 (s, $\mathrm{N}\mathit{C}\mathrm{HN}$), 124.04 (s, $\mathrm{N}\mathit{C}\mathrm{HCHN}$), 122.73 (s, $\mathrm{NCH}\mathit{C}\mathrm{HN}$), 49.16 (s, $\mathrm{N}\mathit{C}\mathrm{H_2(CH_2)_{10}CH_3}$), 40.43 (s, $\mathrm{N}\mathit{C}\mathrm{H_3}$), 36.18 (s, $\mathrm{NCH_2}\mathit{C}\mathrm{H_2(CH_2)_9CH_3}$), 31.77 (s, $\mathrm{N(CH_2)_2}\mathit{C}\mathrm{H_2(CH_2)_8CH_3}$), 29.91 (s, $\mathrm{N(CH_2)_3}\mathit{C}\mathrm{H_2(CH_2)_7CH_3}$), 29.50 (s, $\mathrm{N(CH_2)_4}\mathit{C}\mathrm{H_2(CH_2)_6CH_3}$), 29.43 (s, $\mathrm{N(CH_2)_5}\mathit{C}\mathrm{H_2(CH_2)_5CH_3}$), 29.32 (s, $\mathrm{N(CH_2)_6}\mathit{C}\mathrm{H_2(CH_2)_4CH_3}$), 29.19 (s, $\mathrm{N(CH_2)_7}\mathit{C}\mathrm{H_2(CH_2)_3CH_3}$), 28.88 (s, $\mathrm{N(CH_2)_8}\mathit{C}\mathrm{H_2(CH_2)_2CH_3}$), 25.98 (s, $\mathrm{N(CH_2)_9}\mathit{C}\mathrm{H_2CH_2CH_3}$), 22.57 (s, $\mathrm{N(CH_2)_{10}}\mathit{C}\mathrm{H_2CH_3}$), 14.41 (s, $\mathrm{N(CH_{2)11}}\mathit{C}\mathrm{H_3}$).

Synthesis of 1-dodecyl-3-methylimidazolium bis(trifluoromethylsulfonyl)imide [$C_{12}C_1$im][NTf_2]

Solid lithium bis(trifluoromethylsulfonyl)imide (50.00 g, 0.174 mol, 1 eq) was added to a stirred solution of 1-dodecyl-3-methylimidazolium chloride (49.97 g, 0.174 mol, 1 eq) in 200 mL dichloromethane and stirred for 24 hours being filtration to remove the lithium chloride precipitate. The ionic liquid layer was washed with distilled water (6 × 50 mL) until the aqueous washings tested negative for halide ions using the silver nitrate test. Excess solvent was removed *in vacuo*, and the resulting liquid was washed with 50 mL n-hexane. The oil was then treated with activated charcoal at room temperature overnight. The charcoal was removed by filtration with filter paper and a sterile 0.2 µm PTFE filter. The filtrate was then dried overnight at 55 °C to yield a clear, colourless liquid (79.75 g, 86% yield).

^{1}H NMR (400 MHz, DMSO-d_6) δ 8.14 (1H, s, $\mathrm{N}\mathit{C}\mathrm{HN}$), 6.99 (1H, s, $\mathrm{NC}\mathit{H}\mathrm{CHN}$), 6.91 (1H, s, $\mathrm{NCHC}\mathit{H}\mathrm{N}$), 3.88 - 3.56(2H, m, $\mathrm{NC}\mathit{H_2}\mathrm{(CH_2)_{10}CH_3}$), 3.41 (3H, s, $\mathrm{NC}\mathit{H_3}$), 1.40 (2H, s, $\mathrm{NCH_2C}\mathit{H_2}\mathrm{(CH_2)_9CH_3}$), 1.08 - 0.59 (18H, m, $\mathrm{N(CH_2)_2(C}\mathit{H_2}\mathrm{)_9CH_3}$), 0.41 (3H, t, $^3J_{HH}$ = 6.2 Hz, $\mathrm{N(CH_2)_{11}C}\mathit{H_3}$).

^{13}C NMR (101 MHz, DMSO-d_6 capillary) δ 135.31 (s, $\mathrm{N}\mathit{C}\mathrm{HN}$), 123.00 (s, $\mathrm{N}\mathit{C}\mathrm{HCHN}$), 121.69 (s, $\mathrm{NCH}\mathit{C}\mathrm{HN}$), 116.18 (q, $^1J_{CF}$ = 320.9 Hz, $\mathit{C}\mathrm{F_3}$), 49.20 (s, $\mathrm{N}\mathit{C}\mathrm{H_2(CH_2)_{10}CH_3}$), 35.09 (s, $\mathrm{N}\mathit{C}\mathrm{H_3}$), 31.40 (s, $\mathrm{NCH_2}\mathit{C}\mathrm{H_2(CH_2)_9CH_3}$), 29.40 (s, $\mathrm{N(CH_2)_2}\mathit{C}\mathrm{H_2(CH_2)_8CH_3}$), 29.12 (s, $\mathrm{N(CH_2)_3}\mathit{C}\mathrm{H_2(CH_2)_7CH_3}$), 29.02 (s, $\mathrm{N(CH_2)_4}\mathit{C}\mathrm{H_2(CH_2)_6CH_3}$), 29.00 (s, $\mathrm{N(CH_2)_5}\mathit{C}\mathrm{H_2(CH_2)_5CH_3}$), 28.85 (s, $\mathrm{N(CH_2)_6}\mathit{C}\mathrm{H_2(CH_2)_4CH_3}$), 28.81 (s, $\mathrm{N(CH_2)_7}\mathit{C}\mathrm{H_2(CH_2)_3CH_3}$), 28.37 (s, $\mathrm{N(CH_2)_8}\mathit{C}\mathrm{H_2(CH_2)_2CH_3}$), 25.47 (s, $\mathrm{N(CH_2)_9}\mathit{C}\mathrm{H_2CH_2CH_3}$), 22.08 (s, $\mathrm{N(CH_2)_{10}}\mathit{C}\mathrm{H_2CH_3}$), 13.14 (s, $\mathrm{N(CH_2)_{11}}\mathit{C}\mathrm{H_3}$).

m/z (M^+) 251.2 ([$C_{12}C_1$im]$^+$, 100%); (M^-) 279.9([NTf_2]$^-$, 100%)

Found: C, 40.7; H, 5.9; N, 7.9. Calc. for $C_{18}H_{31}F_6N_3O_4S_2$: C, 40.7; H, 5.9; N, 7.9%

Synthesis of tributylhexylphosphonium bromide [P_{4446}]Br

1-bromohexane (44.93 g, 38.21ml, 272.19 mmol) was added dropwise to a stirred and cooled solution of tributylphosphonium (55.07 g, 67.99ml, 272.19 mmol) in 100 mL dichloromethane and stirred for two days. The resulting solid was recrystallised 15 times from diethyl ether:ethyl acetate (2:1) with cooling in dry ice. Excess solvent was removed in vacuo to give a white solid (85.42 g, 85 % yield)

^{1}H NMR (400 MHz, DMSO-d_6) δ 2.22 (8H, m, $\mathrm{P[C}\mathit{H_2}\mathrm{(CH_2)_2CH_3]_3[C}\mathit{H_2}\mathrm{(CH_2)_4CH_3]}$), 1.42 (16H, m, $\mathrm{P[CH_2(C}\mathit{H_2}\mathrm{)_2CH_3]_3[CH_2(C}\mathit{H_2}\mathrm{)_2(CH_2)_2CH_3]}$), 1.29 (4H, m, $\mathrm{P[(CH_2)_3(C}\mathit{H_2}\mathrm{)_2CH_3]}$), 0.92 (12H, m, $\mathrm{P[(CH_2)_3C}\mathit{H_3}\mathrm{]_3[(CH_2)_5C}\mathit{H_3}\mathrm{]}$)

^{13}C NMR (101 MHz, DMSO-d_6) 30.87 (s, $\mathrm{P[}\mathit{C}\mathrm{H_2(CH_2)_4CH_3]}$), 30.24 (d, $\mathrm{P[}\mathit{C}\mathrm{H_2(CH_2)_2CH_3]_3}$), 23.83 (d, $\mathrm{P[CH_2}\mathit{C}\mathrm{H_2(CH_2)_3CH_3]}$), 23.15(d, $\mathrm{P[CH_2}\mathit{C}\mathrm{H_2CH_2CH_3]_3}$), 22.31 (s, $\mathrm{P[(CH_2)_2}\mathit{C}\mathrm{H_2(CH_2)_2CH_3]}$), 21.04 (d, $\mathrm{P[(CH_2)_2}\mathit{C}\mathrm{H_2CH_3]_3}$), 18.06 (d, $\mathrm{P[(CH_2)_3}\mathit{C}\mathrm{H_2CH_2CH_3]}$), 17.84 (d, $\mathrm{P[(CH_2)_3}\mathit{C}\mathrm{H_3]_3}$), 14.35 (d, $\mathrm{P[(CH_2)_4}\mathit{C}\mathrm{H_2CH_3]}$), 13.75 (d, $\mathrm{P[(CH_2)_5}\mathit{C}\mathrm{H_3]}$).

Synthesis of tributylhexylphosphonium bis(trifluoromethylsulfonyl)imide $[P_{4446}][NTf_2]$

Solid lithium bis(trifluoromethylsulfonyl)imide (15.17 g, 52.85 mol, 1 eq) was added to a stirred solution of tributylhexyphosphonium bromide (19.42g, 52.85 mmol, 1 eq) in 100 mL dichloromethane and left overnight at room temperature. The solid lithium bromide was removed by filtration and the filtrate was washed with distilled water (15 × 50 mL) until the aqueous washings tested negative for halide ions using the silver nitrate test. Excess solvent was removed *in vacuo* at 60 °C for two days then the liquid was treated with activated charcoal overnight. The charcoal was removed by filtration with filter paper and a sterile 0.2 µm PTFE filter. The filtrate was then dried *in vacuo* overnight at 60 °C to give a clear viscous liquid (21.55 g, 72 % yield)

^{1}H NMR (400 MHz, DMSO-d_6) δ 2.18 (8H, m, $P[CH_2(CH_2)_2CH_3]_3[CH_2(CH_2)_4CH_3]$), 1.44 (16H, m, $P[CH_2(CH_2)_2CH_3]_3[CH_2(CH_2)_2(CH_2)_2CH_3]$), 1.30 (4H, m, $P[(CH_2)_3(CH_2)_2CH_3]$), 0.93 (12H, m, $P[(CH_2)_3CH_3]_3[(CH_2)_5CH_3]$)

^{13}C NMR (101 MHz, DMSO-d_6) δ 119.65 (q, $^1J_{CF}$ = 320.6 Hz, CF_3), 30.37 (s, $P[CH_2(CH_2)_4CH_3]$), 29.76 (d, $P[CH_2(CH_2)_2CH_3]_3$), 23.34 (d, $P[CH_2CH_2(CH_2)_3CH_3]$), 22.62 (d, $P[CH_2CH_2CH_2CH_3]_3$), 21.81 (s, $P[(CH_2)_2CH_2(CH_2)_2CH_3]$), 20.51 (d, $P[(CH_2)_2CH_2CH_3]_3$), 17.48 (d, $P[(CH_2)_3CH_2CH_2CH_3]$), 17.29 (d, $P[(CH_2)_3CH_3]_3$), 13.78 (d, $P[(CH_2)_4CH_2CH_3]$), 13.16 (d, $P[(CH_2)_4CH_3]$).

S2: Metathesis of Cy3 Dyes

General method

Experiments were carried out in air unless otherwise stated. Cy3 iodide was purchased from TCI and used as received. $LiNTf_2$, AgOTf, KPF_6, $NaBF_4$ and $AgBF_4$ were purchased from Sigma and used as received. $NaCHTf_2$ was synthesized according to the procedure of Waller *et al.*[1] MeOH, Et_2O (both HPLC grade) and CH_2Cl_2 were purchased from VWR and used as received.

^1H NMR, $^{13}C\{^1H\}$, $^{19}F\{^1H\}$ and $^{31}P\{^1H\}$ NMR spectra were obtained on a Bruker Avance 400 spectrometer at 298 K and referenced to the residual protio-solvent signal (^1H, $^{13}C\{^1H\}$), $CFCl_3$ ($^{19}F\{^1H\}$) or an 85% solution of H_3PO_4 in water ($^{31}P\{^1H\}$). DMSO-d_6 was bought from Sigma and used as received. Mass spectra were obtained on a Waters LCT Premier Acquity i-Class using electrospray ionisation. IR spectra were collected on a Perkin Elmer Spectrum RX1 and UV-vis spectra on a Perkin Elmer Lambda 25. Melting points were obtained on a Stuart SMP30 and elemental analyses were carried out by Stephen Boyer at London Metropolitan University.

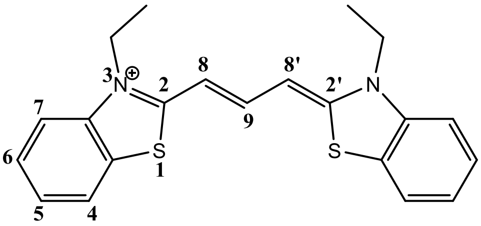

Figure S2 A: numbering scheme used in this section

Cy3 NTf_2

Under an atmosphere of N_2, Cy3 iodide (0.25 g, 0.49 mmol) was dissolved in CH_2Cl_2 (50 mL). Solid $LiNTf_2$ (0.14 g, 0.49 mmol) was added under a counterflow of N_2 and the reaction was stirred at RT for 2 days. After this time the reaction was filtered and volatiles were removed *in vacuo*, affording a dark green solid which was recrystallised from CH_2Cl_2. Yield: 0.22 g of gold crystals, 69%. M.p. 259 °C (dec.).

^1H NMR (400.1 MHz, DMSO-d_6): 7.92 (d, *J* = 7.8 Hz, [2H], H4/7), 7.63–7.75 (m, [3H], H4/7, H9), 7.50 (t, *J* = 7.6 Hz, [2H], H5/6), 7.32 (t, *J* = 7.6 Hz, [2H], H5/6), 6.56 (d, *J* = 12.7 Hz, [2H], H8,8'), 4.32 (br d, *J* = 7.0 Hz, [4H], CH_2), 1.31 (t, *J* = 7.0 Hz, [6H], CH_3) ppm.

$^{13}C\{^1H\}$ NMR (100.6 MHz, DMSO-d_6): 164.01 (C2), 146.40 (C9), 140.70 (CS), 128.03 (C5), 125.08 (C6,CN), 123.03 (C7), 119.49 (q, *J* = 322 Hz, CF_3), 113.26 (C4), 98.52 (CH, C8,8'), 41.46 (CH_2), 12.60 (CH_3) ppm.

$^{19}F\{^1H\}$ NMR (376.5 MHz, DMSO-d_6): –78.70 (NTf_2) ppm.

MS (ES^+): m/z 365.1 (M^+, 100%). (ES^-): m/z 279.9 (NTf_2^-, 100%).

IR (nujol, KBr plates): 3746, 3735, 2361, 2341, 1918, 1869, 1844, 1830, 1792, 1772, 1750, 1734, 1717, 1700, 1684, 1670, 1654, 1636, 1624, 1617, 1576, 1559, 1541, 1522, 1507, 1489, 1419, 1319, 1266, 1205, 1126, 1076, 825 cm^{-1}.

UV-vis (CH_2Cl_2, 5.0 µM): λ_{max} = 564.60 nm (ε= 1.78 x 10^5 $dm^3mol^{-1}cm^{-1}$).

Analysis calc. for $C_{23}H_{21}F_6N_3O_4S_4$ (645.03): C 42.79; H 3.28; N 6.51. Found: C 42.99; H 3.18; N 6.53.

Cy3 OTf

To a solution of Cy3 iodide (0.25 g, 0.51 mmol) in CH_2Cl_2 (100 mL) was added a solution of AgOTf (0.14 g, 0.55 mmol) in Et_2O (50 mL). The reaction was stirred at RT for 4 days. After this time the solution was filtered and volatiles were removed *in vacuo*, affording a dark blue solid which was recrystallised from MeOH. Yield: 0.20 g of gold crystals, 77%. M.p. 246 °C (dec.).

^1H NMR (400.1 MHz, DMSO-d_6): 7.97 (d, *J* = 7.8 Hz, [2H], H4/7), 7.70–7.80 (m, [3H], H4/7, H9), 7.55 (t, *J* = 7.5 Hz, [2H], H5/6), 7.38 (t, *J* = 7.6 Hz, [2H], H5/6), 6.59 (d, *J* = 12.7 Hz, [2H], H8,8'), 4.36 (q, *J* = 7.0 Hz, [4H], CH_2), 1.33 (t, *J* = 7.0 Hz, [6H], CH_3) ppm.

$^{13}C\{^1H\}$ NMR (100.6 MHz, DMSO-d_6): 164.12 (C2), 146.56 (C9), 140.76 (CS), 128.09 (C5), 125.16 (C6,CN), 123.08 (C7), 120.69 (q, *J* = 323 Hz, CF_3), 113.33 (C4), 98.58 (C8,8'), 41.45 (CH_2), 12.60 (CH_3) ppm.

$^{19}F\{^1H\}$ NMR (376.5 MHz, DMSO-d_6): –77.74 (OTf) ppm.

MS (ES$^+$): m/z 365.1 (M$^+$, 100%). (ES$^-$): m/z 149.0 (OTf$^-$, 100%).

IR (nujol, KBr plates): 3746, 2361, 2341, 1869, 1844, 1830, 1792, 1772, 1734, 1717, 1700, 1684, 1670, 1654, 1636, 1624, 1617, 1576, 1558, 1541, 1522, 1507, 1490, 1300, 1260 cm^{-1}.

UV-vis (CH_2Cl_2, 5.0 μM): λ_{max} = 564.14 nm (ε= 1.22 x 10^5 dm^{3}mol^{-1}cm^{-1}).

Analysis calc. for $C_{22}H_{21}F_3N_2O_3S_3$ (514.07): C 51.36; H 4.12; N 5.45. Found: C 51.19; H 4.29; N 5.36.

Cy3 PF_6

To a solution of Cy3 iodide (0.25 g, 0.5 mmol) in CH_2Cl_2 (150 mL) was added KPF_6 (0.09 g, 0.5 mmol). The reaction was stirred at RT for 4 days. After this time the reaction was filtered and volatiles were removed *in vacuo*, affording a blue solid which was recrystallized from CH_2Cl_2. Yield: 0.21 g of gold crystals, 82%. M.p. 255 °C (dec.).

^1H NMR (400.1 MHz, DMSO-d_6): 7.93 (d, *J* = 7.8 Hz, [2H], H4/7), 7.64–7.76 (m, [3H], H4/7, H9), 7.50 (t, *J* = 7.5 Hz, [2H], H5/6), 7.32 (t, *J* = 7.6 Hz, [2H], H5/6), 6.58 (d, *J* = 12.7 Hz, [2H], H8,8'), 4.32 (br d, *J* = 6.8 Hz, [4H], CH_2), 1.31 (t, *J* = 6.8 Hz, [6H], CH_3) ppm.

$^{13}C\{^1H\}$ NMR (100.6 MHz, DMSO-d_6): 164.02 (C2), 146.43 (C9), 140.71 (CS), 128.04 (C5), 125.09 (C6,CN), 123.05 (C7), 113.27 (C4), 98.54 (C8,8'), 41.46 (CH_2), 12.61 (CH_3) ppm.

$^{19}F\{^1H\}$ NMR (376.5 MHz, DMSO-d_6): –70.12 (d, *J* = 711 Hz, PF_6) ppm.

$^{31}P\{^1H\}$ NMR (162.1 MHz, DMSO-d_6): –144.16 (septet, *J* = 711 Hz, PF_6) ppm.

MS (ES$^+$): m/z 365.1 (M$^+$, 100%). (ES$^-$): m/z 145.0 (PF_6^-, 100%).

IR (nujol, KBr plates): 3746, 3735, 2361, 2341, 1918, 1869, 1844, 1830, 1792, 1772, 1750, 1734, 1717, 1700, 1684, 1670, 1654, 1636, 1624, 1617, 1576, 1559, 1540, 1522, 1507, 1490, 1419, 1318, 1076, 825 cm^{-1}.

UV-vis (CH_2Cl_2, 5.0 μM): λ_{max} = 564.21 nm (ε= 2.08 x 10^5 dm^{3}mol^{-1}cm^{-1}).

Analysis calc. for $C_{21}H_{21}F_6N_2PS_2$ (510.08): C 49.40; H 4.15; N 5.49. Found: C 49.32; H 4.20; N 5.57.

Cy3 BF_4/I

To a solution of Cy3 iodide (0.25 g, 0.51 mmol) in CH_2Cl_2 (100 mL) was added $NaBF_4$ (0.23 g, 2.09 mmol). The reaction was stirred at RT for 4 days. After this time the solution was filtered and volatiles were removed *in vacuo*, affording a dark blue solid which was recrystallised from CH_2Cl_2. Yield: 0.24 g of dark blue crystals. M.p. 277 °C (dec.).

^1H NMR (400.1 MHz, DMSO-d_6): 7.98 (d, *J* = 7.8 Hz, [2H], H4/7), 7.69–7.80 (m, [3H], H4/7, H9), 7.55 (t, *J* = 7.5 Hz, [2H], H5/6), 7.38 (t, *J* = 7.6 Hz, [2H], H5/6), 6.62 (d, *J* = 12.7 Hz, [2H], H8,8'), 4.36 (q, *J* = 7.0 Hz, [4H], CH_2), 1.33 (t, *J* = 7.0 Hz, [6H], CH_3) ppm.

$^{13}C\{^1H\}$ NMR (100.6 MHz, DMSO-d_6): 164.10 (C2), 146.56 (C9), 140.76 (CS), 128.08 (C5), 125.15 (C6,CN), 123.10 (C7), 113.34 (C4), 98.60 (C8,8'), 41.46 (CH_2), 12.62 (CH_3) ppm.

$^{19}F\{^1H\}$ NMR (376.5 MHz, DMSO-d_6): –148.19 ($^{10}BF_4$), –148.24 ($^{11}BF_4$) ppm.

MS (ES$^+$): m/z 365.1 (M$^+$, 100%). (ES$^-$): m/z 87.0 (BF_4^-, 25%), 126.9 (I$^-$, 100%).

IR (nujol, KBr plates): 3746, 3735, 2361, 2341, 1869, 1844, 1830, 1792, 1772, 1750, 1734, 1717, 1700, 1684, 1670, 1654, 1636, 1624, 1616, 1576, 1559, 1540, 1522, 1507, 1314, 1270, 1051 cm^{-1}.

UV-vis (CH_2Cl_2, 5.0 µM): λ_{max} = 564.19 nm (ε= 2.26 x 10^5 dm^{3}mol^{-1}cm^{-1}).

Analysis calc. for $C_{21}H_{21}B_{0.43}F_{1.72}I_{0.57}N_2S_2$ (474.86): C 53.07; H 4.46; N 5.90. Found: C 52.84; H 4.52; N 5.79.

Cy3 BF_4

To a solution of Cy3 iodide (0.49 g, 1.0 mmol) in CH_2Cl_2 (100 mL) was added $AgBF_4$ (0.23 g, 1.2 mmol). The reaction was stirred at RT for 7 days. After this time the solution was filtered and volatiles were removed *in vacuo*, affording 0.40 g of a dark blue solid (yield 89%). M.p. 270 °C (dec.).

^{1}H NMR (400.1 MHz, DMSO-d$_6$): 7.96 (d, *J* = 7.8 Hz, [2H], H4/7), 7.69–7.80 (m, [3H], H4/7, H9), 7.54 (t, *J* = 7.5 Hz, [2H], H5/6), 7.37 (t, *J* = 7.6 Hz, [2H], H5/6), 6.57 (d, *J* = 12.7 Hz, [2H], H8,8'), 4.35 (q, *J* = 7.0 Hz, [4H], CH_2), 1.33 (t, *J* = 7.0 Hz, [6H], CH_3) ppm.

^{13}C{^{1}H} NMR (100.6 MHz, DMSO-d$_6$): 164.11 (C2), 146.54 (C9), 140.75 (CS), 128.08 (C5), 125.15 (C6,CN), 123.08 (C7), 113.32 (C4), 98.57 (C8,8'), 41.45 (CH_2), 12.60 (CH_3) ppm.

^{19}F{^{1}H} NMR (376.5 MHz, DMSO-d$_6$): –148.21 ($^{10}BF_4$), –148.26 ($^{11}BF_4$) ppm.

MS (ES$^+$): m/z 365.1 (M$^+$, 100%). (ES$^-$): m/z 87.0 (BF_4^-, 100%).

IR (nujol, KBr plates): 3746, 3735, 2360, 2341, 1869, 1844, 1830, 1792, 1772, 1750, 1734, 1717, 1700, 1684, 1670, 1653, 1636, 1624, 1617, 1576, 1559, 1540, 1522, 1507, 1490, 1319, 1051 cm^{-1}.

UV-vis (CH_2Cl_2, 5.0 µM): λ_{max} = 564.31 nm (ε= 1.68 x 10^5 dm^{3}mol^{-1}cm^{-1}).

Analysis calc. for $C_{21}H_{21}BF_4N_2S_2$ (452.11): C 55.74; H 4.68; N 6.19. Found: C 55.55; H 4.79; N 6.17.

Cy3 $CHTf_2$

To a solution of Cy3 iodide (0.10 g, 0.20 mmol) in CH_2Cl_2 (25 mL) was added a solution of $NaCHTf_2$ (0.06 g, 0.20 mmol) in CH_2Cl_2 (25 mL). The reaction was stirred at RT for 4 days. After this time the organic layer was extracted and washed with distilled water until no sodium iodide was observed using the $AgNO_3$ test (typically 3 x 20 mL). Volatiles were removed *in vacuo*, affording a dark green solid which was recrystallised from CH_2Cl_2. Yield: 0.12 g of gold crystals, 93%. M.p. 257 °C (dec.).

^{1}H NMR (400.1 MHz, DMSO-d$_6$): 7.97 (d, *J* = 7.8 Hz, [2H], H4/7), 7.69–7.82 (m, [3H], H4/7, H9), 7.55 (t, *J* = 7.5 Hz, [2H], H5/6), 7.39 (t, *J* = 7.6 Hz, [2H], H5/6), 6.58 (d, *J* = 12.7 Hz, [2H], H8,8'), 4.36 (q, *J* = 7.0 Hz, [4H], CH_2), 3.91 (s, [1H], $CHTf_2$), 1.33 (t, *J* = 7.0 Hz, [6H], CH_3) ppm.

^{13}C{^{1}H} NMR (100.6 MHz, DMSO-d$_6$): 164.15 (C2), 146.59 (C9), 140.77 (CS), 128.09 (C5), 125.17 (C6,CN), 123.08 (C7), 120.75 (q, *J* = 326 Hz, CF_3), 113.34 (C4), 98.57 (C8,8'), 53.94 ($CHTf_2$), 41.45 (CH_2), 12.59 (CH_3) ppm.

^{19}F{^{1}H} NMR (376.5 MHz, DMSO-d$_6$): –75.93 ($CHTf_2$) ppm.

MS (ES$^+$): m/z 365.1 (M$^+$, 100%). (ES$^-$): m/z 278.9 ($CHTf_2^-$, 100%).

IR (nujol, KBr plates): 3746, 3735, 2361, 2341, 1918, 1869, 1844, 1830, 1792, 1772, 1750, 1734, 1717, 1700, 1684, 1670, 1654, 1636, 1624, 1616, 1576, 1559, 1540, 1522, 1507, 1264, 1072 cm^{-1}.

UV-vis (CH_2Cl_2, 5.0 µM): λ_{max} = 564.31 nm (ε= 1.66 x 10^5 dm^{3}mol^{-1}cm^{-1}).

Analysis calc. for $C_{24}H_{22}F_6N_2O_4S_4$ (644.04): C 44.72; H 3.44; N 4.35. Found: C 44.81; H 3.47; N 4.40.

S3: Simulation of $[P_{4446}][NTf_2]$

All simulations were run using LAMMPS[2] in a canonical [fixed number of molecules, volume, and temperature (NVT)] ensemble with a time step of 0.5 fs. Periodic boundary conditions were applied, and long-range interactions were treated with a particle-particle particle-mesh solver method (PPPM) with a relative error in forces of 1×10^{-6}. Short-range Coulomb interactions were damped by Thole functions with a damping parameter of 2.6.[3] Lennard-Jones interactions were cut off after 12 Å, and Coulomb interactions were treated in the reciprocal space beyond this distance. All simulations were run at 400 K.

The methodology used for the simulations was a polarisable force field discussed elsewhere, but is included here for completeness.[4] The methodology uses a thermalized Drude oscillator model implemented in LAMMPS by Dequidt, Devémy, and Pádua.[3] It involves the addition of Drude particles to each atom to account for the polarisability, where the Drude particles are attached with a high spring constant ($K/2 = 500$ kcal mol^{-1}) and are thermalized at 1 K using a decoupled Nosé-Hoover (NH) thermostat with a time constant of 5 fs.

The Drude particles are assigned a small mass (0.4 amu) and a negative charge to account for the polarisability of the atoms. Charges on the Drude particles were calculated from the polarizability and spring constant by $q = \sqrt{K/\alpha}$, and the mass and charge on the core atom were adjusted, so the total charge and mass of the atom-Drude pair remains the same as the atom before addition of the Drude particle.

The force field used adapts the commonly used CL&P force field[5] by the addition of Drude oscillator particles. The simulation box was built, and Drude particles added using the polarizer script within the fftool package.[6] The polarisabilities used were the additive polarisabilities from Bernardes *et al.*[7] For hydrogen and fluorine atoms, the polarizability is accounted for on the direct neighbour atom, rather than assigning it a Drude particle.

To build the simulation box 512 ion pairs of $[P_{4446}][NTf_2]$ were packed into a cubic simulation box using the fftool[6] and PACKMOL[8] algorithms and any unfavourable initial configurations were relaxed by a short (1000 step) conjugate gradient energy minimization.

The simulation was thermally equilibrated and relaxed by an initial 2.5 ns isobaric-isothermal run, with the average box size from the final 500 ps being used to set the box size for the production canonical run. This gave a final box size of 75.68 Å with a density of 1.113 g/mol, an error of 0.3% from experimental density.[9] The box size was changed, and a canonical equilibration of 2 ns was performed, followed by a production run of 2 ns, with coordinates output every 100 fs for analysis.

Domain analysis was performed using the Voronoi tessellation feature of the TRAVIS software package.[10,11] The Drude particles were excluded from the domain Voronoi analysis, the polar domain was assigned to be all of the atoms in the anion, and the phosphorous and adjacent CH_2 groups in the cation as these carry the majority of the charge in this force field. The non-polar domain was assigned to be the rest of the CH_n groups on the alkyl chains. Voronoi parameters are shown below in Table S3

Table S3: *Average domain properties of* $[P_{4446}][NTf_2]$

Domain	No. of Domains	Volume (Å^3)	Surface Area (Å^2)
Polar	1.00 ± 0.00	190087 ± 221	153232 ± 513
Non-Polar	1.00 ± 0.00	243372 ± 221	153232 ± 513

The Voronoi analysis indicates that one continuous polar and non-polar domains are a permanent feature of this ionic liquid. Both of these domains are very large, with the non-polar domain accounting for approximately 55% of the total volume, and the polar domain accounting for approximately 45% of the total volume.

An estimation of the non-polar domain volumes of the imidazolium based ionic liquids can be calculated based upon extrapolation from known values using the numbers of carbons in the alkyl chain. Known non-polar domain volume ratios, calculated to be 22% for $[C_4C_1im][NTf_2]$ and 34% for $[C_8C_1im][NTf_2]$, lead to a non-polar domain accounting for 45% of the total volume in $[C_{12}C_1im][NTf_2]$.

Comparing this to non-polar domain volume ratios calculated from the molar volumes of these ionic liquids, these show that the non-polar domain in $[C_8C_1im][NTf_2]$ accounts for 32% of the total volume, and the non-polar domain in $[C_{12}C_1im][NTf_2]$ accounts for 43% of the total volume.[12,13]

Therefore $[P_{4446}][NTf_2]$ has a larger volume of non-polar moieties (55% of the total volume) than all of the imidazolium based ionic liquids that have BODIPY-C10 fully partitioned. As the polar domains are of a similar size (~400 Å^3 per ion pair in imidazolium ionic liquids, ~380 Å^3 per ion pair in phosphonium ionic liquids), we can deduce that there is likely a much larger non-polar domain for the BODIPY-C10 to partition into. Therefore it can be reasonably assumed that BODIPY-C10 is indeed fully partitioning into the non-polar domain.

S4: Crystallography

Crystals of commercially obtained Cy3 iodide were obtained by slow evaporation of a concentrated CH_2Cl_2 solution. All other crystals were obtained as described above.

Datasets were collected using the following hardware: **Cy3 NTf$_2$**, **Cy3 CHTf$_2$**, **BODIPY-C10**: an Oxford Diffraction PX Ultra diffractometer (Cu K_α radiation, 1.54184 Å); **Cy3 OTf**, **Cy3 BF$_4$/I**, **Cy3 I** and **Cy3 PF$_6$**: an Oxford Diffraction Xcalibur 3E (Mo K_α radiation, 0.71073 Å). Data processing was carried out using CrysAlisPro,[14] solutions were solved and refined using SHELX-97 and SHELXTL,[15] as well as Olex-2,[16] and WinGX.[17] Hydrogen atoms were placed in geometrically assigned positions with C–H distances of 0.95 Å (CH) or 0.98 Å (CH_3) and refined using a riding model, with $U_{\mathrm{iso}}(\mathrm{H}) = 1.2\ U_{\mathrm{eq}}(\mathrm{C})$ (CH) or $1.5\ U_{\mathrm{eq}}(\mathrm{C})$ (CH_3). Graphics were generated using ORTEP-III[17] and Mercury.[18] CCDC reference numbers 1995025 (**BODIPY-C10**), 1995224 (**Cy3 NTf$_2$**), 1995225 (**Cy3 OTf**), 1995226 (**Cy3 PF$_6$**), 1995229 (**Cy3 BF$_4$/I**), 1995227 (**Cy3 CHTf$_2$**) and 1995228 (**Cy3 I**) contain crystallographic data in CIF format.

In the Cy3 BF_4/I structure, the anion is a 43:57 mixture of BF_4 and I resulting from an incomplete salt metathesis of Cy3 iodide. Both anions occupied the same site within the unit cell; this was modelled using standard PART instructions and the occupancy was left free to refine. This approach necessitated the use of DFIX and ISOR restraints to keep the BF_4 anion in a sensible geometry with sensible ellipsoids. Isotropic restraints were also required for two oxygen atoms in Cy3 NTf_2 which were potentially disordered over two positions, but could not be modelled as such.

Disordered solvent which could not be satisfactorily modelled was present in the asymmetric units of Cy3 PF_6 (0.5 molecules of CH_2Cl_2) and Cy3 BF_4/I (one molecule each of CH_2Cl_2 and MeOH). These were removed using SQUEEZE. Positional disorder was also present in Cy3 PF_6 (the PF_6 anion was disordered over two positions) and Cy3 $CHTf_2$ (two of the CF_3 groups were disordered) which required restraints to retain a sensible geometry.

Data

Cy3

Table S4 A: crystallographic data for all structures of Cy3 X. All datasets were collected at 173.0(1) K.

Compound	**Cy3 NTf$_2$**	**Cy3 OTf**	**Cy3 PF$_6$**	**Cy3 BF$_4$/I**	**Cy3 CHTf$_2$**	**Cy3 I**
Formula	$C_{23}H_{21}F_6N_3O_4S_4$	$C_{22}H_{21}F_3N_2O_3S_3$	$C_{21}H_{21}F_6N_2PS_2$	$C_{21}H_{21}B_{0.43}F_{1.72}I_{0.57}N_2S_2$	$C_{24}H_{22}F_6N_2O_4S_4$	$C_{22}H_{23}Cl_2IN_2S_2$
M/g mol^{-1}	645.67	514.59	510.49	475.22	642.73	577.34
Crystal system	monoclinic	monoclinic	monoclinic	monoclinic	triclinic	triclinic
Space group (No.)	$I\ 2/a$ (15)	$P2_1/n$ (14)	$C2/c$ (15)	$C\ 2/c$ (15)	P–1 (2)	P–1 (2)
a/Å	14.7979(2)	13.3057(4)	17.6864(8)	17.7575(9)	13.7964(7)	7.9187(4)
b/Å	21.9313(3)	12.0660(4)	18.6880(8)	19.0198(8)	14.4462(6)	12.1261(7)
c/Å	18.0080(3)	14.7108(5)	15.7950(8)	15.2682(7)	14.8908(7)	13.0689(4)
α/°	90	90	90	90	103.965(3)	82.760(4)
β/°	112.854(2)	108.185(4)	114.792(6)	114.649(6)	99.568(4)	78.619(4)
γ/°	90	90	90	90	104.025(4)	79.315(5)
U/Å^3	5385.47(16)	2243.81(14)	4739.5(4)	4686.9(4)	2713.5(2)	1203.50(11)
Z	8	4	8	8	4	2
μ(Mo-Kα) /mm^{-1}	3.964	0.384	0.351	1.001	1.578	1.738
F(000)	2640	1064	2096	1927	1320	576
Total reflections	8357	7912	12437	9207	16043	8396
Unique reflections	4679	4549	4180	5366	10314	5456
R_{int}	0.033	0.028	0.019	0.019	0.033	0.036
GooF on F^2	1.048	1.028	1.042	1.008	1.040	1.048
$R_1{}^b$ [$I_o > 2\sigma(I_o)$]	0.069	0.037	0.066	0.037	0.049	0.033
R_1 (all data)	0.081	0.053	0.078	0.061	0.067	0.040
$wR_2{}^b$ [$I_o > 2\sigma(I_o)$]	0.180	0.077	0.191	0.074	0.136	0.074
wR_2 (all data)	0.193	0.085	0.203	0.083	0.151	0.079

BODIPY-C10

Table S4 B: crystallographic data for the structure of BODIPY-C10. Dataset collected at 173.0(2) K.

Compound	**BODIPY-C10**
Formula	$C_{25}H_{31}BF_2N_2O$
M/g mol^{-1}	424.33
Crystal system	triclinic
Space group (No.)	P–1 (2)
a/Å	7.9871(4)
b/Å	15.6608(8)
c/Å	19.3410(11)
α/°	74.494(5)
β/°	87.660(4)
γ/°	76.490(4)
U/Å^3	5385.47(16)
Z	4
μ(Mo-Kα) /mm^{-1}	0.698
F(000)	904
Total reflections	15553
Unique reflections	8578
R_{int}	0.046
GooF on F^2	1.032
$R_1{}^b$ $[I_o > 2\sigma(I_o)]$	0.048
R_1 (all data)	0.071
$wR_2{}^b$ $[I_o > 2\sigma(I_o)]$	0.123
wR_2 (all data)	0.137

Cy3 Crystallography Discussion

In order to understand how the Cy3 cation interacts with weakly coordinating anions, we turned to X-ray crystallography. A search of the CCDC revealed seven structures with an exact match to the Cy3 cation, with Br,[19,20] BF_4,[21] $AuCl_2$,[22] OTs[23] and tetracyanoquinodimethane[24,25] anions. However, six of these structures were 40+ years old and were run at room temperature, hence the data quality indicators were poor (high R factors, large ESDs on bond lengths, etc.). The exception is the BF_4 salt: a high quality dataset was obtained at 123 K in 2016, hence this structure is the only one which will be included in the resulting analysis.

Crystals suitable for single-crystal X-ray diffraction studies were grown by slow evaporation of a CH_2Cl_2 solution (the OTf complex was crystallized from MeOH). In comparison to the literature structure of Cy3 BF_4, two structures had very similar unit cell parameters: Cy3 PF_6 and Cy3 BF_4/I. Each of these crystallized in the C-centred monoclinic spacegroup *C* 2/*c* with small differences (<0.5 Å) in the cell lengths. This resulted in very similar packing interactions between cation and anion, with the only significant interactions being hydrogen bonding between the anion and one of the CH units of the conjugated linker (Figure S4 A).

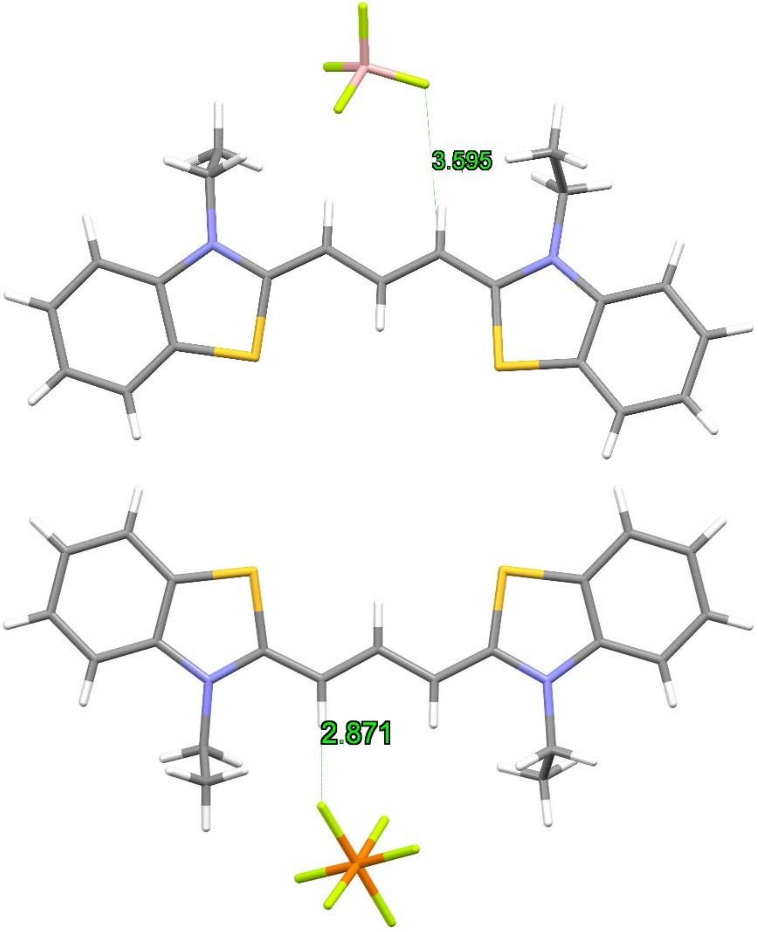

Figure S4 A: the interactions between the Cy3 cation and BF4 in BF4/I (top), and PF6 in Cy3 PF6 (bottom).

The CH···F distances to the BF_4 anions are consistent with weak hydrogen bonds, in keeping with the notion that BF_4 is a weakly coordinating anion (WCA). The CH···F distance is slightly shorter in the 'pure' BF_4 compound (3.362(3) Å) compared to the mixed BF_4/I salt (3.595(4) Å). Notably the CH···F distance to the PF_6 anion is much shorter at 2.87(2) Å, although this is most likely a packing effect: the larger PF_6 anion is occupying the same crystallographic site as the smaller BF_4 anion hence it is forced to be in closer proximity to the Cy3 cation.

Also of note is the difference between pure Cy3 iodide and the mixed anion Cy3 I/BF_4. Whilst the latter is structurally similar to Cy3 BF_4, with iodide and BF_4 occupying the same lattice position in a 57:43 ratio, the former crystallizes in a different crystal system entirely (triclinic *P*–1) with different cation-anion interactions. For pure Cy3 iodide, the dominant interaction is a sigma hole-type interaction between iodide and one of the sulfur atoms in the benzothiazole ring, compared to hydrogen bonding in the mixed BF_4/I salt (Figure S4 B). The sum of van der Waals radii for S and I is 3.93 Å,[26] indicating that the sigma hole interaction is very weak.

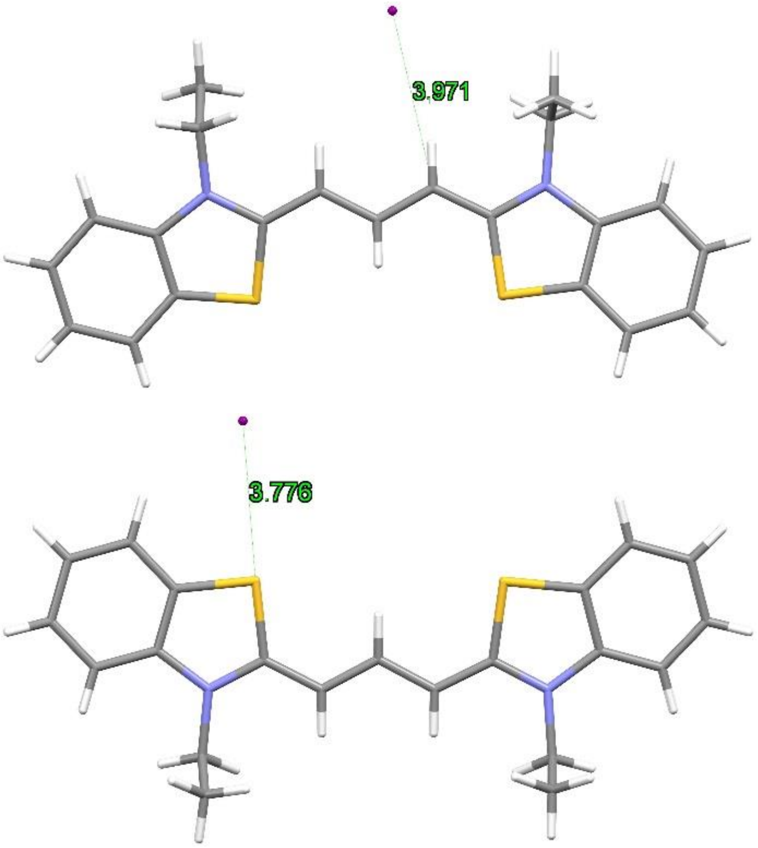

Figure S4 B: the interactions between the Cy3 cation and iodide in (top) the BF4/I complex and (bottom) pure Cy3 iodide.

As the shape of the anion becomes less spherical, the complexity of the cation-anion interactions increases. Cy3 OTf crystallized in the monoclinic space group $P\ 2_1/n$ with notably different cell parameters to any previous Cy3 salt. The OTf anion interacts with the Cy3 cation in two different ways, both via oxygen atoms of the sulfonyl group: hydrogen bonding through one of the conjugated CH units and sigma hole bonding to one of the sulfur atoms in a benzothiazole ring (Figure S4 C). However, both of these are weak interactions, with the sigma hole interaction about 0.1 Å shorter than the sum of van der Waals radii for S and O (3.39 Å).[26]

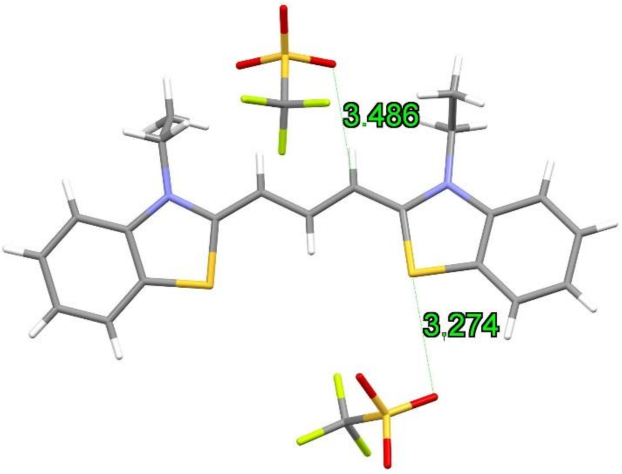

Figure S4 C: diagram of the cation-anion interactions in Cy3 OTf.

Further complexity in the cation-anion interactions was observed for Cy3 NTf_2. The asymmetric unit contained two symmetry-independent cations interacting with two symmetry-independent NTf2 anions, resulting in the formation of 1D chains of interconnecting cations and anions running parallel to the x/y/z axis (Figure S4 D).

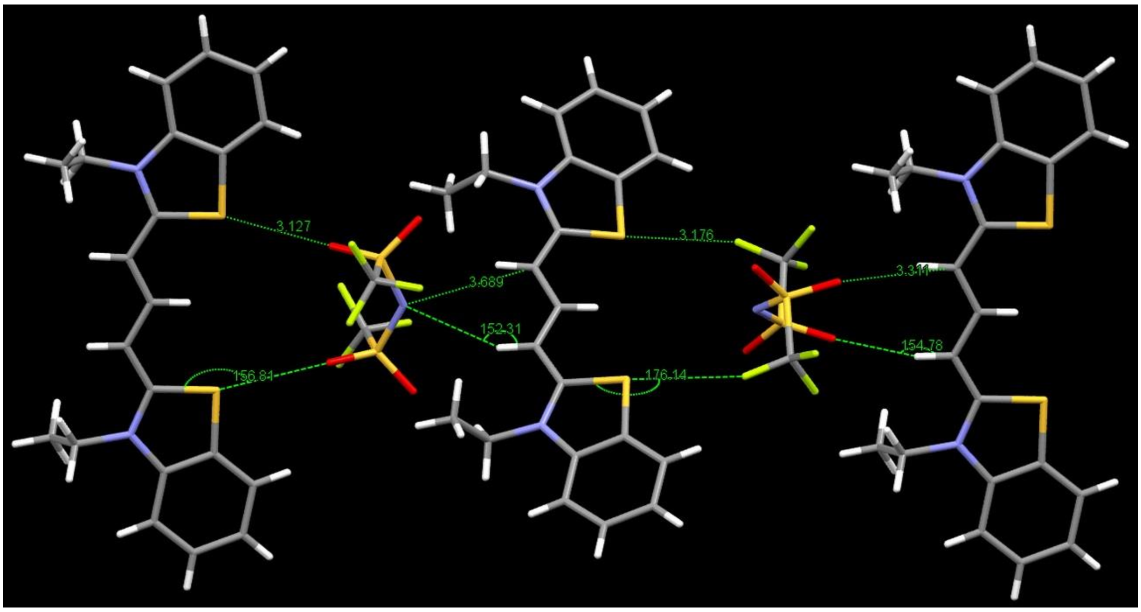

Figure S4 D: diagram of the cation-anion interactions in Cy3 NTf_2.

Each NTf_2 anion interacts with two Cy3 cations, one via a sigma hole-type interaction to a sulfur in the benzothiazole ring and the other via hydrogen bonding to the conjugated CH units. However, the atoms involved are different for each symmetry-independent NTf_2 anion. One anion exhibits sigma hole binding through the sulfoxide oxygens and hydrogen bonding through the central nitrogen, whereas the other NTf_2 anion has the sulfoxide oxygens involved in hydrogen bonding and the fluorine atoms are involved with the sigma hole bonding. The sigma hole interaction in Cy3 NTf_2 is stronger than the equivalent interaction in the Cy3 OTf structure, and even the sigma hole interaction through the CF_3 groups are shorter than the S···O distance in Cy3 OTf. It is not clear why the NTf_2 anion interacts more strongly with the Cy3 cation than other WCAs in this study, but the multiple points of interaction between cation and anion imply a synergistic bonding effect is increasing the strength of interactions.

A 1D chain structure with similar cation-anion interactions was observed in Cy3 $CHTf_2$ (Figure S4 E), although the atoms involved are slightly different. The sigma hole interactions are of similar strength in both $CHTf_2$ and NTf_2, but the hydrogen bonding interactions are solely through the S···O oxygens. These hydrogen bonding interactions are still classified as weak, as are those observed in Cy3 NTf_2.

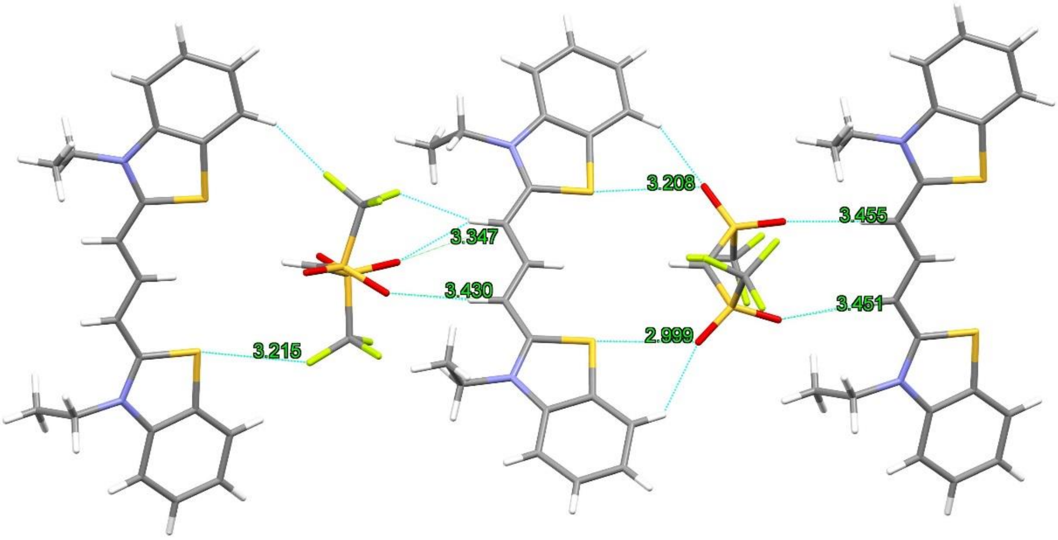

Figure S4 E: diagram of the cation-anion interactions in Cy3 $CHTf_2$.

Further evidence that the cation-anion interactions are weak comes from an examination of the structural parameters, particularly the conjugated C–C bonds (Table S4 C). These are all mid-way between a classical C=C double bond (~1.33 Å) and a C–C single bond (~1.54 Å), consistent with the notion that there is complete delocalisation across both benzothiazole rings and the C3 linker. However, when experimental error is considered, only one bond across all 9 structures is different to the others (C3-C4 in Cy3 OTf which is slightly shorter) hence the interactions between anion and cation do not appear to influence the bonding in the Cy3 cation.

Table S4 C: summary of relevant C–C bond lengths in Cy3 structures. Notes: (a) cation with bigger twist; (b) cation with smaller twist; (c) related by symmetry to C8–C9; (d) related by symmetry to C2–C8

	θ	**C2–C8**	**C8–C9**	**C9–C8′**	**C8′–C2′**
BF$_4$(MeCN)	10.4	1.394(4)	1.384(4)	1.383(4)	1.392(4)
NTf$_2$ (a)	26.8	1.389(5)	1.380(5)	c	d
NTf$_2$ (b)	10.4	1.391(6)	1.386(5)	c	d
CHTf$_2$ (a)	21.8	1.398(4)	1.387(4)	1.380(4)	1.393(4)
CHTf$_2$ (b)	8.31	1.394(4)	1.387(4)	1.392(4)	1.397(4)
OTf	15.07	1.387(3)	1.392(3)	1.376(3)	1.400(3)
BF$_4$/I	9.02	1.388(3)	1.385(3)	1.382(3)	1.393(3)
PF$_6$	5.12	1.400(6)	1.388(6)	1.382(6)	1.389(6)
I	3.28	1.385(4)	1.383(4)	1.381(4)	1.388(4)

Despite the similarities in bond lengths across the entire range of structurally characterised Cy3 cations there are still some marked differences. The most obvious is the twist angle between the benzothiazole rings. This is the dihedral angle between the mean planes defined by the 9 atoms in each benzothiazole ring (Figure F and *Θ*, Table S4 C). There is a range of twist angles from 3.28 to 26.8°, indicating that there is a high degree of flexibility across the Cy3 cation despite the formal complete delocalisation of the pi-symmetry orbitals. This is especially notable within Cy3 NTf$_2$ and Cy3 CHTf$_2$ where each structure has two symmetry-independent cations with hugely different twist angles in the same structure. The combined evidence of the Cy3-anion distances indicating only weak interactions, the similarity of the intramolecular bonds across the different structures and yet the significantly different twists around the bonds of the linking conjugated chain in Cy3 indicate the extreme flexibility and ease of distortion of the Cy3 cation.

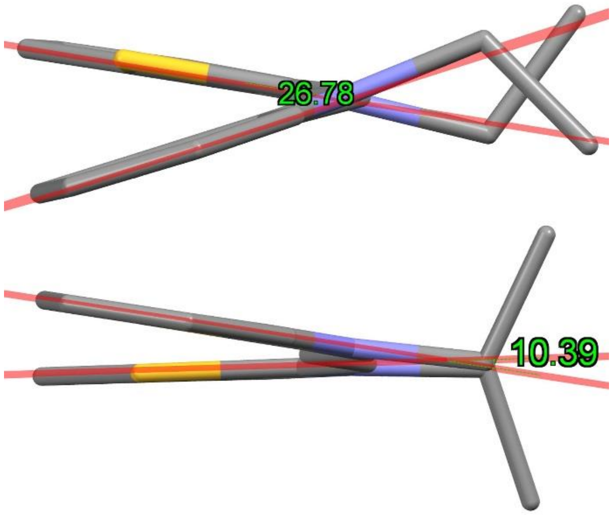

Figure S4 F: the two symmetry-independent cations in Cy3 NTf2 showing the marked difference in twist angle.

The cyanine-based molecules used in this study are commonly used as molecular rotors, although the mechanism by which photoexcitation breaks the conjugation of the cation is still not fully understood. Initially it was thought that photoexcitation of the Cy3 cation caused a cis/trans isomerism about the C8–C9 bond. However, ^{1}H NMR spectroscopic evidence obtained by Ponterini and Momicchioli suggested an alternative explanation that rotation occurred around the C2–C8 bond. This was assigned as a formal E/Z isomerism process whereby the ground state

(Z) isomer was fully converted to the photoexcited (E) isomer.[27] Follow-up theoretical calculations on a model conjugated system supported the full twist theory around the C2–C8 bond.[28] However, subsequent calculations from Vladirimova *et al.* on the entire Cy3 cation (rather than a model system) found that the 90° "perpendicular" twist about C2–C8 was a local minimum on the potential energy surface, and more favourable than the full 180° rotation.[29]

Table S4 D: summary of relevant torsion angles in Cy3 structures. Notes: (a) cation with bigger twist; (b) cation with smaller twist; (c) related by symmetry to C2C8C9C8'; (d) related by symmetry to NC2C8C9; (e) related by symmetry to SC2C8C9.

	θ	**NC2C8C9**	**SC2C8C9**	**C2C8C9C8'**	**C8C9C8'C2'**	**C9C8'C2'N'**	**C9C8'C2'S'**
BF_4(MeCN)	10.4	175.4(3)	–4.4(5)	–180.0(3)	177.2(3)	175.8(3)	–5.6(5)
NTf_2 (a)	26.8	–170.9(3)	10.7(5)	–174.5(4)	c	d	e
NTf_2 (b)	10.4	174.7(3)	–5.2(5)	178.8(4)	c	d	e
$CHTf_2$ (a)	21.8	–169.4(3)	11.1(4)	–176.6(3)	–175.1(3)	–174.0(3)	6.4(4)
$CHTf_2$ (b)	8.31	–173.2(3)	5.7(4)	–179.9(3)	–178.3(3)	–177.0(3)	3.5(4)
OTf	15.07	179.80(18)	–0.4(3)	178.08(19)	178.18(19)	168.42(19)	–12.7(3)
BF_4/I	9.02	175.95(18)	–4.2(3)	–178.95(19)	176.58(19)	176.54(19)	–5.0(3)
PF_6	5.12	178.2(4)	–3.1(6)	177.7(4)	–179.3(4)	176.6(4)	–3.4(6)
I	3.28	179.8(2)	1.5(4)	–178.3(2)	178.2(2)	–177.8(2)	1.0(4)

Examination of the 3-bond torsion angles across the conjugated C3 linker (Table S4 D) supports the idea that the C2–C8 bond is more likely to rotate than the C8–C9 bond. For an ideal planar molecule, all of these torsion angles should either be 0° or 180°. In most cases the deviation from planarity is small, being 5° or less. This indicates that the overall twist angle between the benzothiazole rings is comprised of lots of small twists, which sum to a larger twist across the entire delocalised C_3 linker. However, the cations with the biggest overall twists (Cy3 OTf, Cy3 $CHTf_2$ and Cy3 NTf_2) have torsion angles which deviate by 11° or more. These relatively large torsion angles are across the C2–C8 bond (or C8'–C2') with only small torsion angles noted across the C8–C9 (or C9–C8') bond, implying that the C2–C8 bond is the most flexible across the entire conjugated linker.

S5: Absorbance and Emission of Cy3 in Ionic Liquids

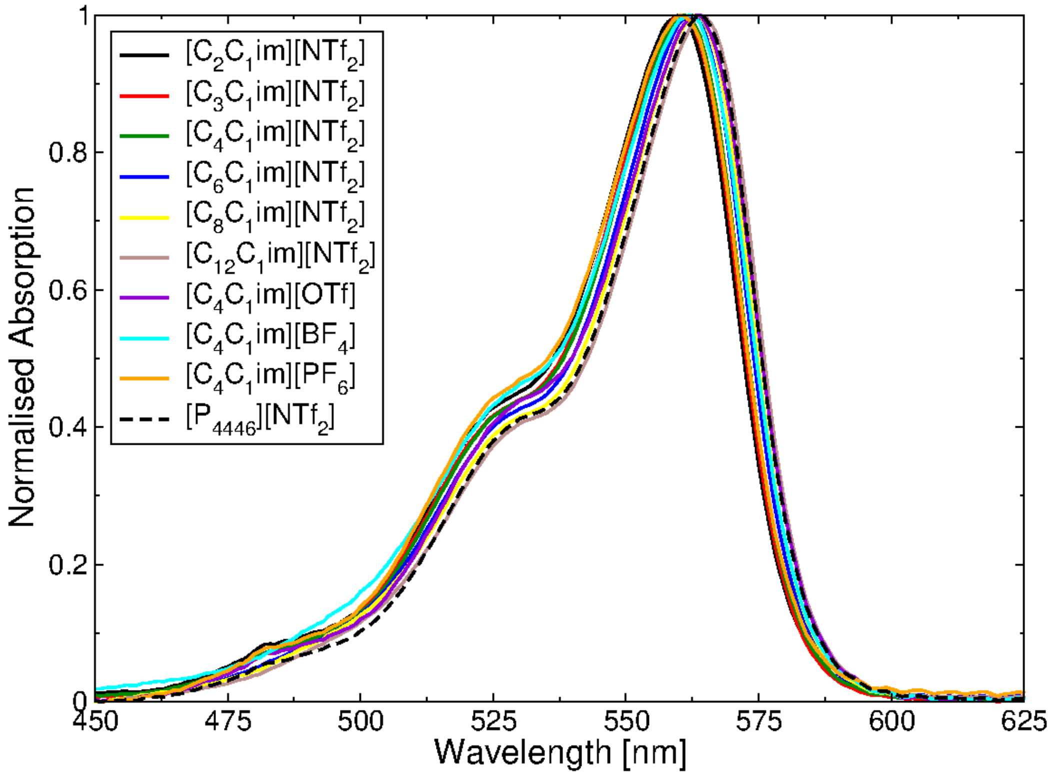

Figure S5 A: Absorbance of Cy3 in various ionic liquids normalised to a maximum of 1.

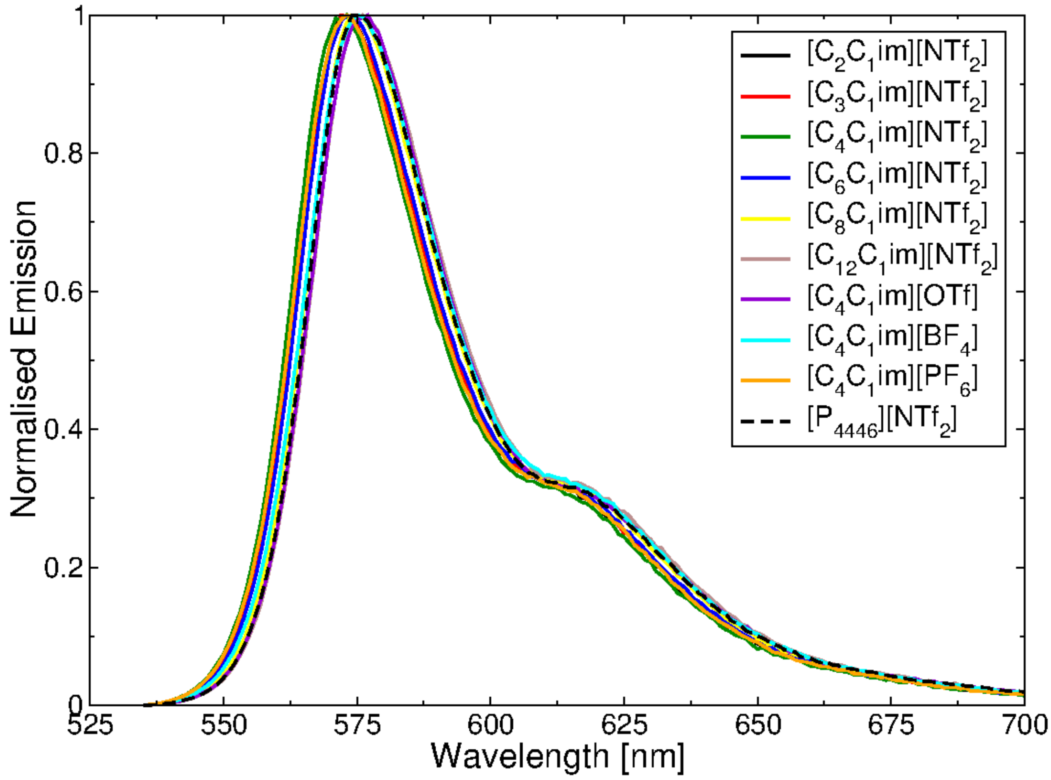

Figure S5 B: Emission of Cy3 in various ionic liquids normalised to a maximum of 1. Excitation wavelength used was 520 nm.

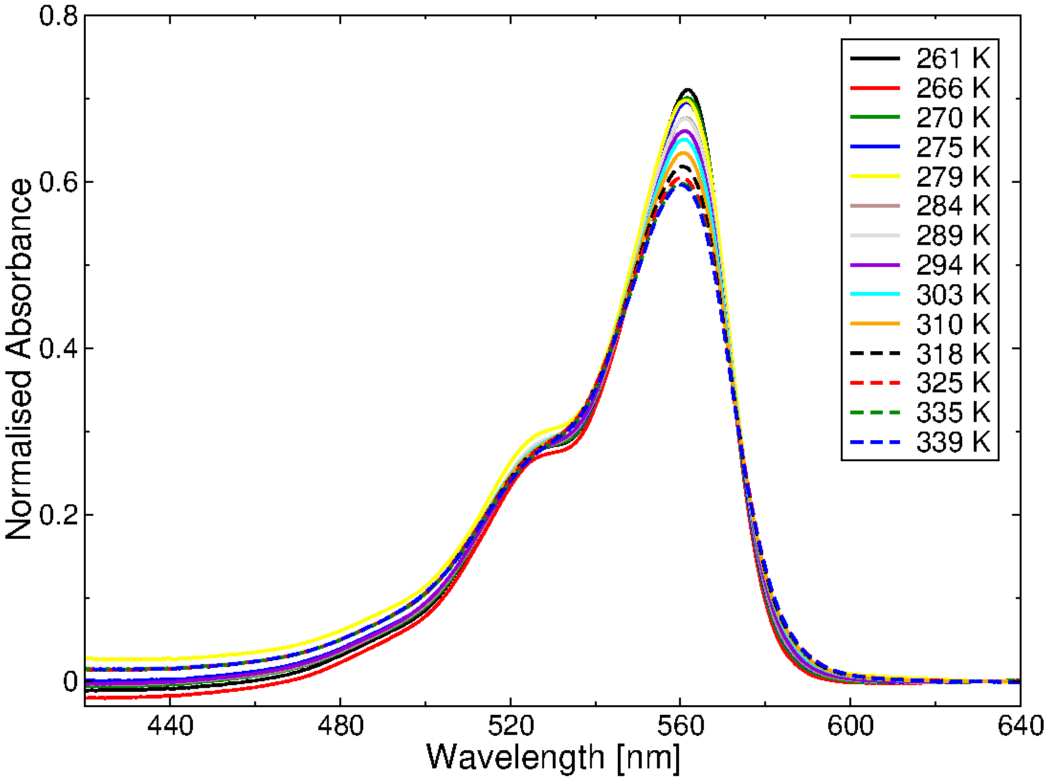

Figure S5 C: Absorbance of Cy3 in [C_4C_1im][NTf_2] at various temperatures, normalised to a baseline of zero.

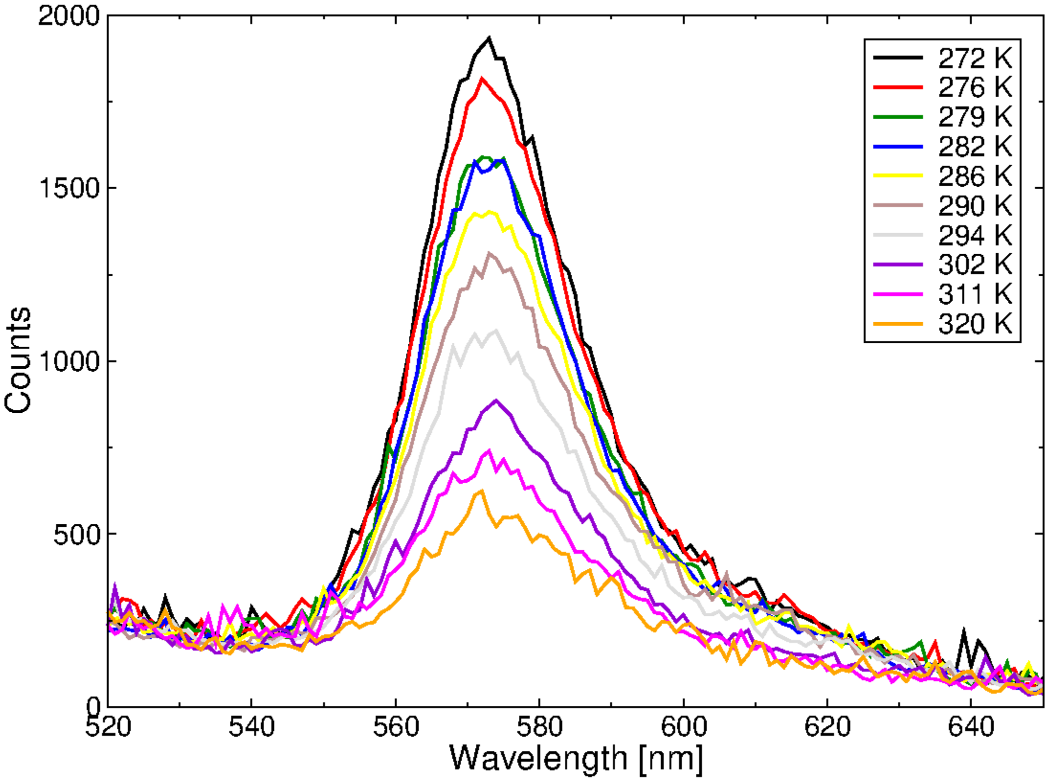

Figure S5 D: Emission of Cy3 in [C_4C_1im][NTf_2] at various temperatures. Excitation wavelength used was 467 nm.

Table S5 A: Wavelength of the maximum absorbance of Cy3 in the different ionic liquids

Ionic liquid	$[C_2C_1im]$ $[NTf_2]$	$[C_3C_1im]$ $[NTf_2]$	$[C_4C_1im]$ $[NTf_2]$	$[C_6C_1im]$ $[NTf_2]$	$[C_8C_1im]$ $[NTf_2]$	$[C_{12}C_1im]$ $[NTf_2]$	$[P_{4446}]$ $[NTf_2]$	$[C_4C_1im]$ $[BF_4]$	$[C_4C_1im]$ [OTf]	$[C_4C_1im]$ $[PF_6]$
λ_{max} (ABS) [nm]	560	560	561	562	563	564	564	562	564	560

Table S5 B: Wavelength of the maximum emission of Cy3 in the different ionic liquids. Excitation wavelength used was 520 nm.

Ionic liquid	$[C_2C_1im]$ $[NTf_2]$	$[C_3C_1im]$ $[NTf_2]$	$[C_4C_1im]$ $[NTf_2]$	$[C_6C_1im]$ $[NTf_2]$	$[C_8C_1im]$ $[NTf_2]$	$[C_{12}C_1im]$ $[NTf_2]$	$[P_{4446}]$ $[NTf_2]$	$[C_4C_1im]$ $[BF_4]$	$[C_4C_1im]$ [OTf]	$[C_4C_1im]$ $[PF_6]$
λ_{max} (Em) [nm]	572	572	573	573	574	576	575	575	577	573

Table S5 C: Wavelength of the maximum absorbance of Cy3 in [C4C1im][NTf2] at different temperatures

Temp (K)	261	266	270	275	279	284	289	294	303	310	318	325	335	339
λ_{max} (ABS) [nm]	562	562	562	561	561	561	561	561	561	561	560	560	560	560

Table S5 D: Wavelength of the maximum emission of Cy3 in [C4C1im][NTf2] at different temperatures. Excitation wavelength used was 467 nm.

Temp (K)	272	276	279	282	286	290	294	302	311	320
λ_{max} (Em) [nm]	572	572	572	573	573	573	573	574	574	574

S6: Absorbance and Emission of BODIPY-C10 in Ionic Liquids

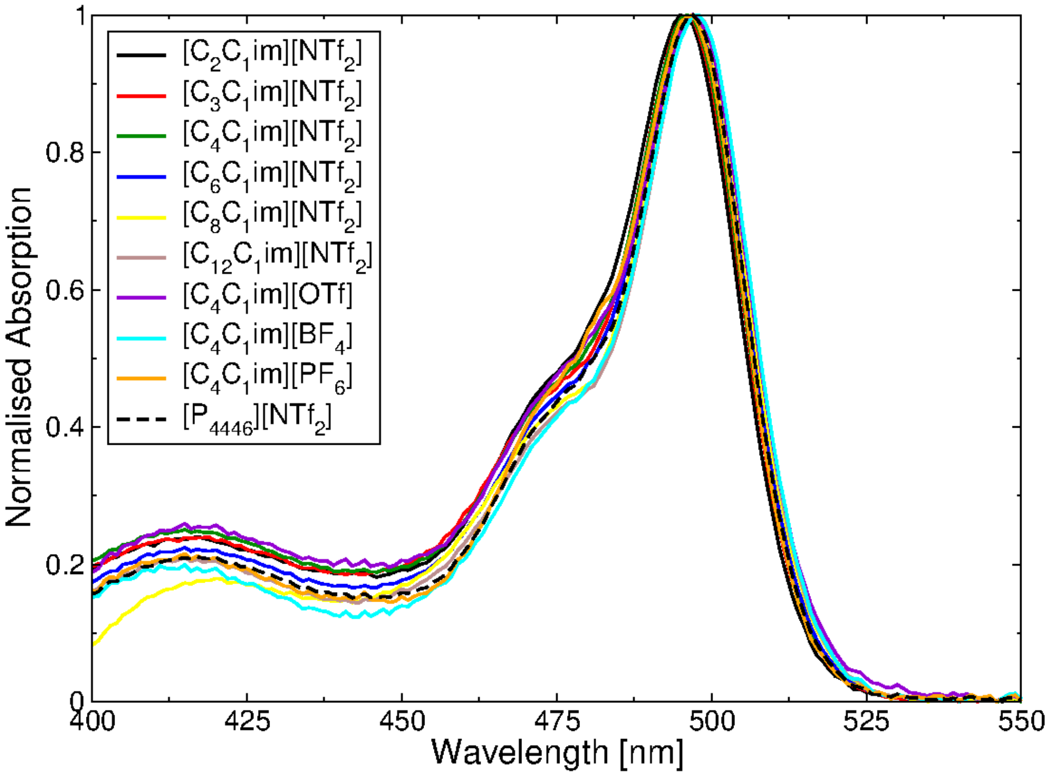

Figure S6 A: Absorbance of BODIPY-C10 in various ionic liquids normalised to a maximum of 1.

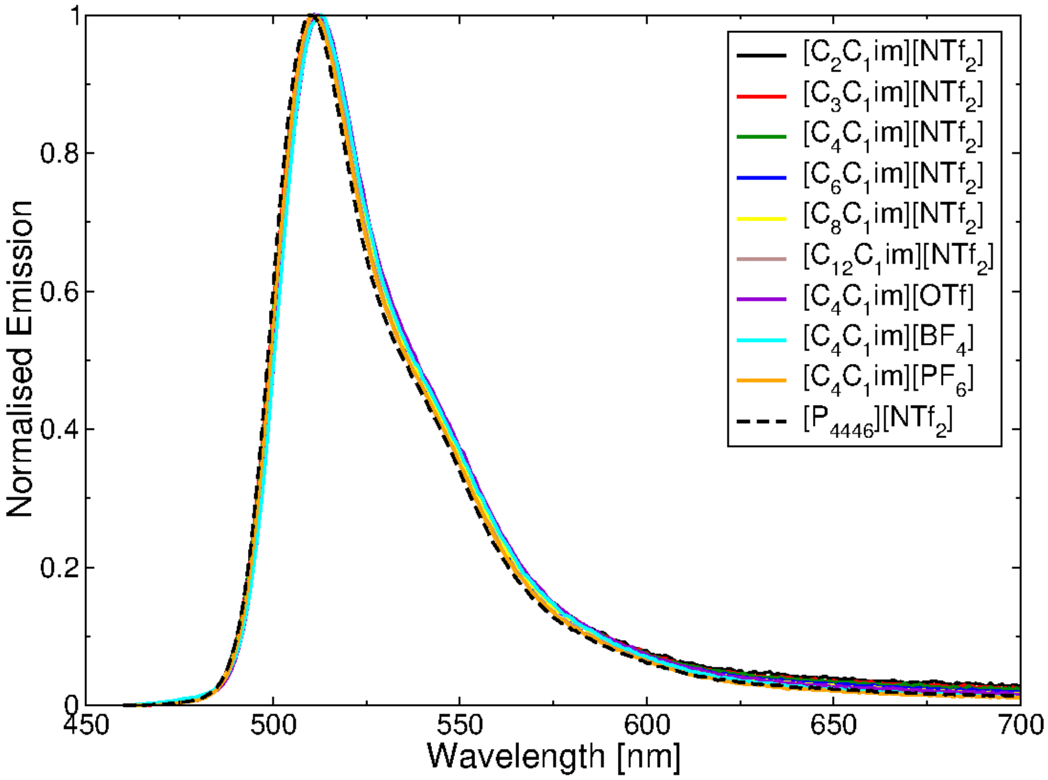

Figure S6 B: Emission of BODIPY-C10 in various ionic liquids. Excitation wavelength used was 445 nm.

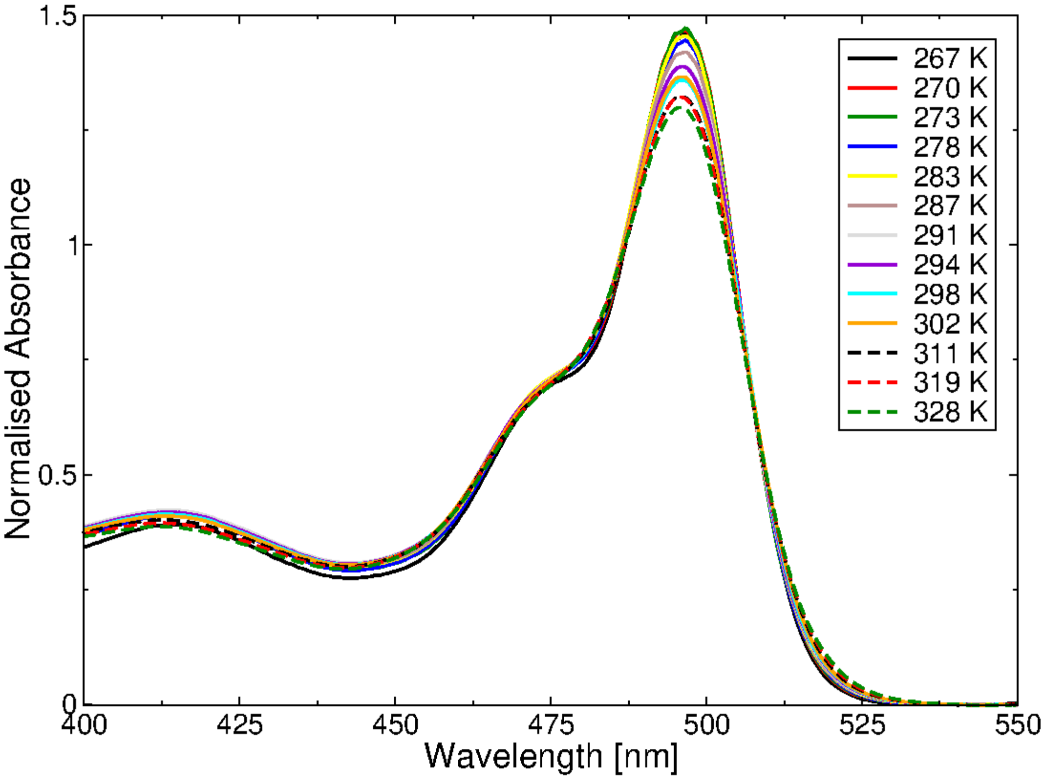

Figure S6 C: Absorbance of BODIPY-C10 in [C_4C_1im][NTf_2] at various temperatures normalised to a baseline of zero.

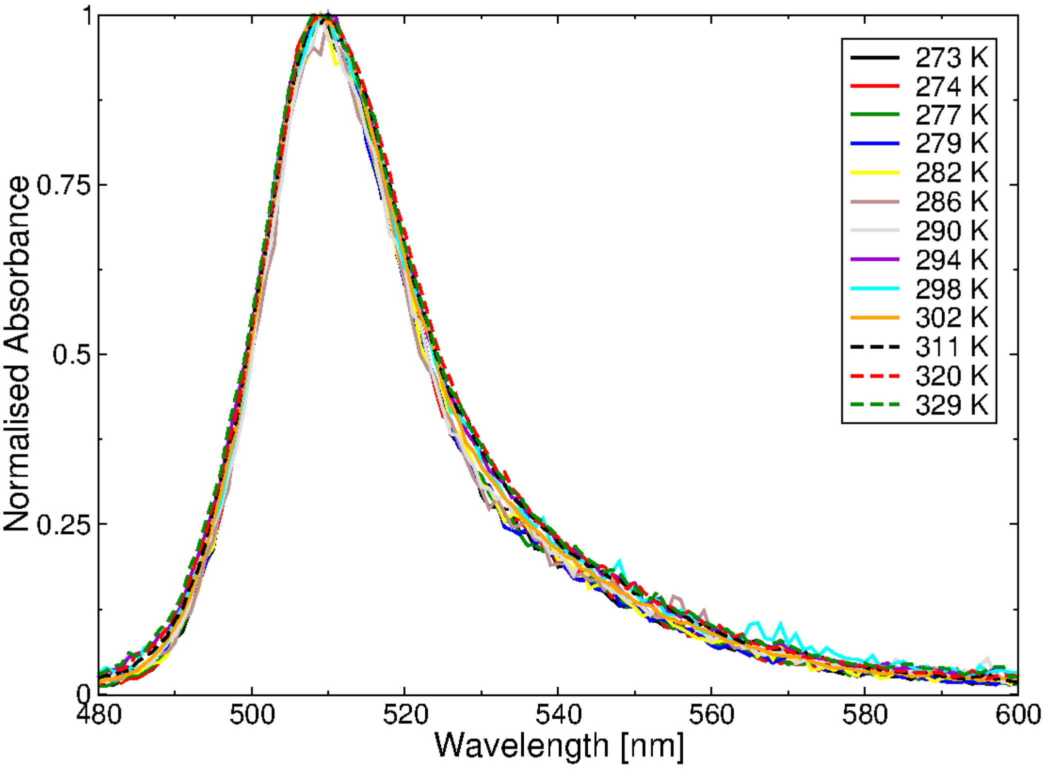

Figure S6 D: Normalised emission of BODIPY-C10 in [C_4C_1im][NTf_2] at various temperatures. Excitation wavelength used was 467 nm.

Table S6 A: Wavelength of the maximum absorbance of BODIPY-C10 in the different ionic liquids

Ionic liquid	[C$_2$C$_1$im] [NTf$_2$]	[C$_3$C$_1$im] [NTf$_2$]	[C$_4$C$_1$im] [NTf$_2$]	[C$_6$C$_1$im] [NTf$_2$]	[C$_8$C$_1$im] [NTf$_2$]	[C$_{12}$C$_1$im] [NTf$_2$]	[P$_{4446}$] [NTf$_2$]	[C$_4$C$_1$im] [BF$_4$]	[C$_4$C$_1$im] [OTf]	[C$_4$C$_1$im] [PF$_6$]
λ_{max} (ABS) [nm]	495	496	496	497	497	497	497	498	497	497

Table S6 B: Wavelength of the maximum emission of BODIPY-C10 in the different ionic liquids. Excitation wavelength used was 445 nm.

Ionic liquid	[C$_2$C$_1$im] [NTf$_2$]	[C$_3$C$_1$im] [NTf$_2$]	[C$_4$C$_1$im] [NTf$_2$]	[C$_6$C$_1$im] [NTf$_2$]	[C$_8$C$_1$im] [NTf$_2$]	[C$_{12}$C$_1$im] [NTf$_2$]	[P$_{4446}$] [NTf$_2$]	[C$_4$C$_1$im] [BF$_4$]	[C$_4$C$_1$im] [OTf]	[C$_4$C$_1$im] [PF$_6$]
λ_{max} (Em) [nm]	511	510	511	511	511	512	510	513	512	510

Table S6 C: Wavelength of the maximum absorbance of BODIPY-C10 in [C$_4$C$_1$im][NTf$_2$] at different temperatures

Temp (K)	267	270	273	278	283	287	291	294	298	302	311	319	328
λ_{max} (ABS) [nm]	497	497	497	497	496	497	496	496	496	496	496	496	496

Table S6 D: Wavelength of the maximum emission of BODIPY-C10 in [C$_4$C$_1$im][NTf$_2$] at different temperatures. Excitation wavelength used was 467 nm.

Temp (K)	273	274	277	279	282	286	290	294	298	302	311	320	329
λ_{max} (Em) [nm]	509	508	510	510	509	510	509	510	509	509	510	509	509

S7: Decay Curves of Neat Ionic Liquids

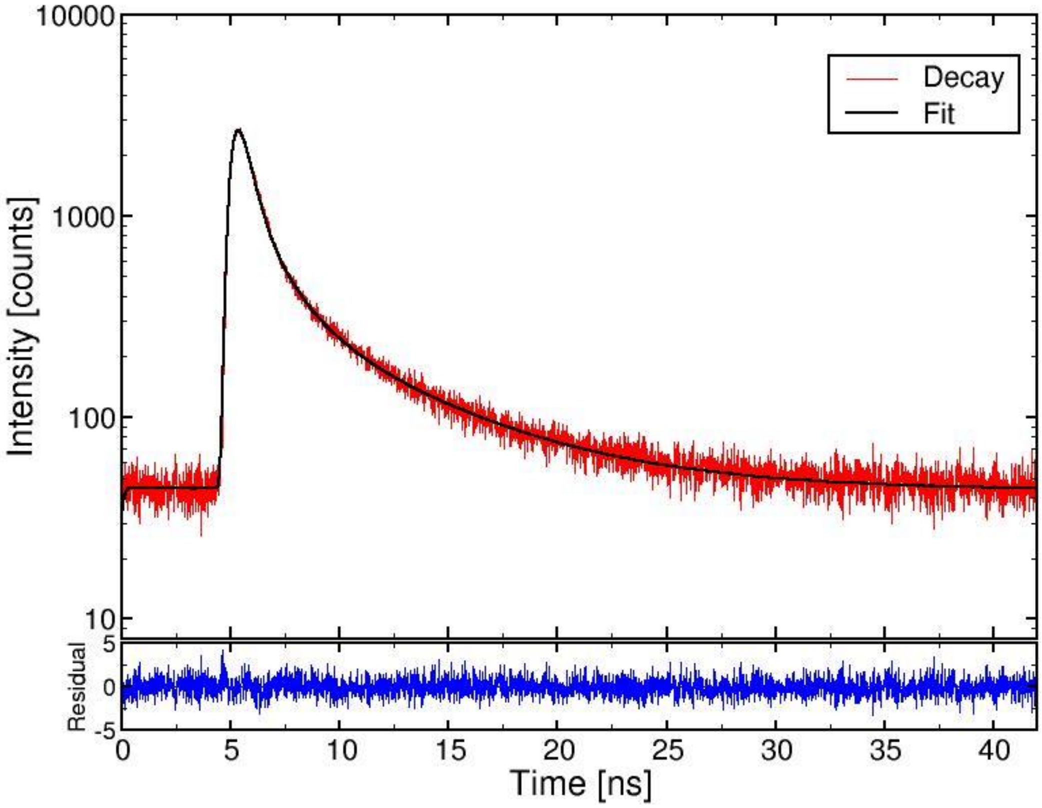

Figure S7 A: Raw decay data and 3 decay component fit for [C_2C_1im][NTf_2]. Bottom graph shows residual values at each point.

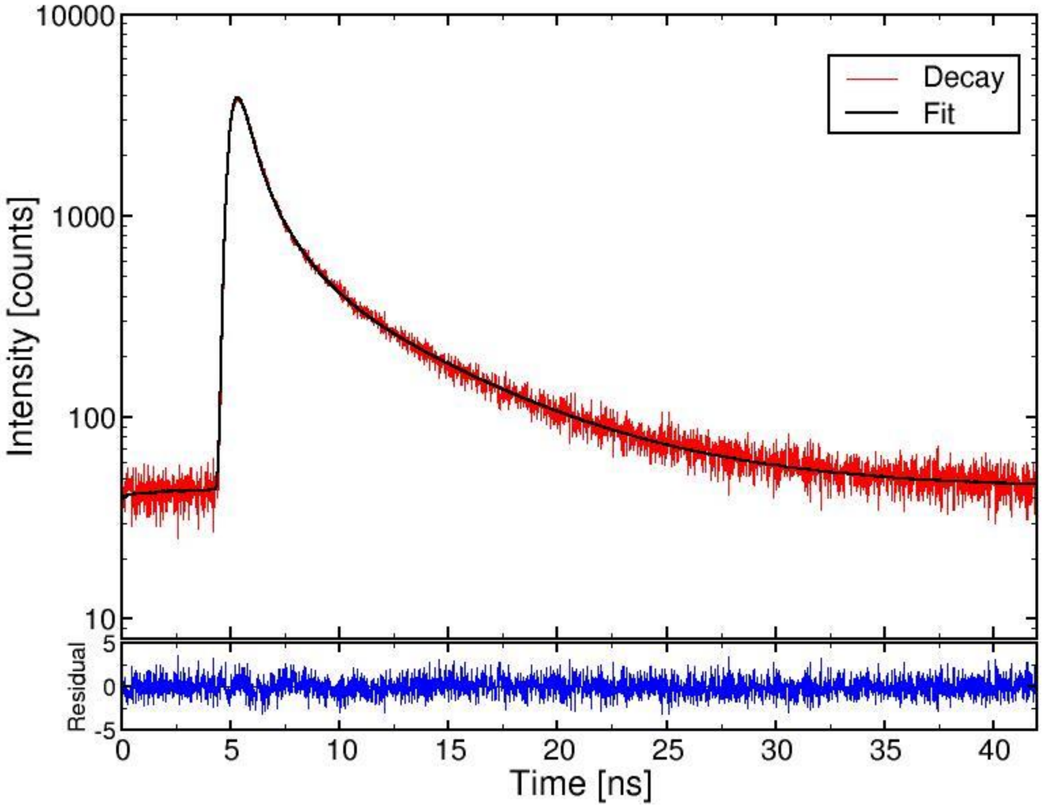

Figure S7 B: Raw decay data and 3 decay component fit for [C_3C_1im][NTf_2]. Bottom graph shows residual values at each point.

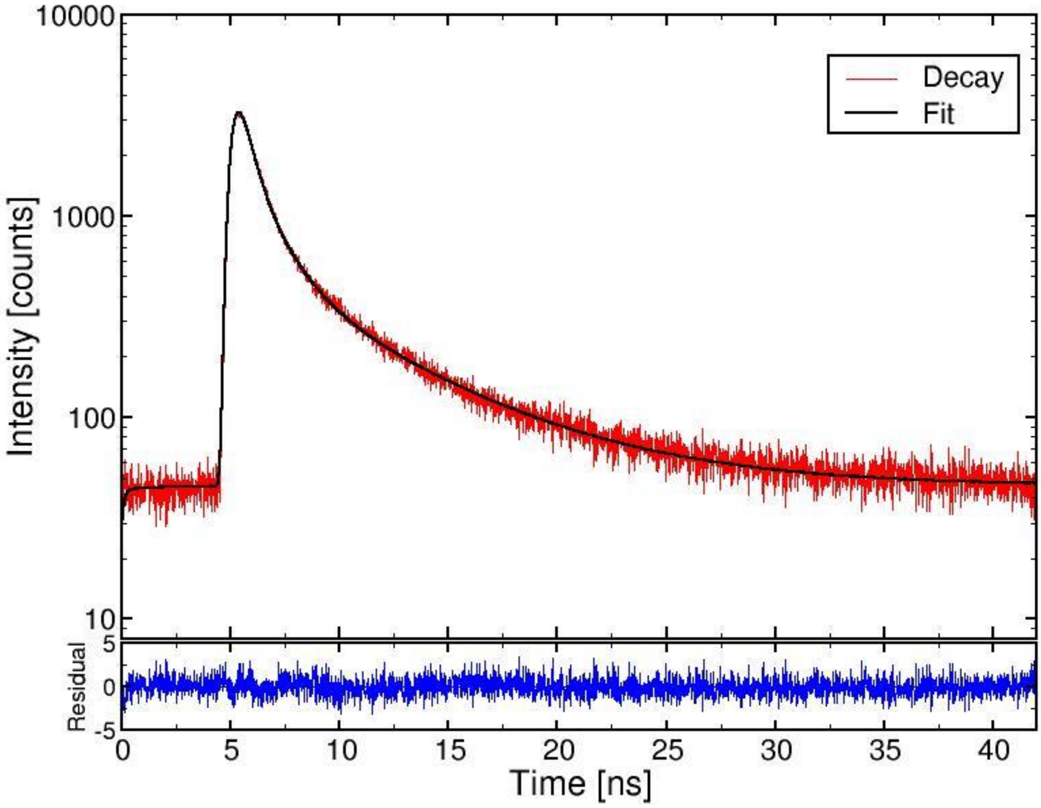

Figure S7 C: Raw decay data and 3 decay component fit for [C_4C_1im][NTf_2]. Bottom graph shows residual values at each point.

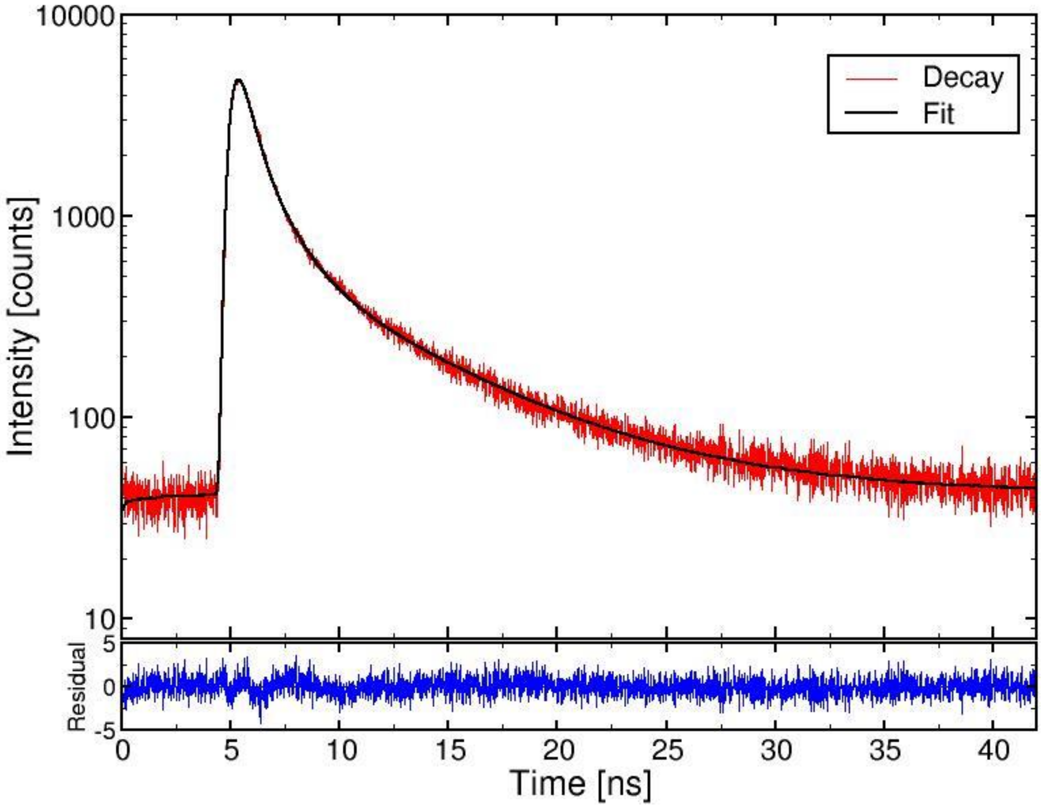

Figure S7 D: Raw decay data and 3 decay component fit for [C_6C_1im][NTf_2]. Bottom graph shows residual values at each point.

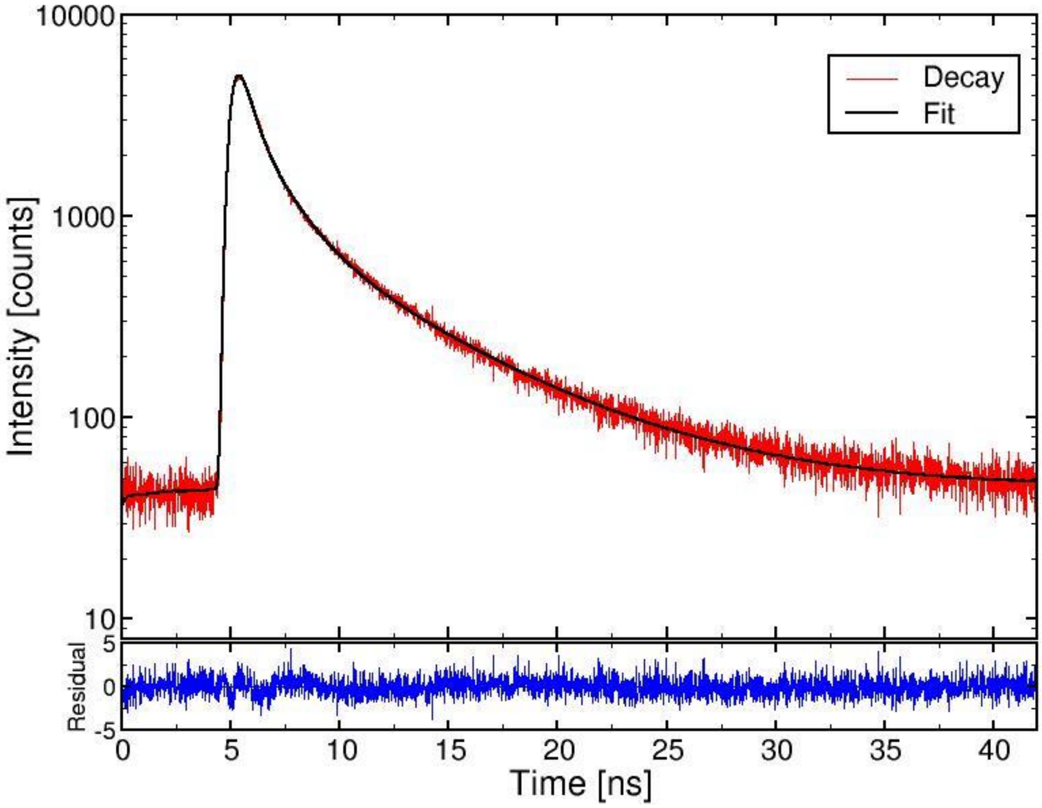

Figure S7 E: Raw decay data and 3 decay component fit for $[C_8C_1im][NTf_2]$. Bottom graph shows residual values at each point.

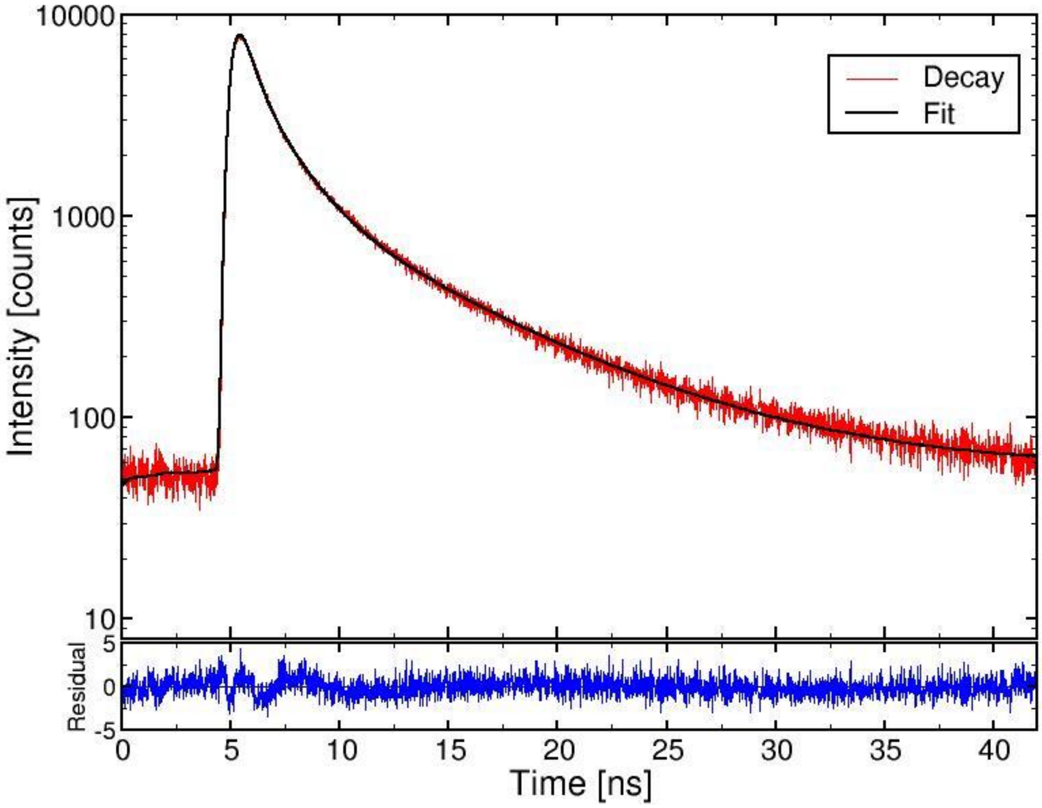

Figure S7 F: Raw decay data and 3 decay component fit for $[C_{12}C_1im][NTf_2]$. Bottom graph shows residual values at each point.

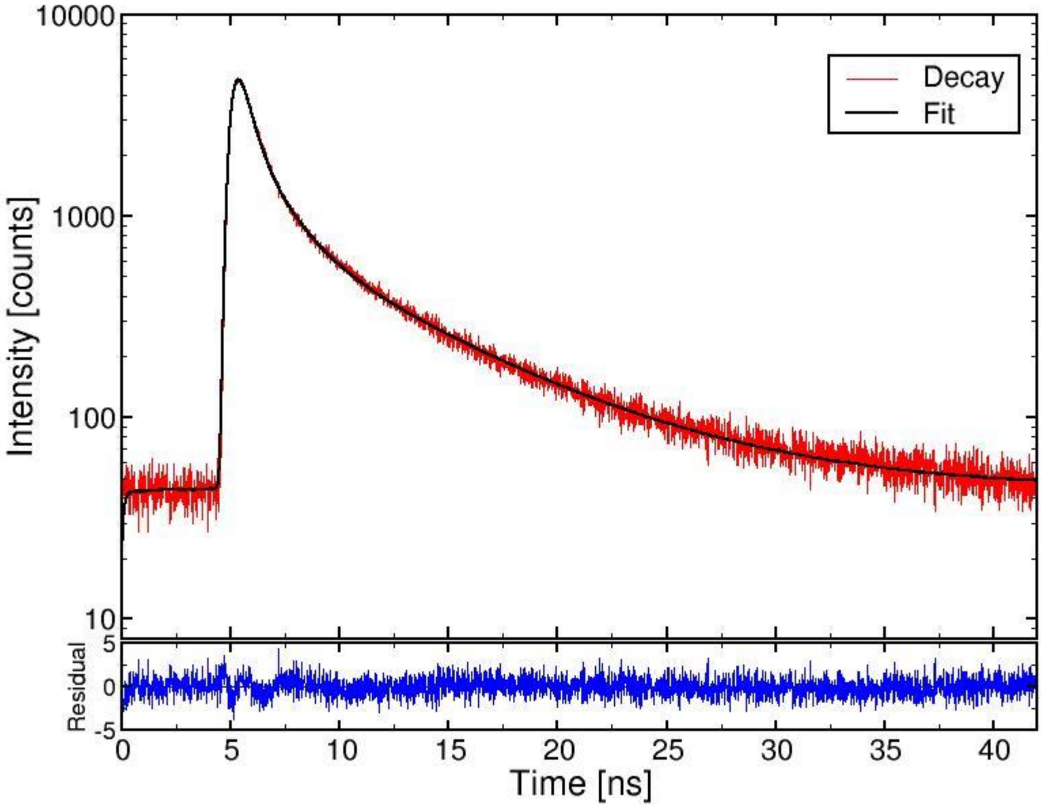

Figure S7 G: Raw decay data and 3 decay component fit for $[P_{4446}][NTf_2]$. Bottom graph shows residual values at each point.

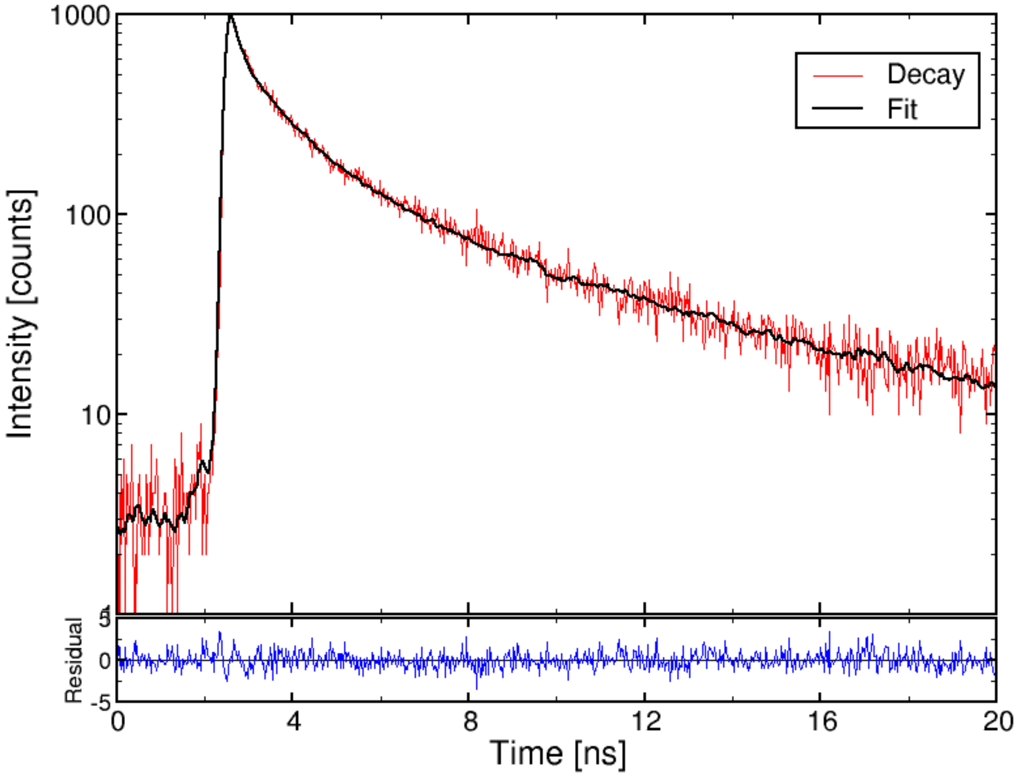

Figure S7 H: Raw decay data and 3 decay component fit for $[C_4C_1im][BF_4]$. Bottom graph shows residual values at each point.

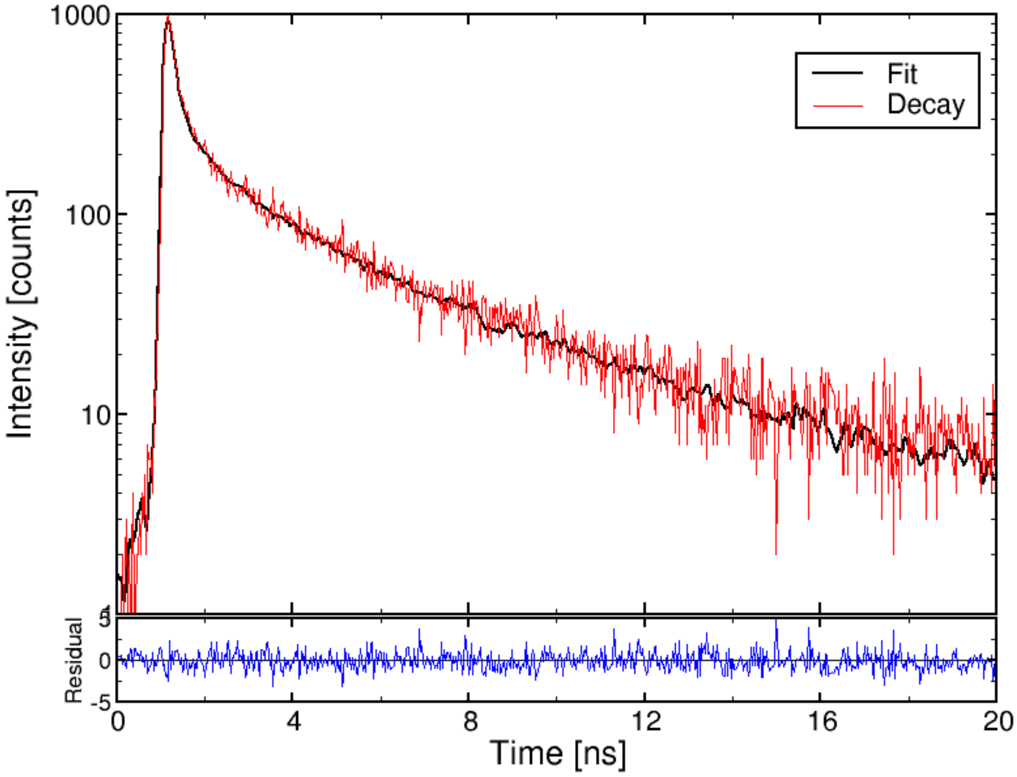

Figure S7 I: Raw decay data and 3 decay component fit for [C_4C_1im][OTf]. Bottom graph shows residual values at each point.

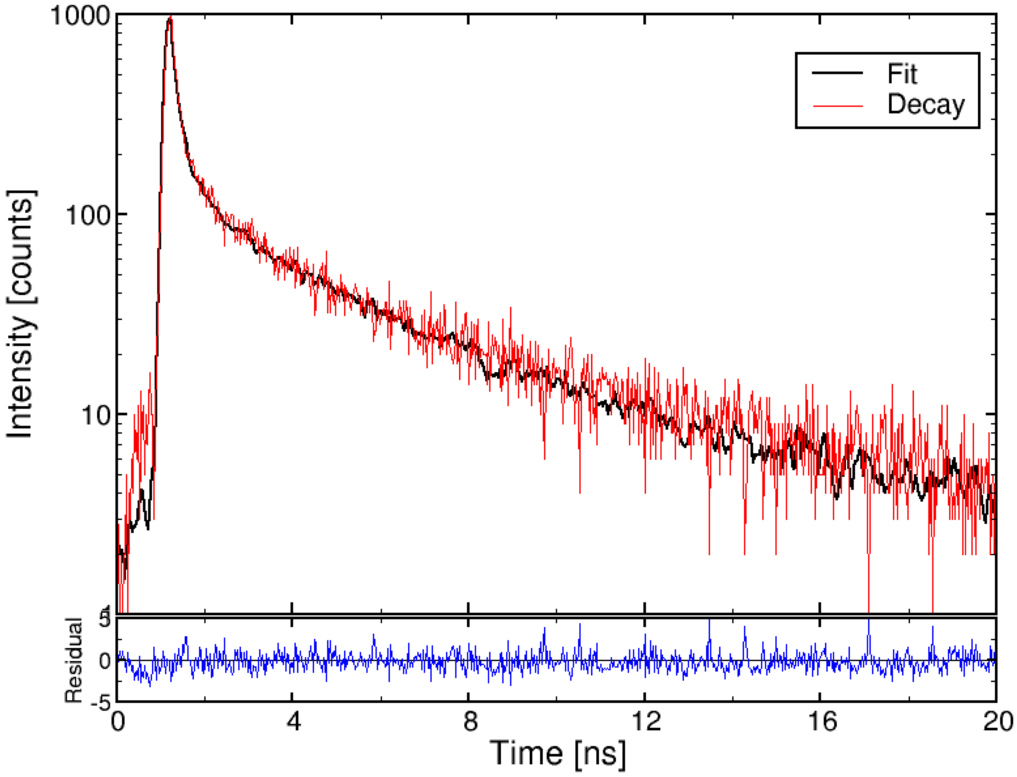

Figure S7 J: Raw decay data and 3 decay component fit for [C_4C_1im][PF_6]. Bottom graph shows residual values at each point.

S8: Decay Curves of Cy3 in Various Ionic Liquids

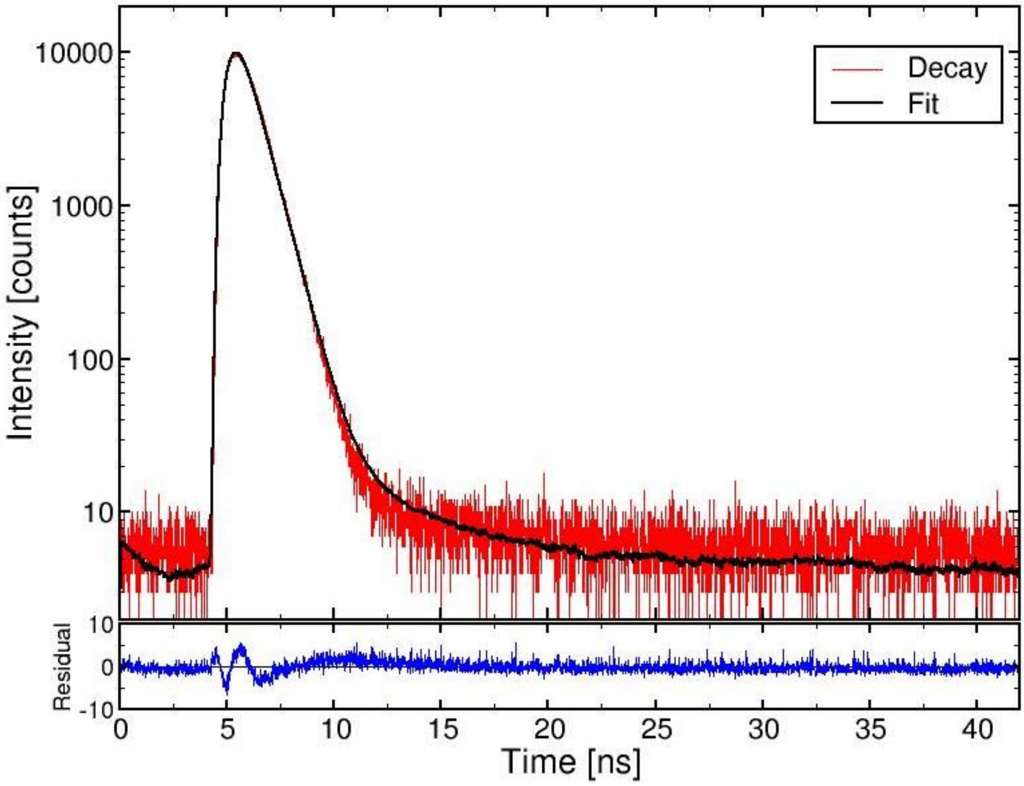

Figure S8 A: Raw decay data and 2 decay component fit for Cy3 in [C_2C_1im][NTf_2]. Bottom graph shows residual values at each point.

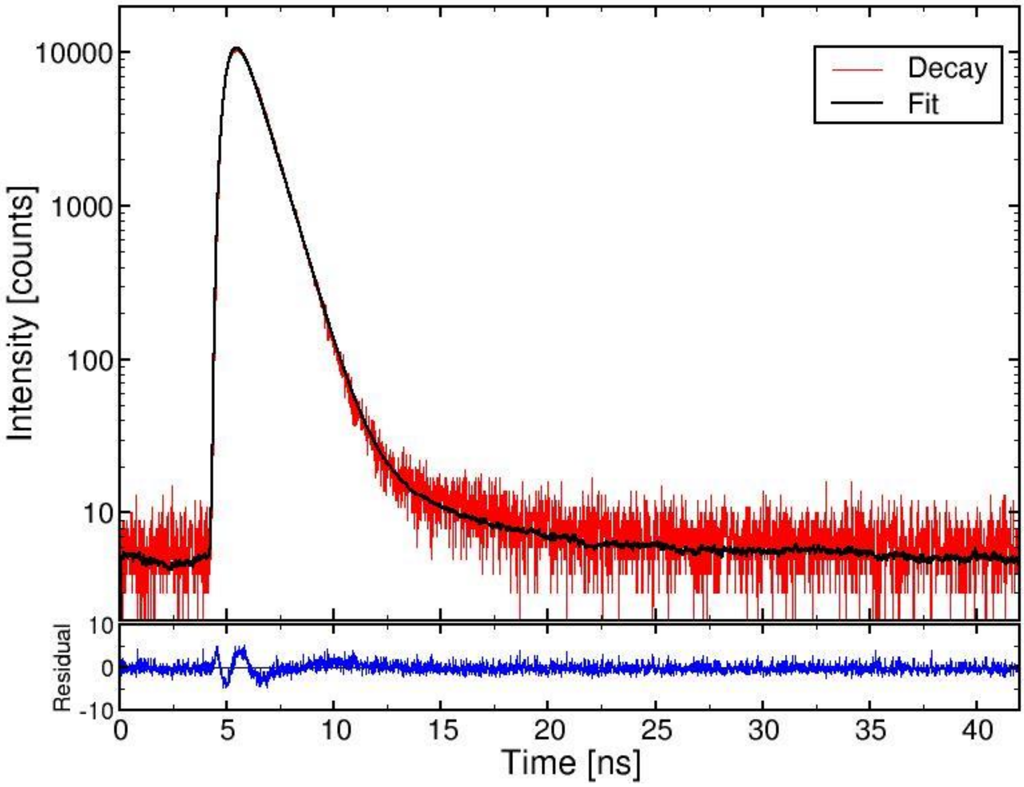

Figure S8 B: Raw decay data and 2 decay component fit for Cy3 in [C_3C_1im][NTf_2]. Bottom graph shows residual values at each point.

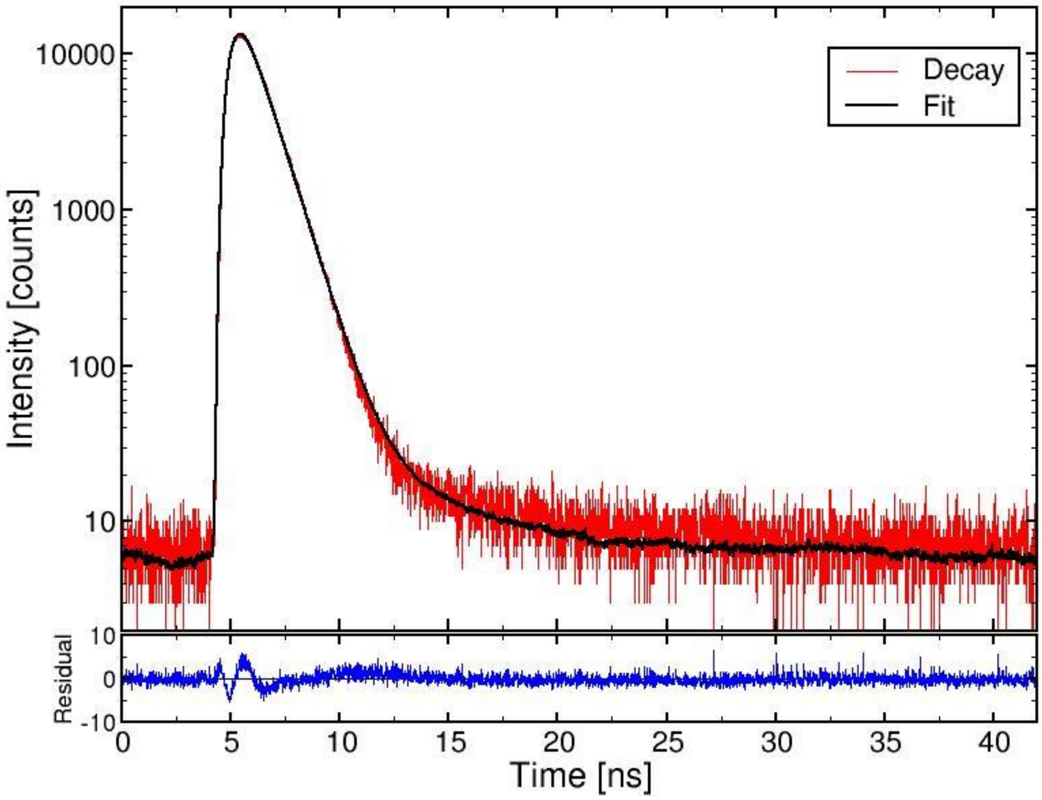

Figure S8 C: Raw decay data and 2 decay component fit for Cy3 in [C_4C_1im][NTf_2]. Bottom graph shows residual values at each point.

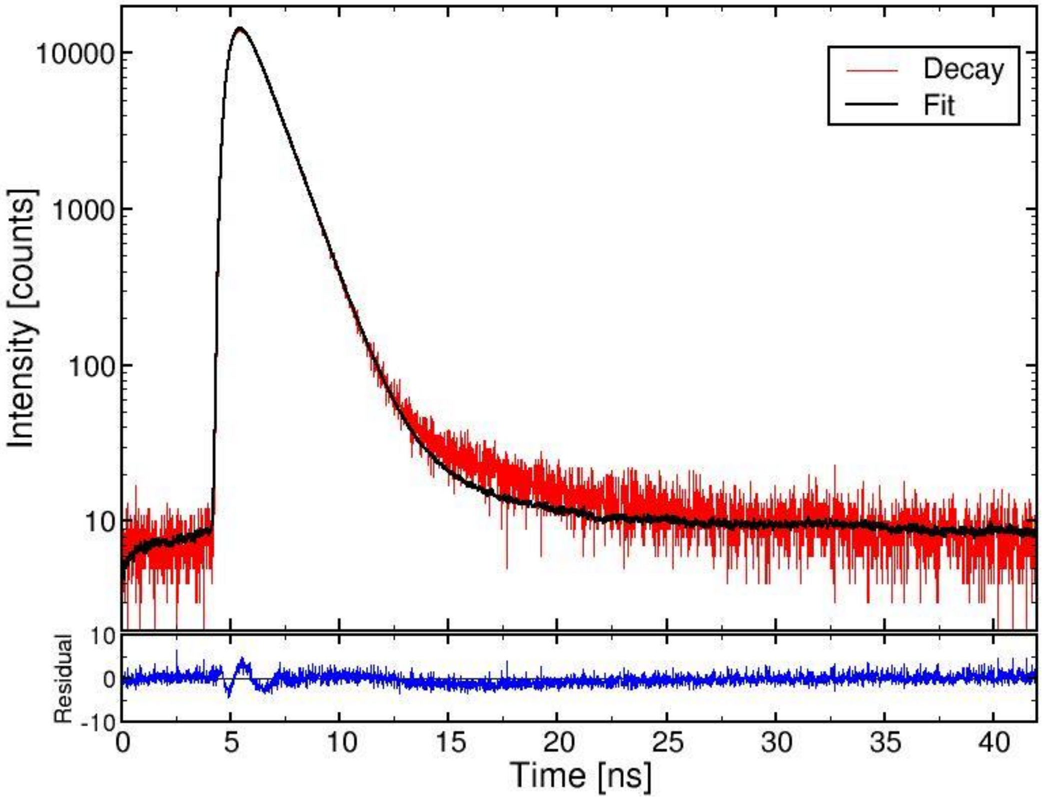

Figure S8 D: Raw decay data and 2 decay component fit for Cy3 in [C_6C_1im][NTf_2]. Bottom graph shows residual values at each point.

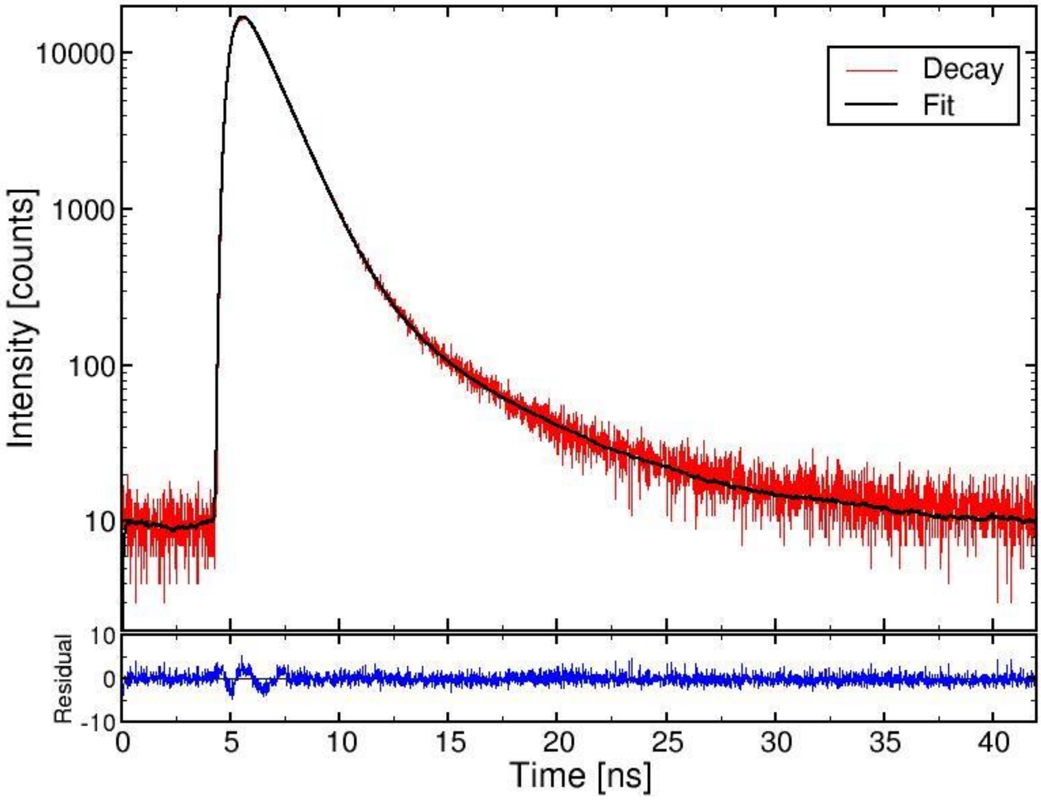

Figure S8 E: Raw decay data and 3 decay component fit for Cy3 in [C_8C_1im][NTf_2]. Bottom graph shows residual values at each point.

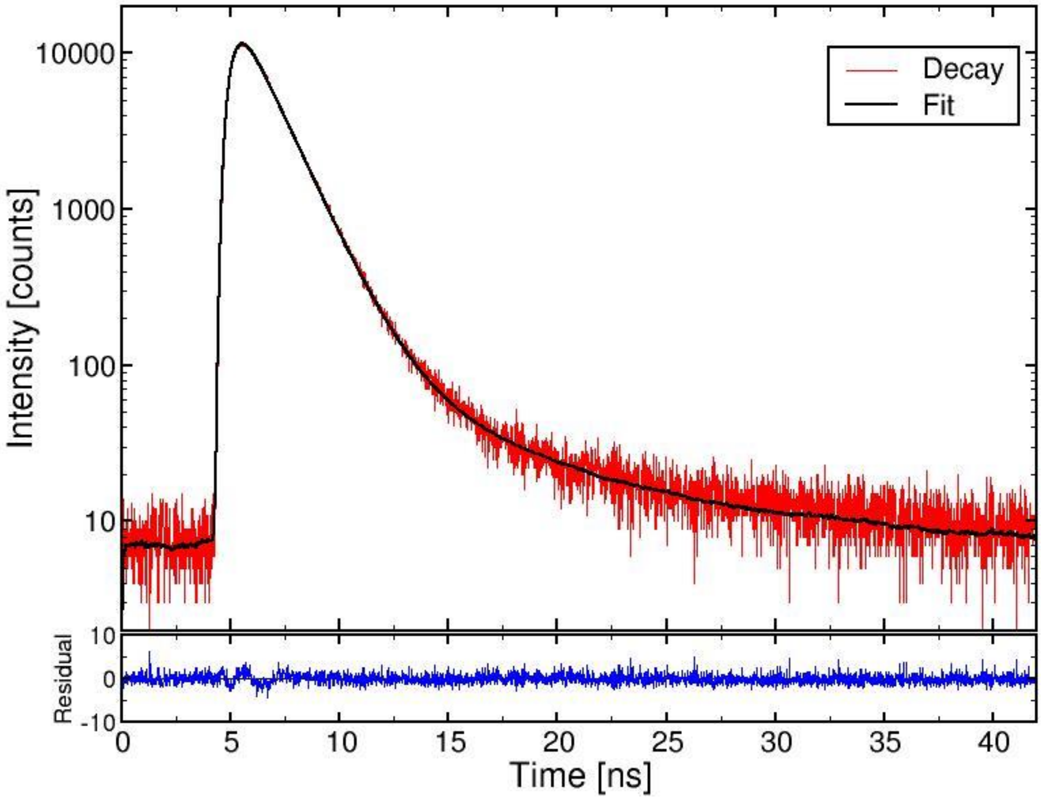

Figure S8 F: Raw decay data and 3 decay component fit for Cy3 in [$C_{12}C_1$im][NTf_2]. Bottom graph shows residual values at each point.

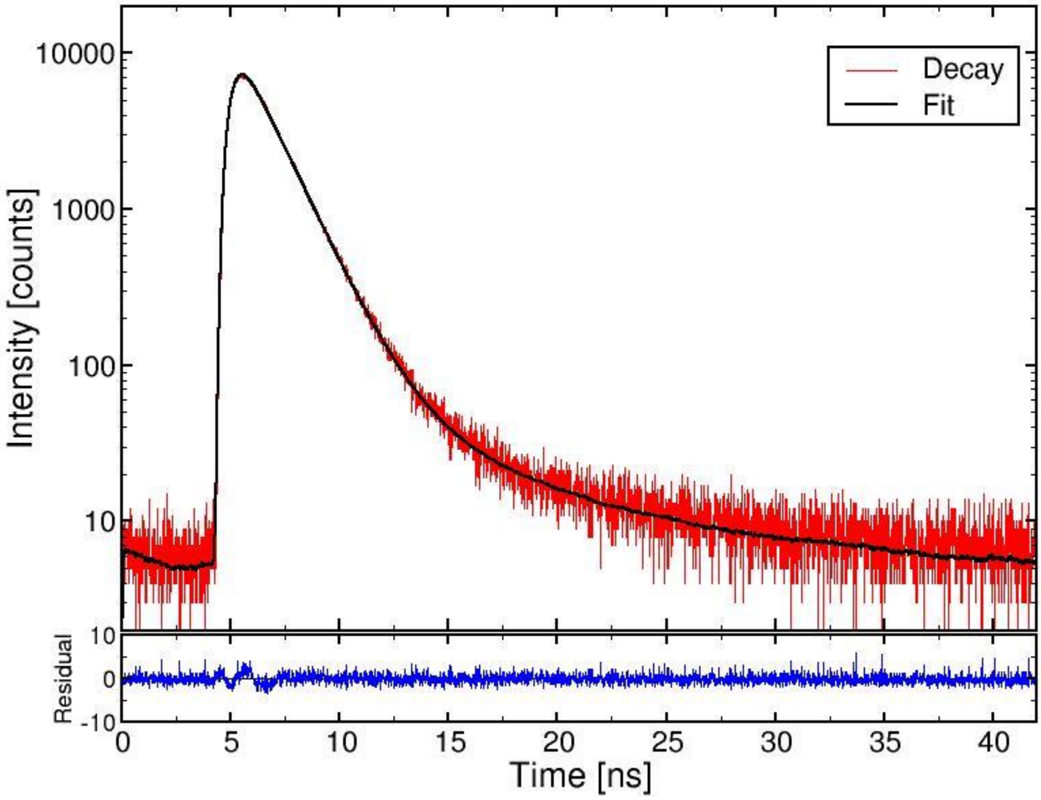

Figure S8 G: Raw decay data and 3 decay component fit for Cy3 in $[P_{4446}][NTf_2]$. Bottom graph shows residual values at each point.

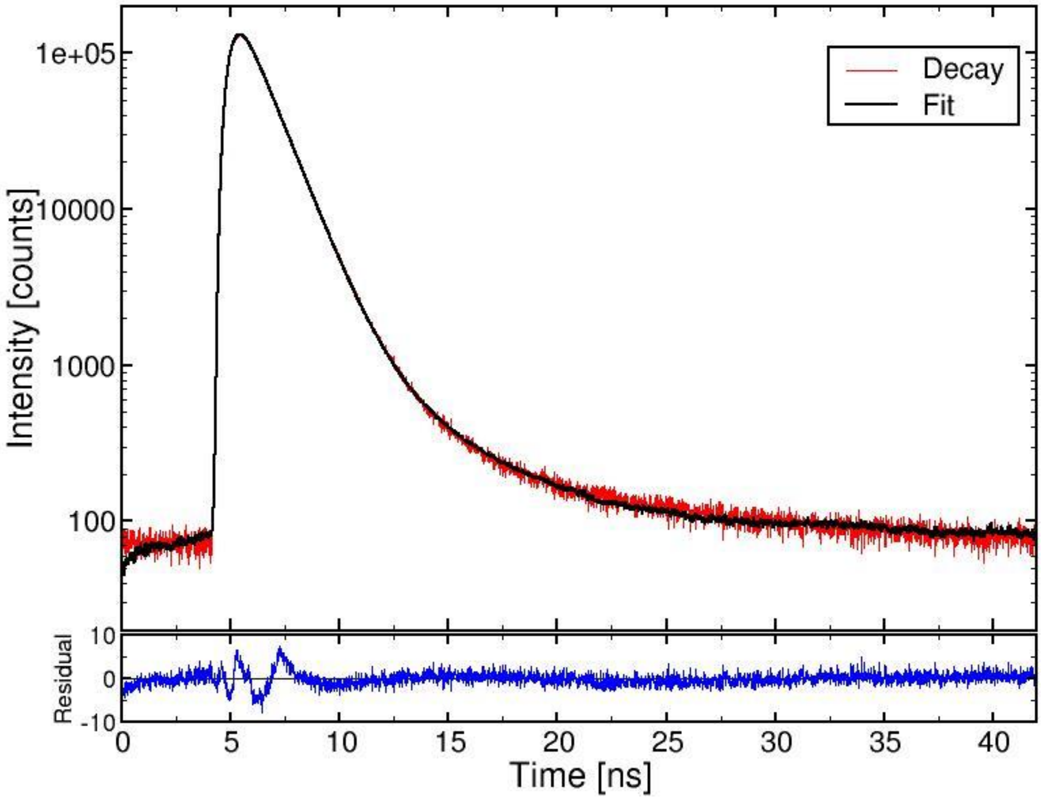

Figure S8 H: Raw decay data and 3 decay component fit for Cy3 in $[C_4C_1im][BF_4]$. Bottom graph shows residual values at each point.

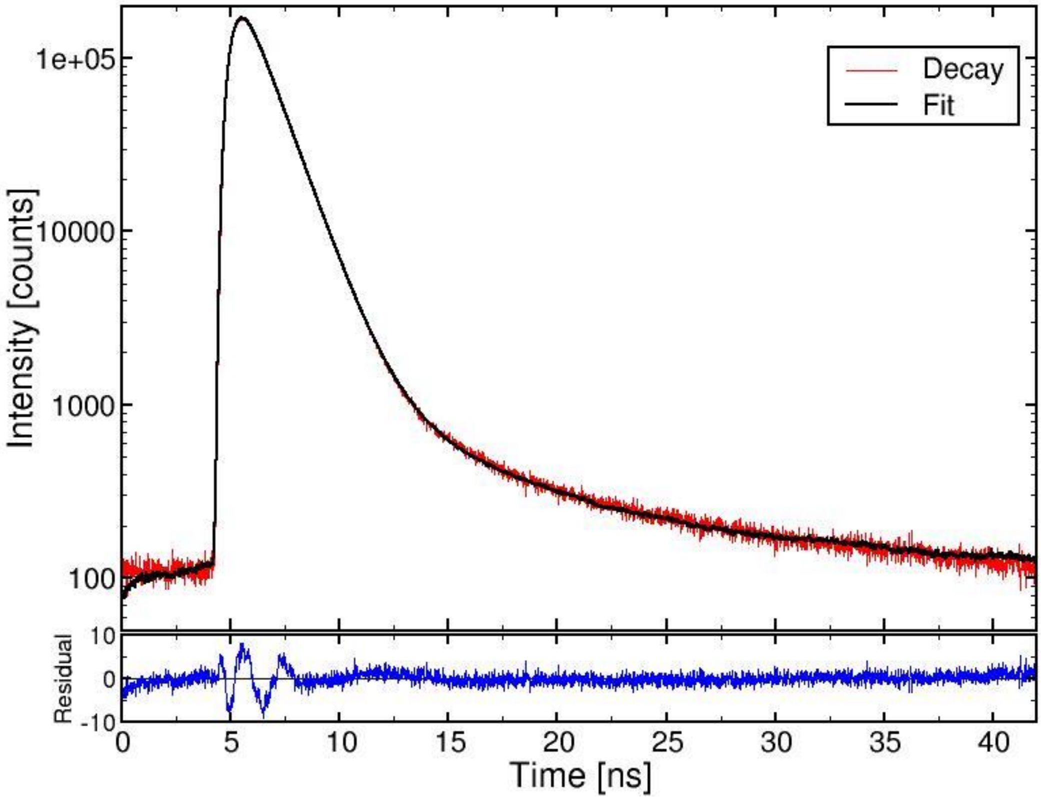

Figure S8 I: Raw decay data and 3 decay component fit for Cy3 in $[C_4C_1im][OTf]$. Bottom graph shows residual values at each point.

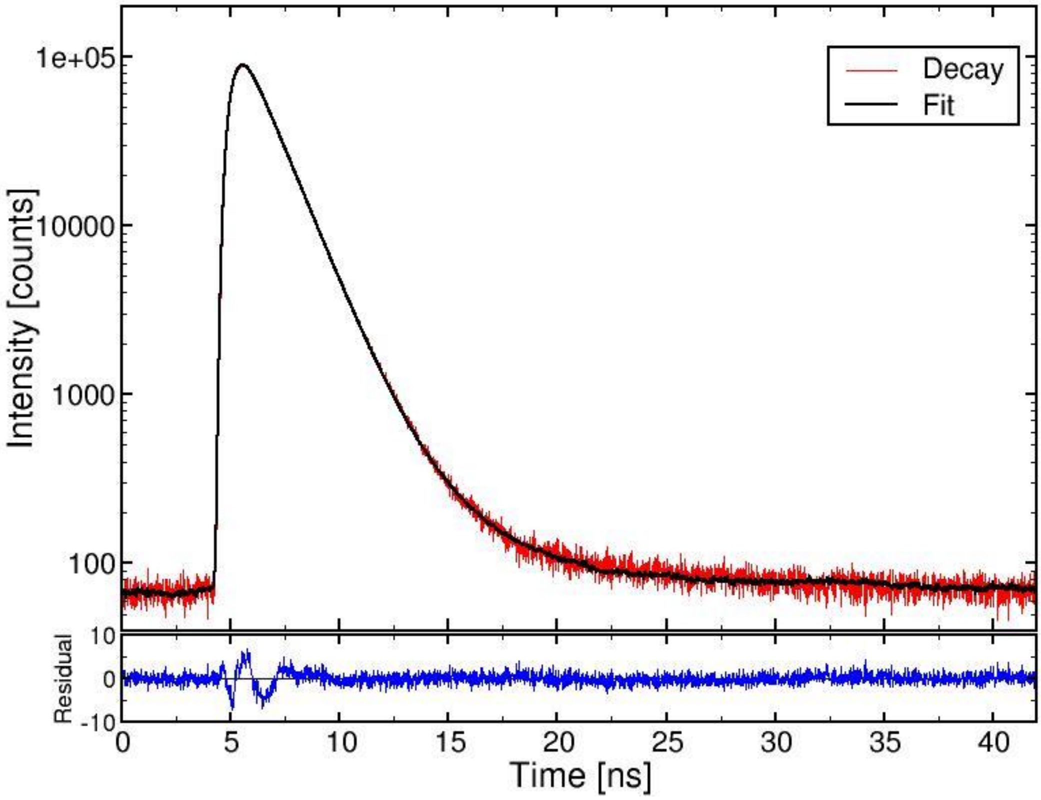

Figure S8 J: Raw decay data and 2 decay component fit for Cy3 in $[C_4C_1im][PF_6]$. Bottom graph shows residual values at each point.

S9: Decay Curves of Cy3 in $[C_4C_1im][NTf_2]$ at Various Temperatures

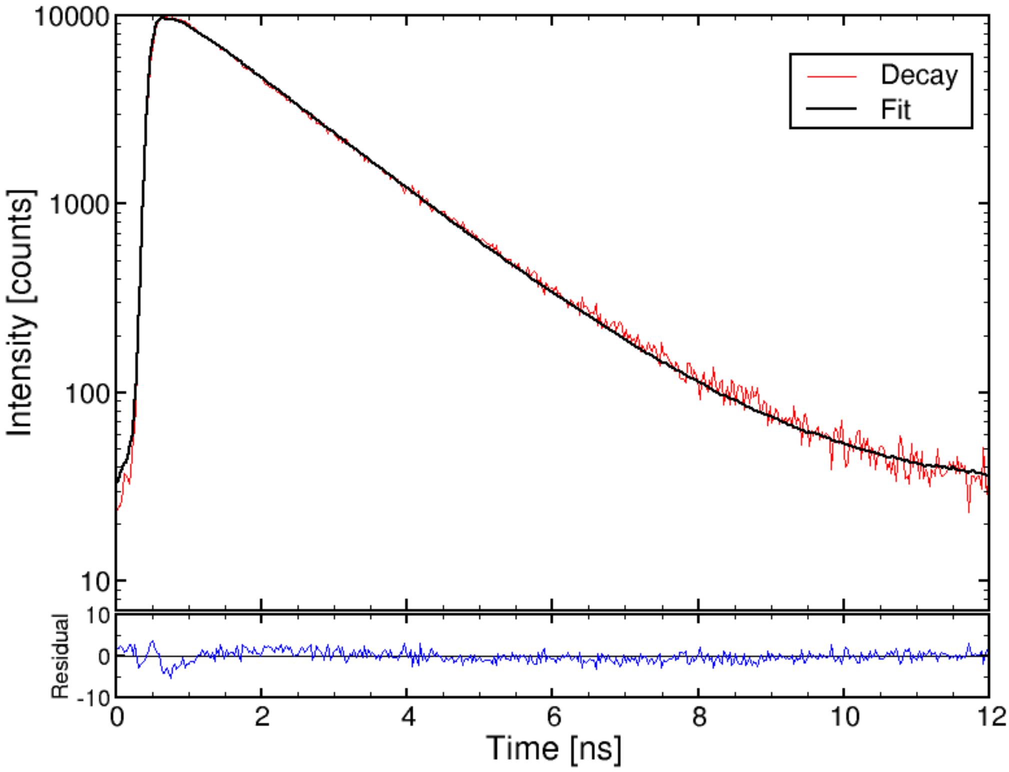

Figure S9 A: Raw decay data and 2 decay component fit for Cy3 in $[C_4C_1im][NTf_2]$ at 272 K. Bottom graph shows residual values at each point.

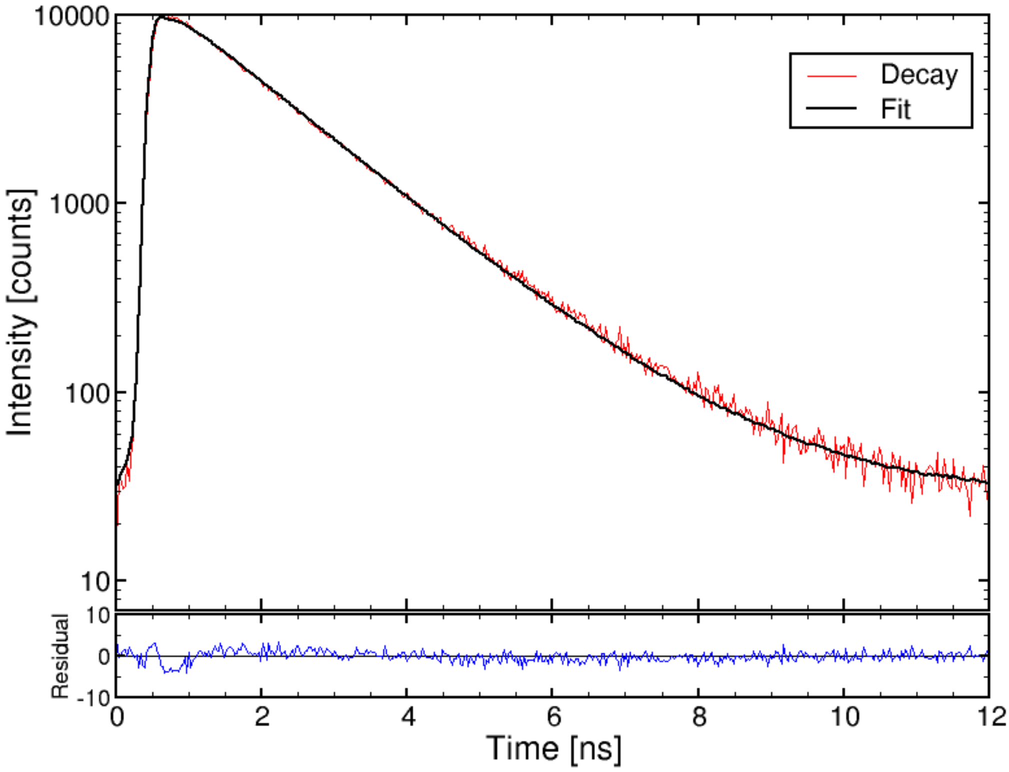

Figure S9 B: Raw decay data and 2 decay component fit for Cy3 in $[C_4C_1im][NTf_2]$ at 276 K. Bottom graph shows residual values at each point.

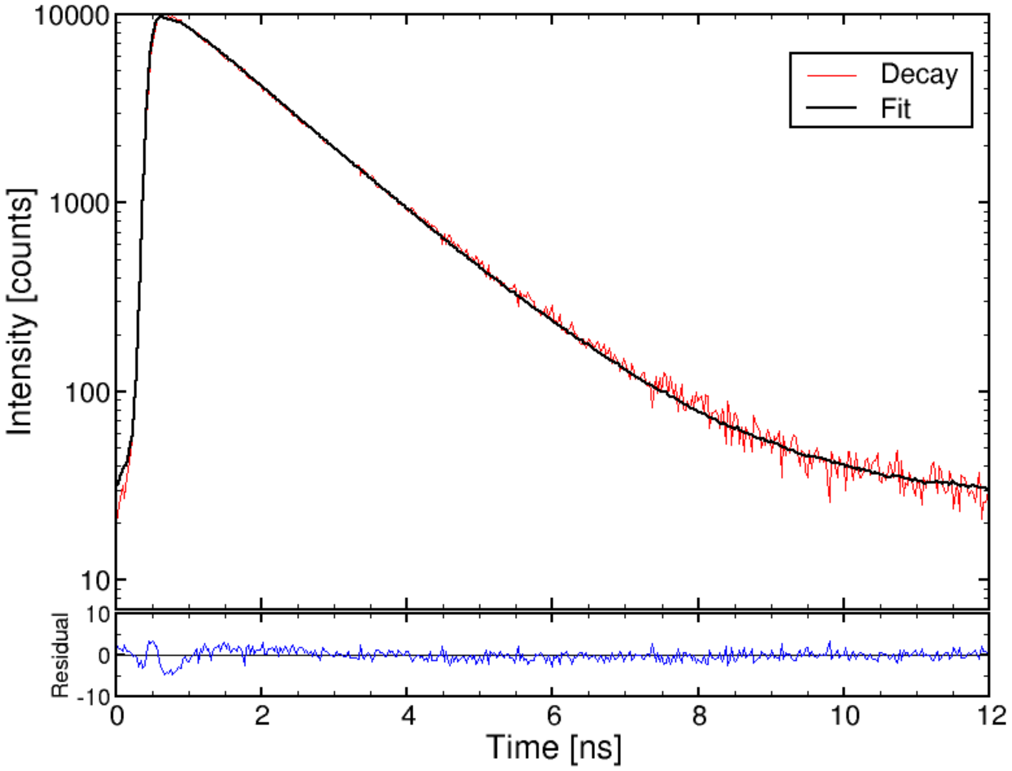

Figure S9 C: Raw decay data and 2 decay component fit for Cy3 in [C_4C_1im][NTf_2] at 279 K. Bottom graph shows residual values at each point.

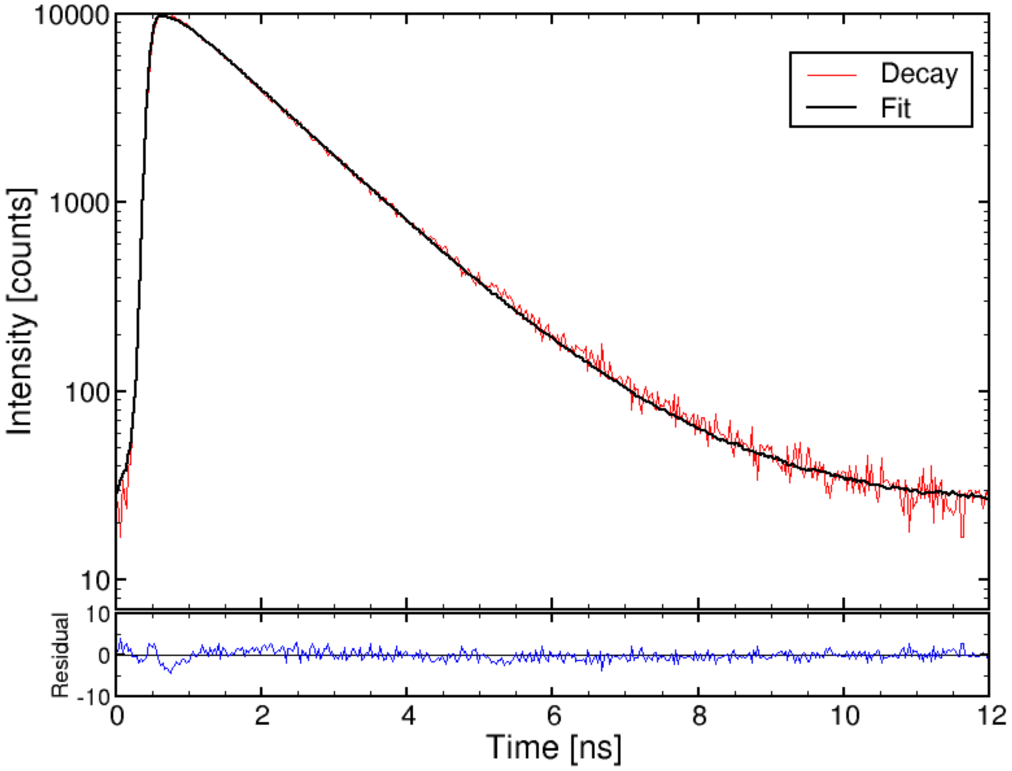

Figure S9 D: Raw decay data and 2 decay component fit for Cy3 in [C_4C_1im][NTf_2] at 282 K. Bottom graph shows residual values at each point.

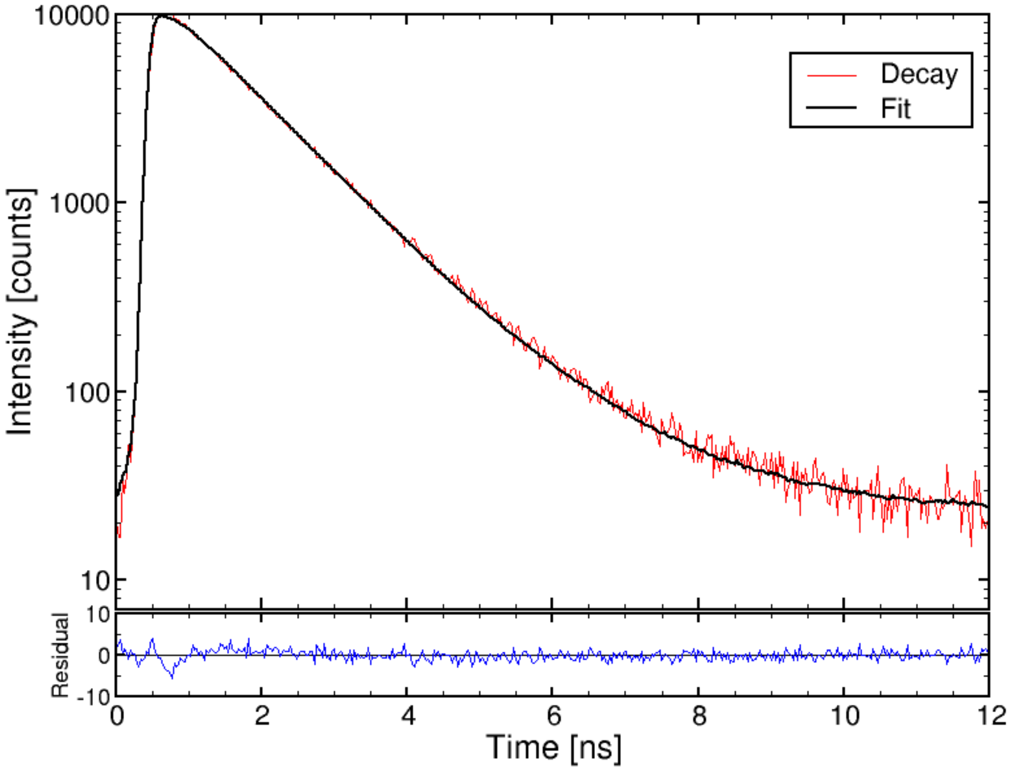

Figure S9 E: Raw decay data and 2 decay component fit for Cy3 in [C_4C_1im][NTf_2] at 286 K. Bottom graph shows residual values at each point.

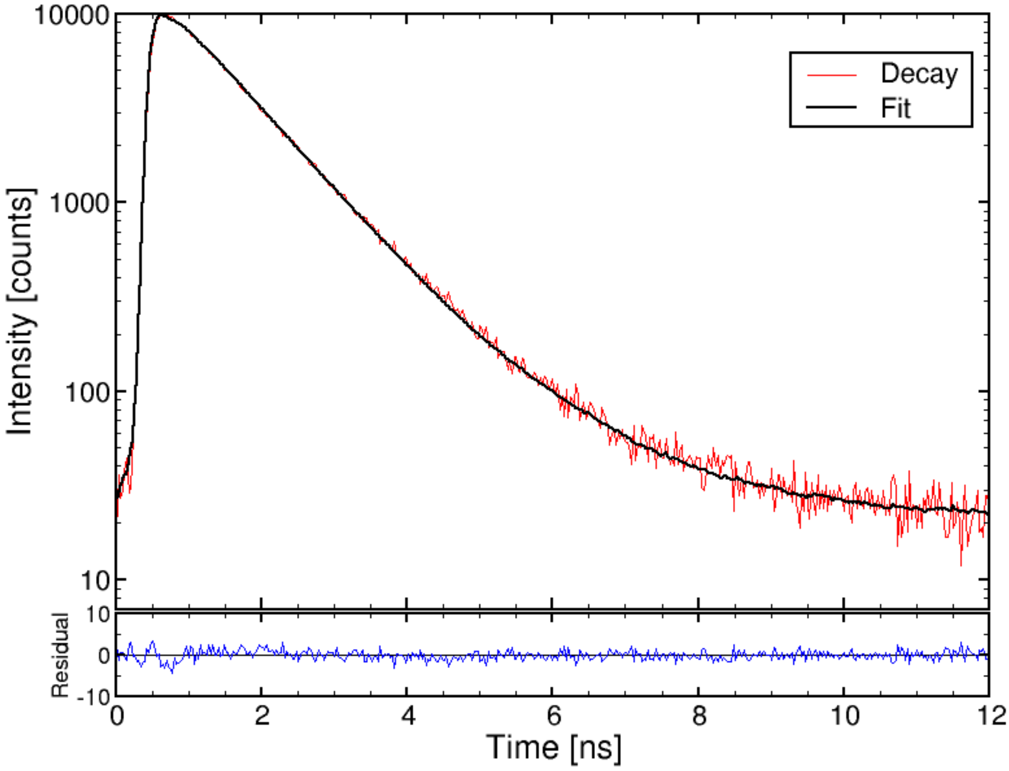

Figure S9 F: Raw decay data and 2 decay component fit for Cy3 in [C_4C_1im][NTf_2] at 290 K. Bottom graph shows residual values at each point.

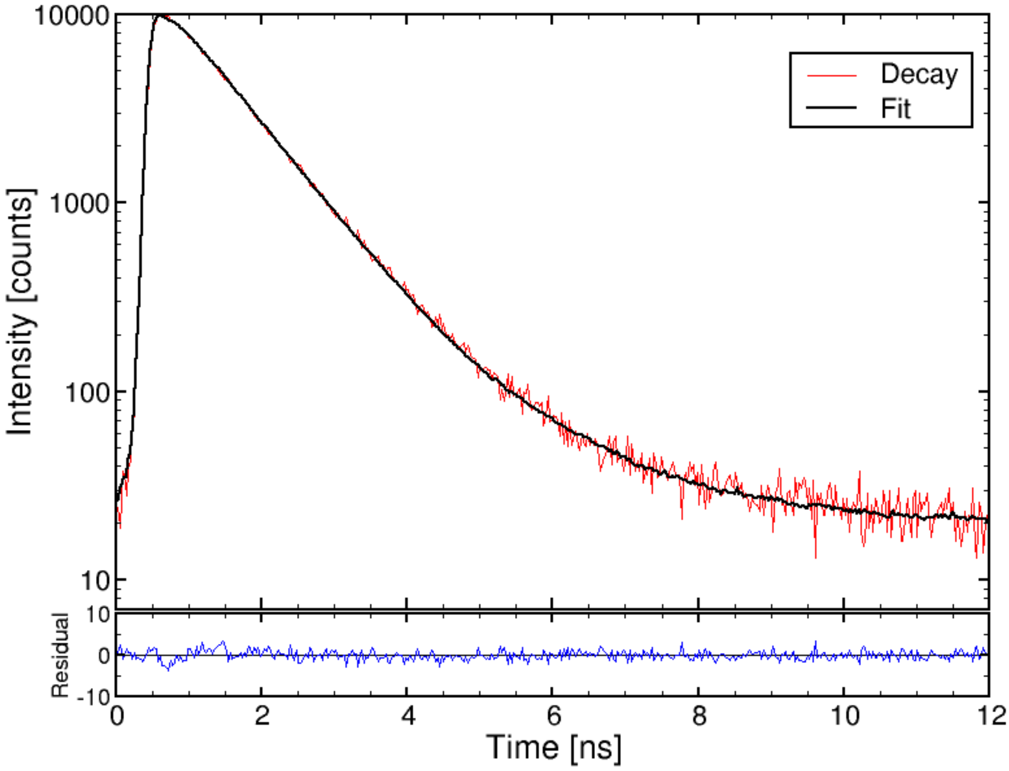

Figure S9 G: Raw decay data and 2 decay component fit for Cy3 in [C_4C_1im][NTf_2] at 294 K. Bottom graph shows residual values at each point.

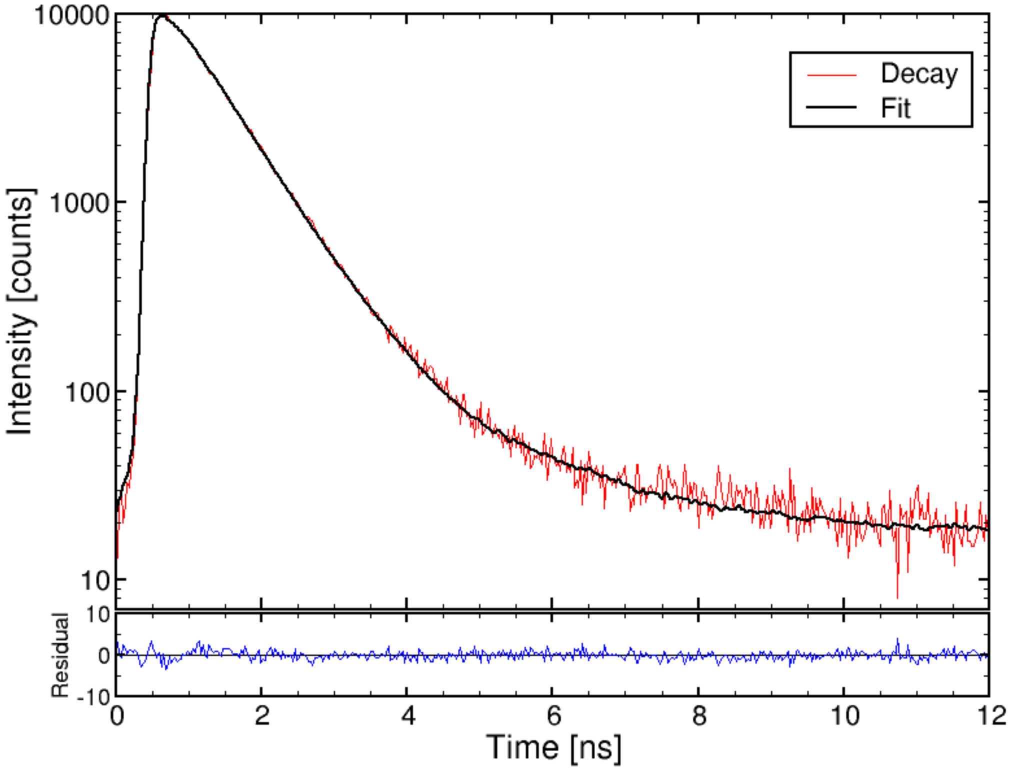

Figure S9 H: Raw decay data and 2 decay component fit for Cy3 in [C_4C_1im][NTf_2] at 302 K. Bottom graph shows residual values at each point.

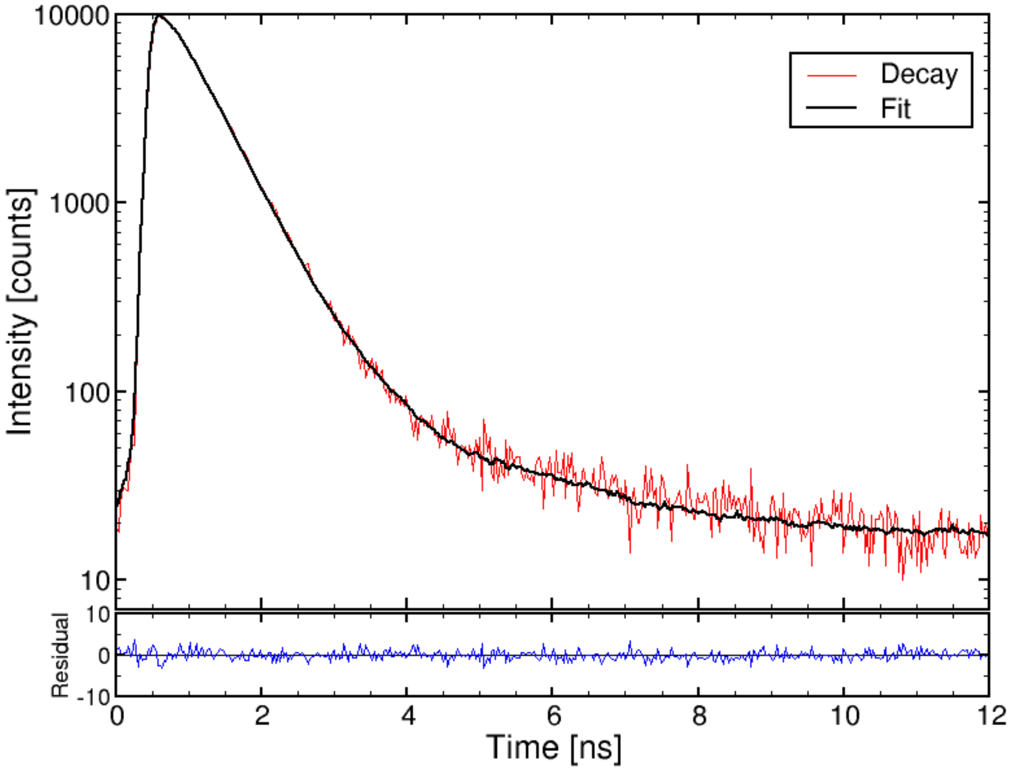

Figure S9 I: Raw decay data and 2 decay component fit for Cy3 in [C_4C_1im][NTf_2] at 311 K. Bottom graph shows residual values at each point.

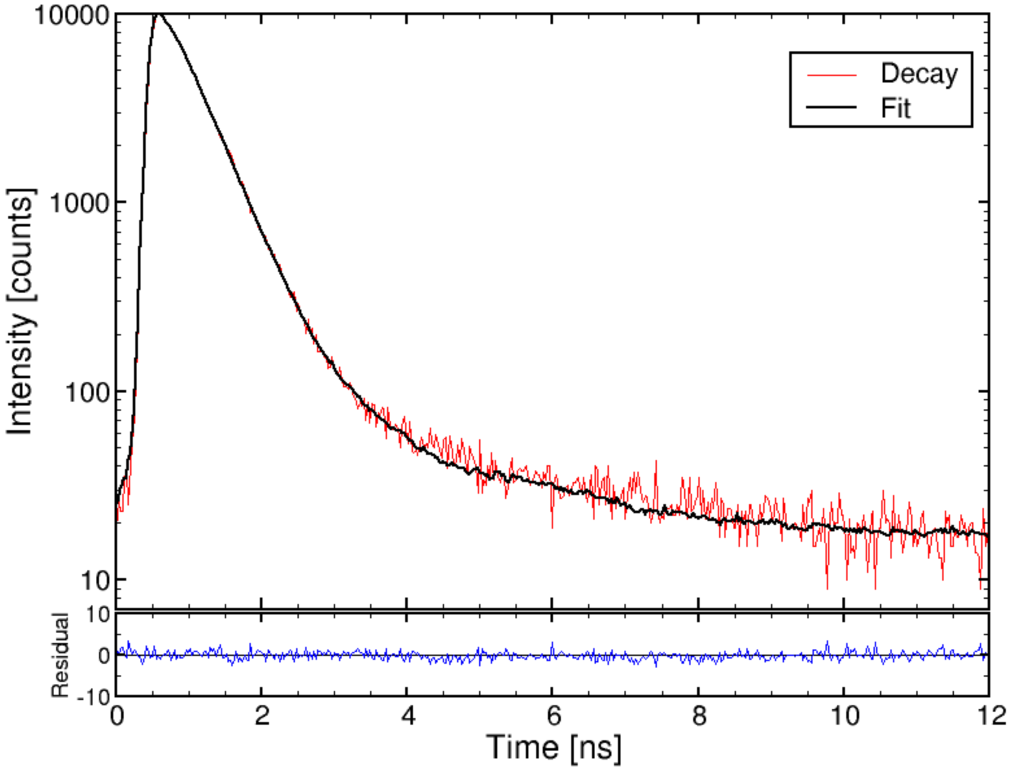

Figure S9 J: Raw decay data and 2 decay component fit for Cy3 in [C_4C_1im][NTf_2] at 320 K. Bottom graph shows residual values at each point.

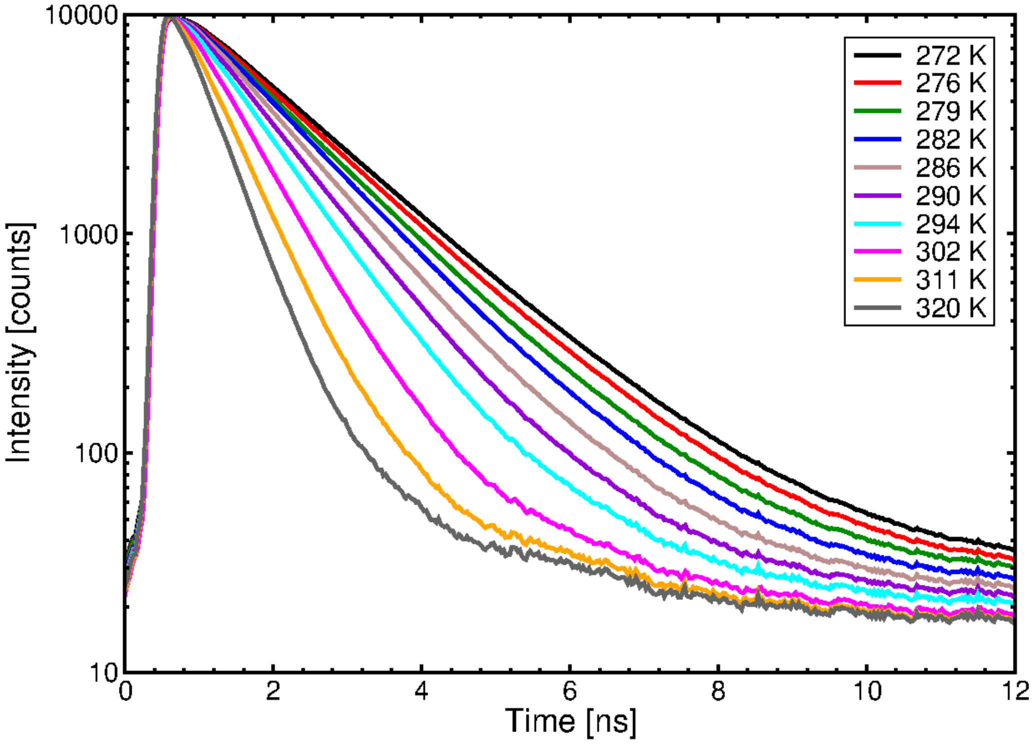

Figure S9 K: Decay data for Cy3 in [C_4C_1im][NTf_2] at various temperatures.

S10: Decay Curves of BODIPY-C10 Solutions of Ionic Liquids

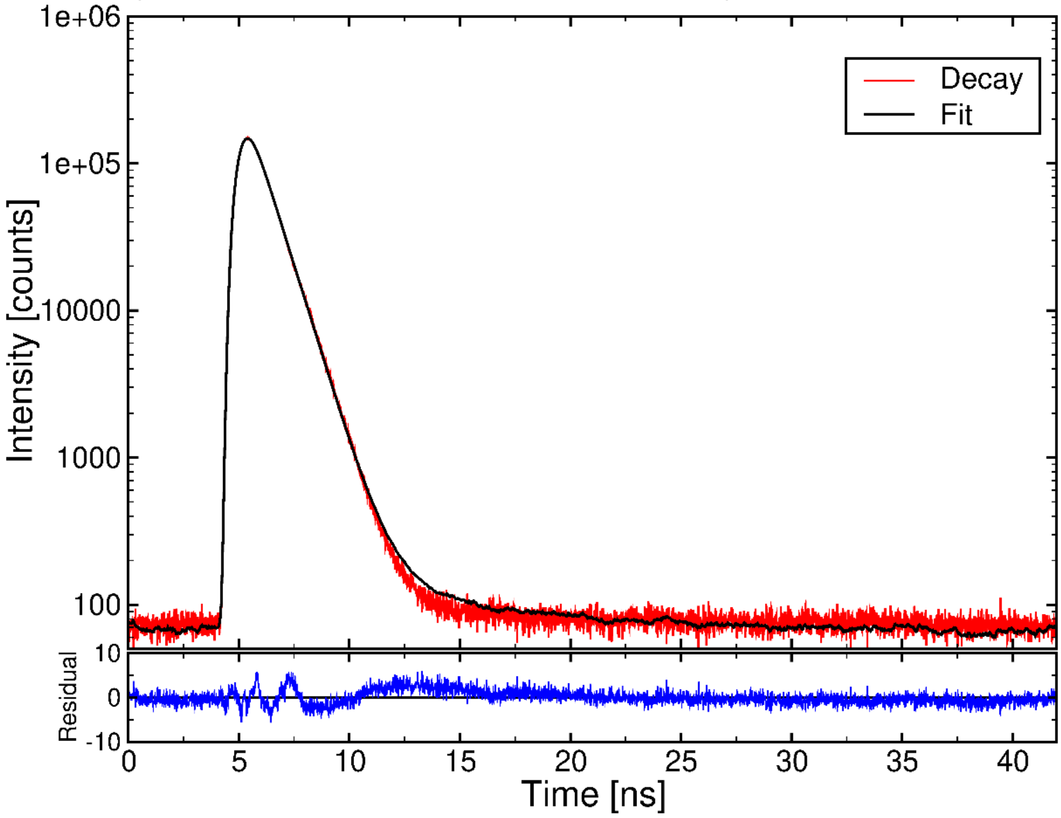

Figure S10 A: Raw decay data and 2 decay component fit for BODIPY-C10 in [C_2C_1im][NTf_2]. Bottom graph shows residual values at each point.

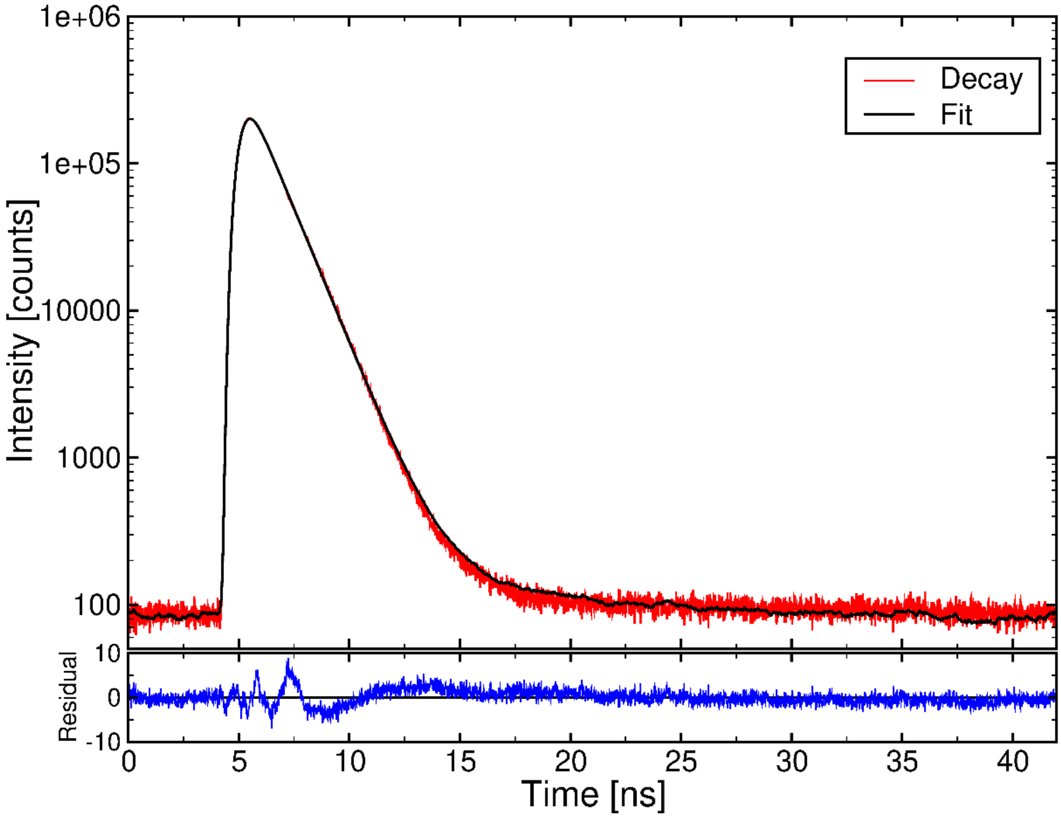

Figure S10 B: Raw decay data and 2 decay component fit for BODIPY-C10 in [C_3C_1im][NTf_2]. Bottom graph shows residual values at each point.

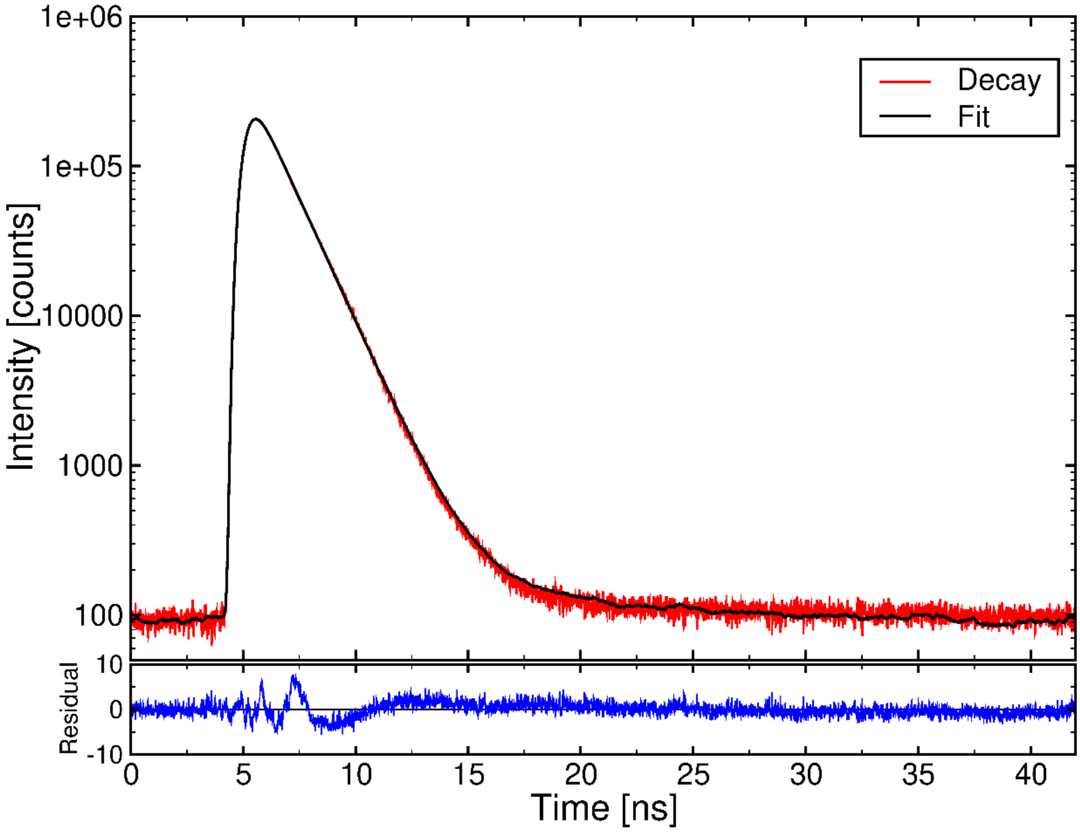

Figure S10 C: Raw decay data and 2 decay component fit for BODIPY-C10 in [C_4C_1im][NTf_2]. Bottom graph shows residual values at each point.

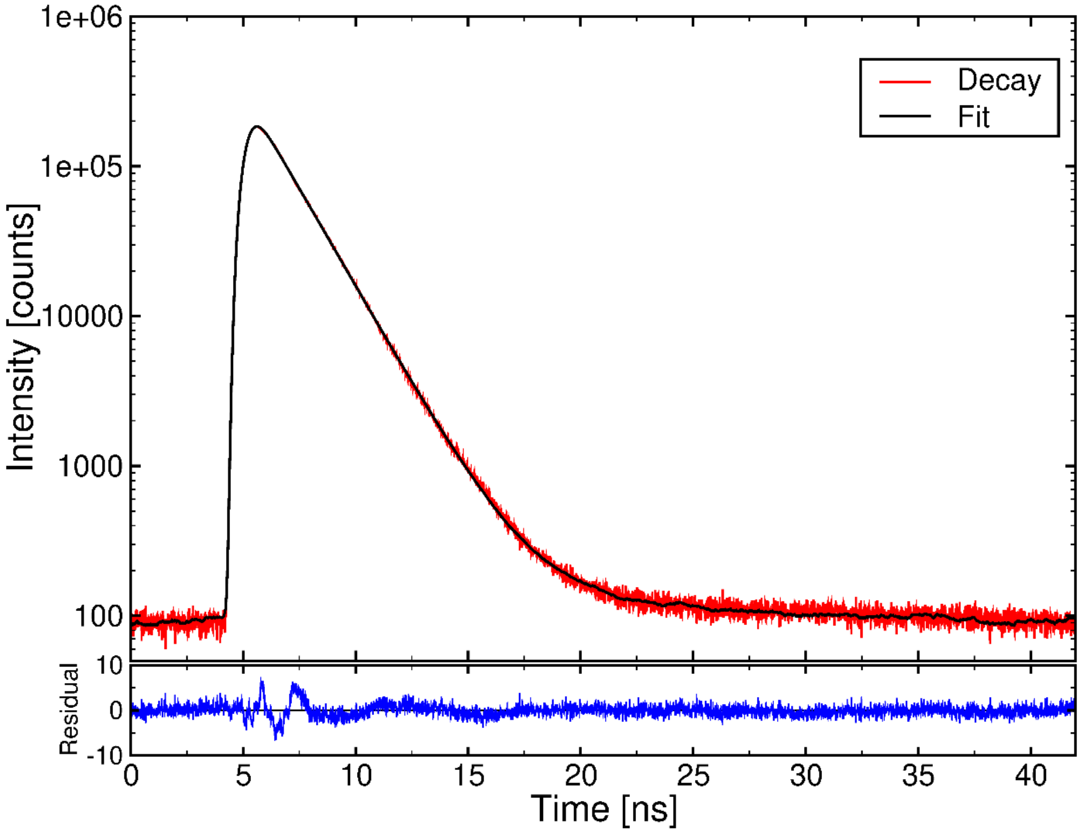

Figure S10 D: Raw decay data and 2 decay component fit for BODIPY-C10 in [C_6C_1im][NTf_2]. Bottom graph shows residual values at each point.

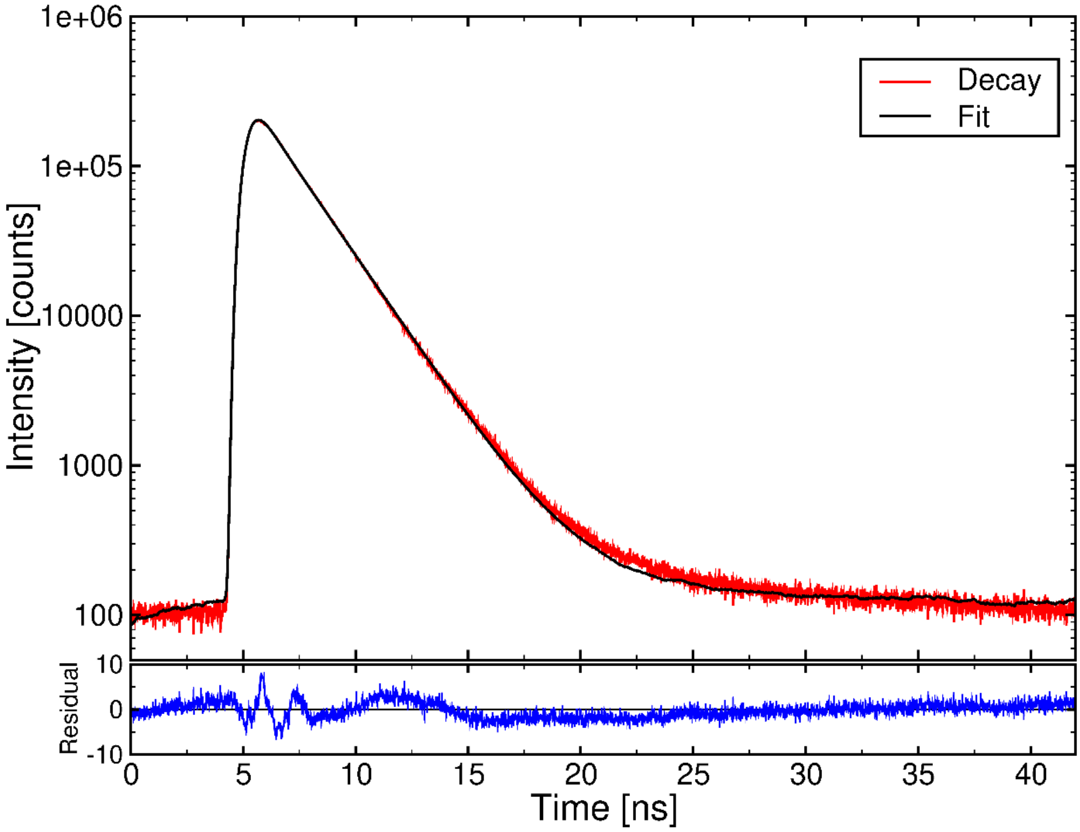

Figure S10 E: Raw decay data and 2 decay component fit for BODIPY-C10 in [C_8C_1im][NTf_2]. Bottom graph shows residual values at each point.

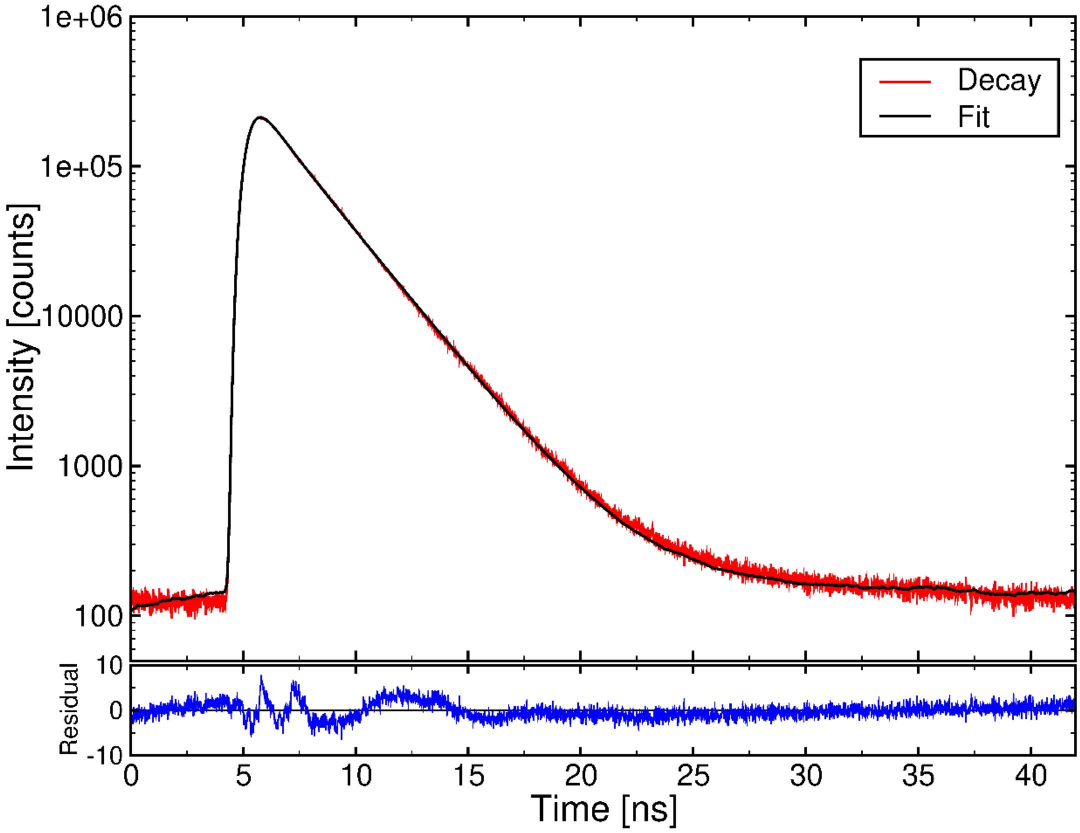

Figure S10 F: Raw decay data and 2 decay component fit for BODIPY-C10 in [$C_{12}C_1$im][NTf_2]. Bottom graph shows residual values at each point.

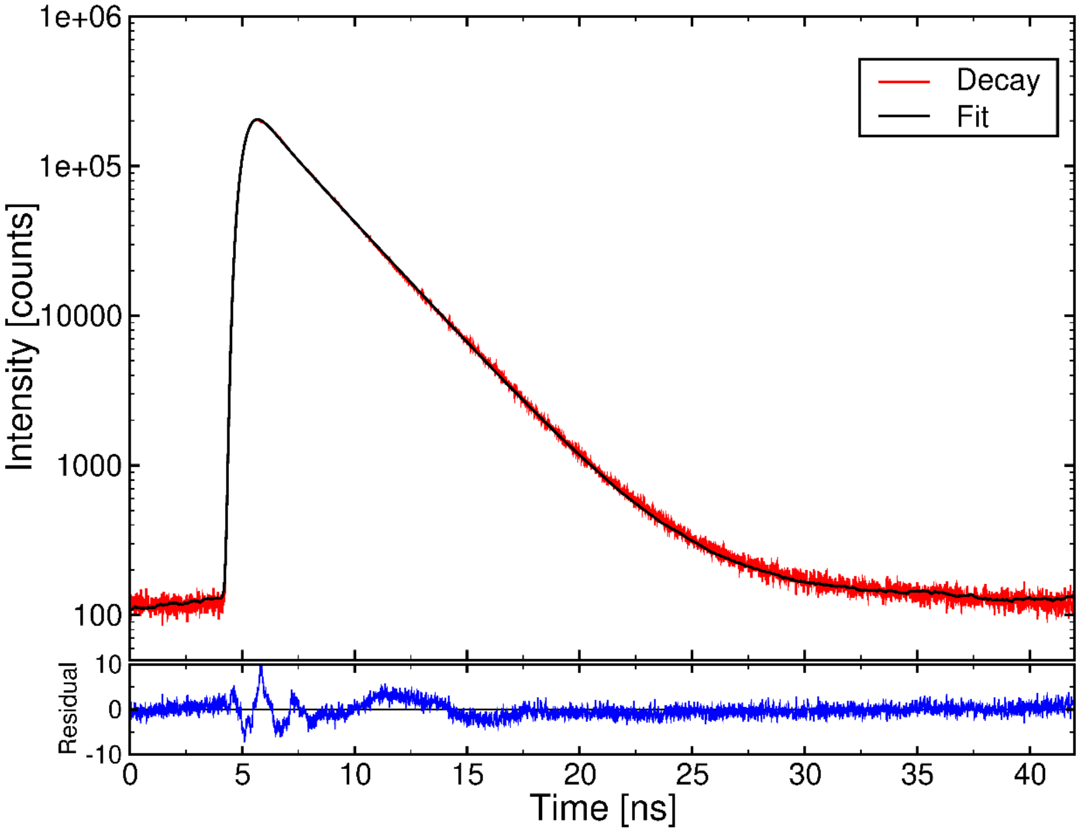

Figure S10 G: Raw decay data and 2 decay component fit for BODIPY-C10 in [P_{4446}][NTf_2]. Bottom graph shows residual values at each point.

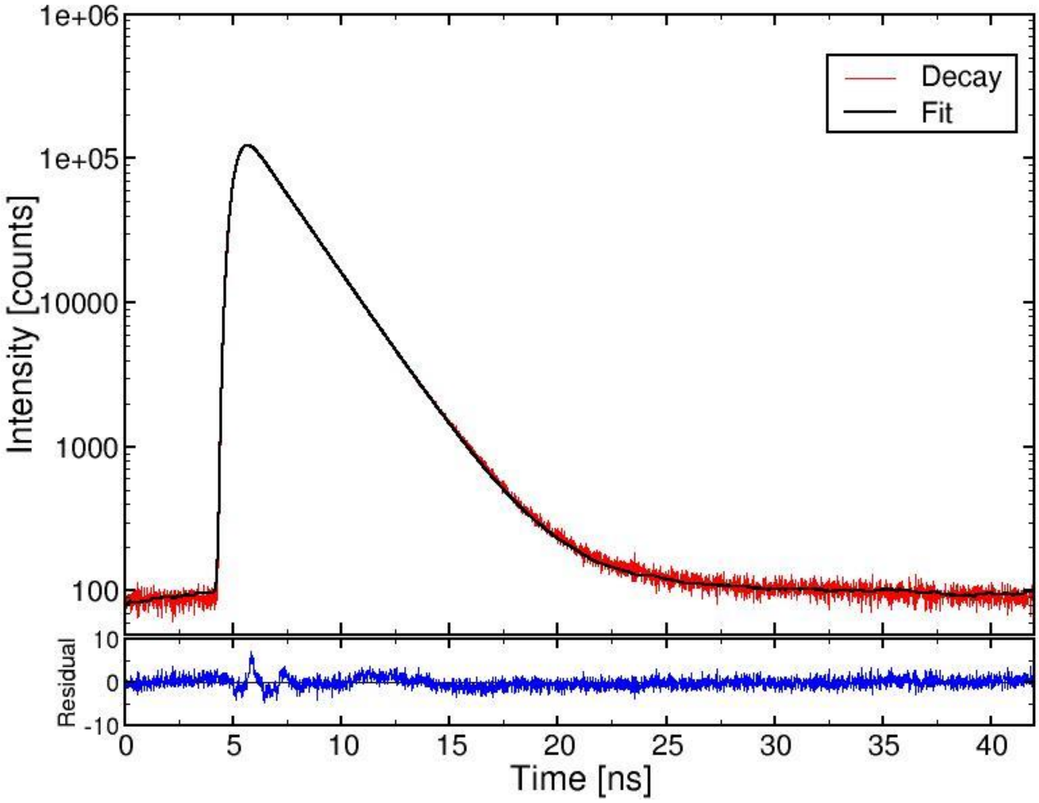

Figure S10 H: Raw decay data and 2 decay component fit for BODIPY-C10 in [C_4C_1im][BF_4]. Bottom graph shows residual values at each point.

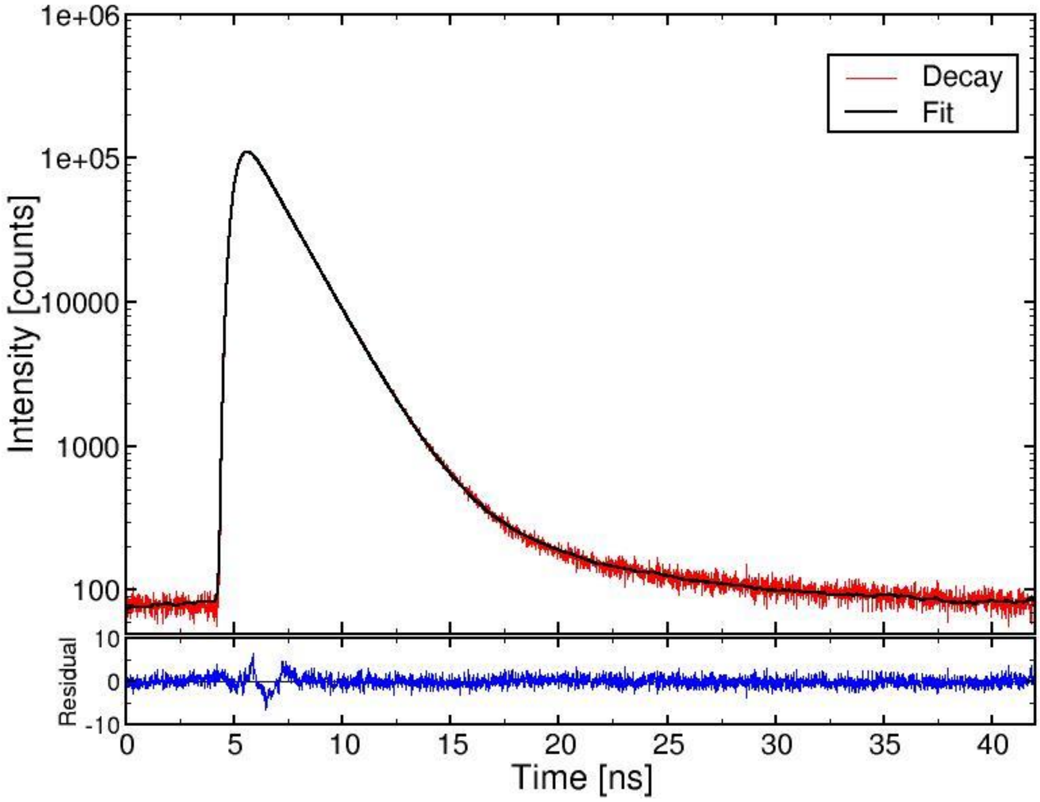

Figure S10 I: Raw decay data and 2 decay component fit for BODIPY-C10 in [C_4C_1im][OTf]. Bottom graph shows residual values at each point.

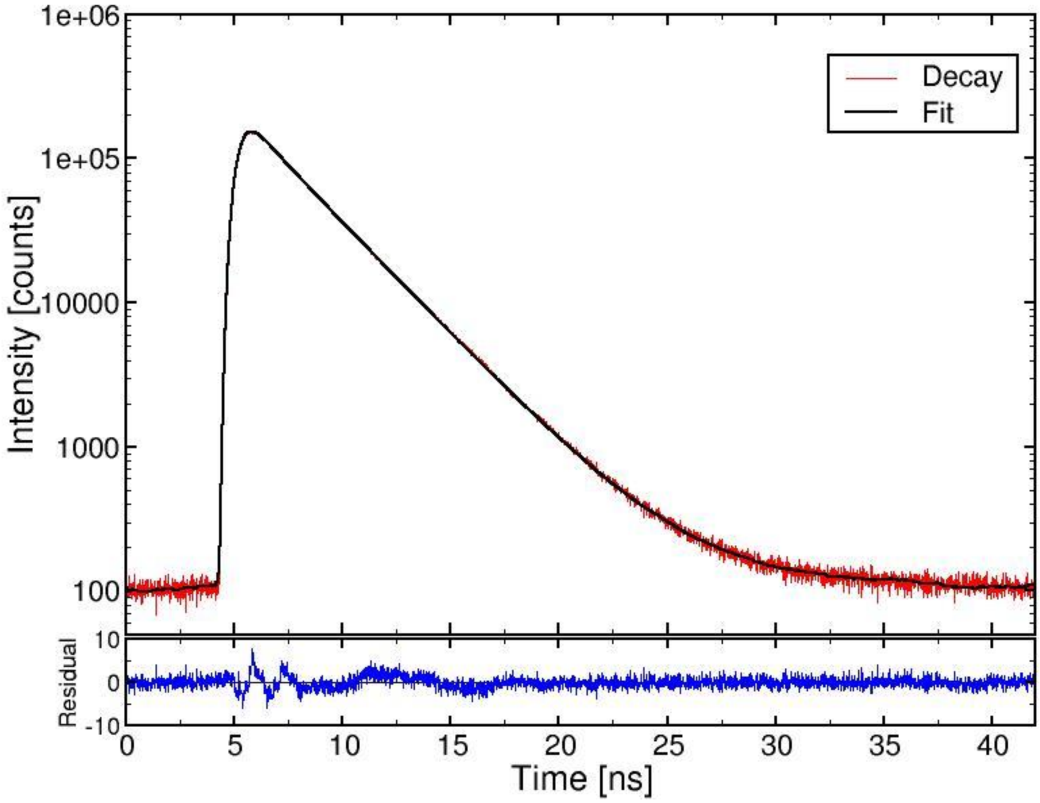

Figure S10 J: Raw decay data and 2 decay component fit for BODIPY-C10 in [C_4C_1im][PF_6]. Bottom graph shows residual values at each point.

S11: Decay Curves of BODIPY-C10 in $[C_4C_1im][NTf_2]$ at Various Temperatures

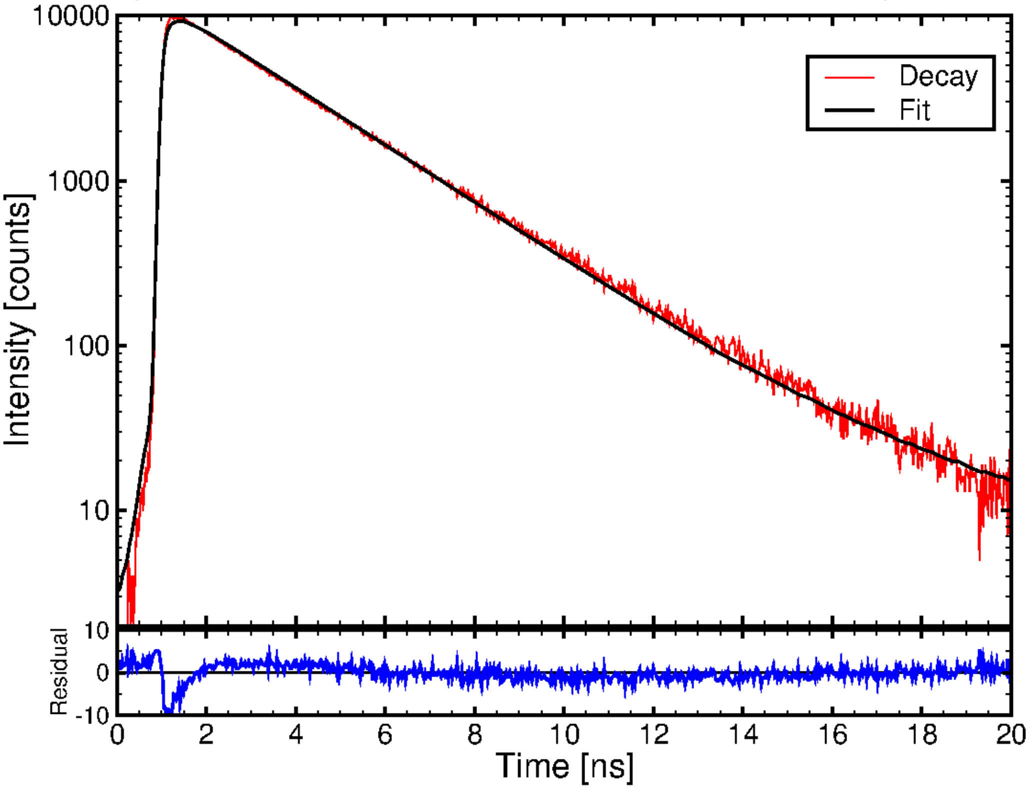

Figure S11 A: Raw decay data and 2 decay component fit for BODIPY-C10 in $[C_4C_1im][NTf_2]$ at 273 K. Bottom graph shows residual values at each point.

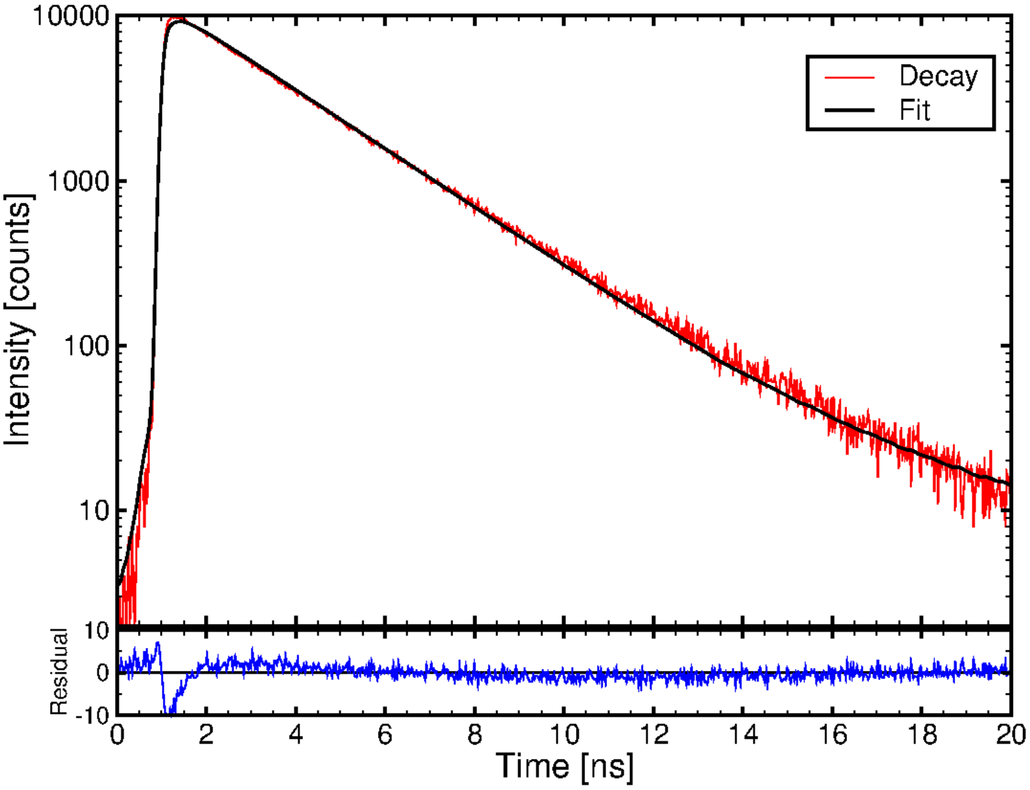

Figure S11 B: Raw decay data and 2 decay component fit for BODIPY-C10 in $[C_4C_1im][NTf_2]$ at 274 K. Bottom graph shows residual values at each point.

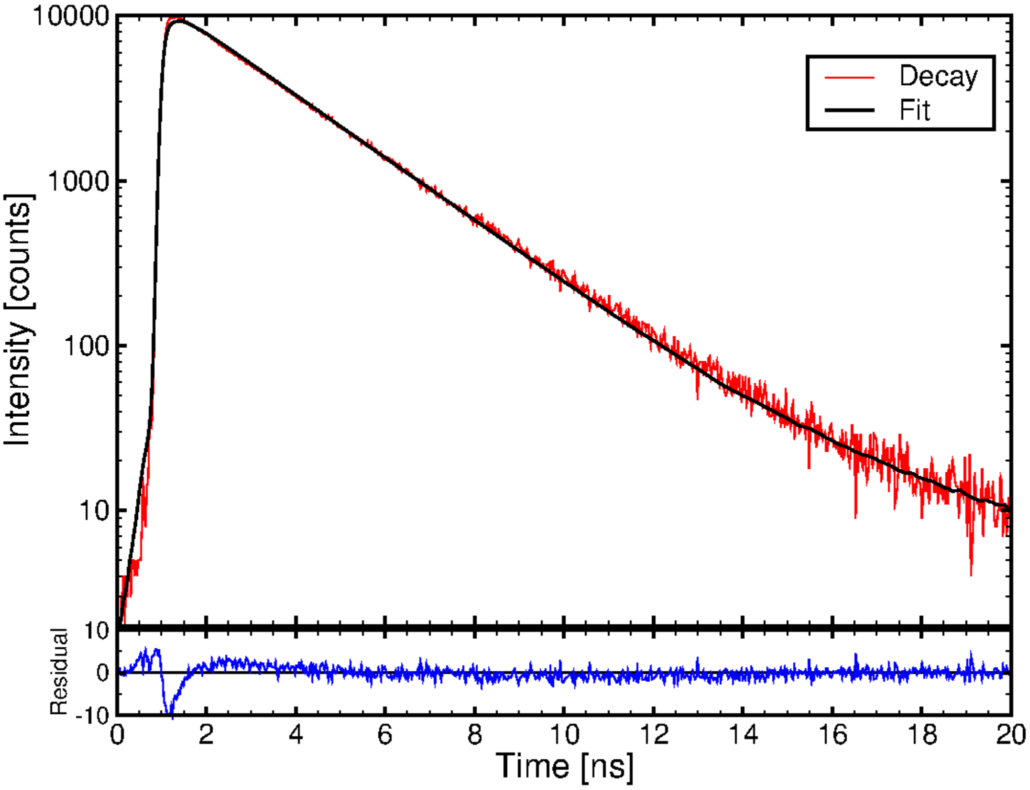

Figure S11 C: Raw decay data and 2 decay component fit for BODIPY-C10 in [C_4C_1im][NTf_2] at 277 K. Bottom graph shows residual values at each point.

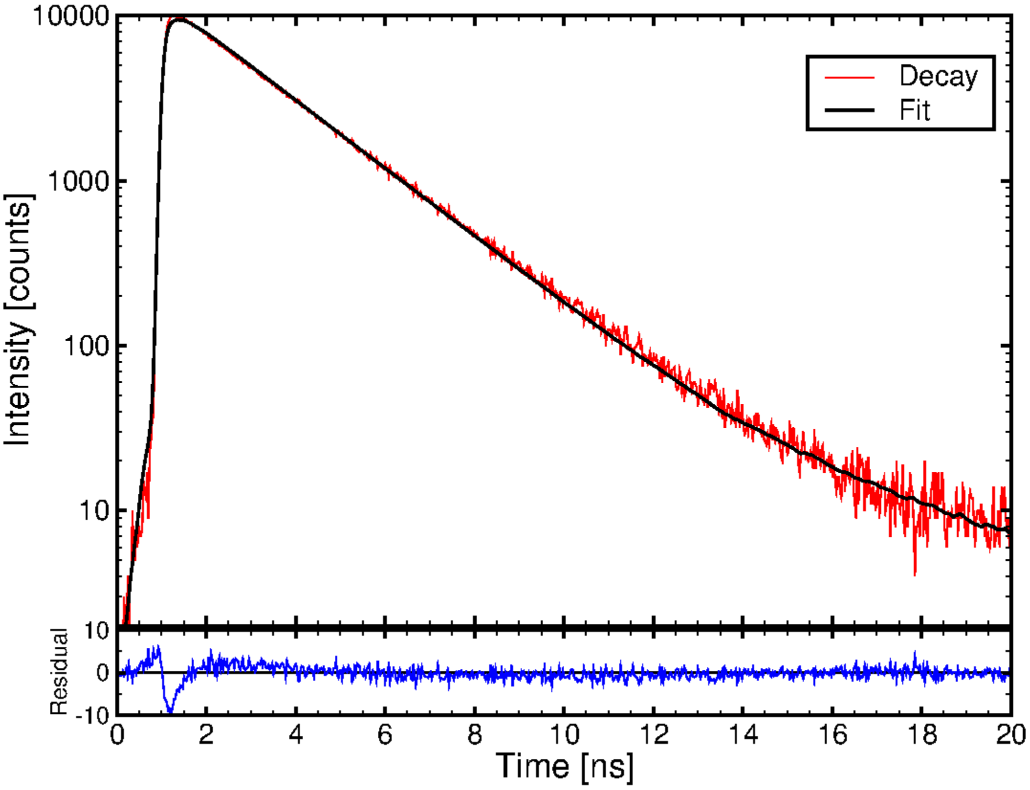

Figure S11 D: Raw decay data and 2 decay component fit for BODIPY-C10 in [C_4C_1im][NTf_2] at 279 K. Bottom graph shows residual values at each point.

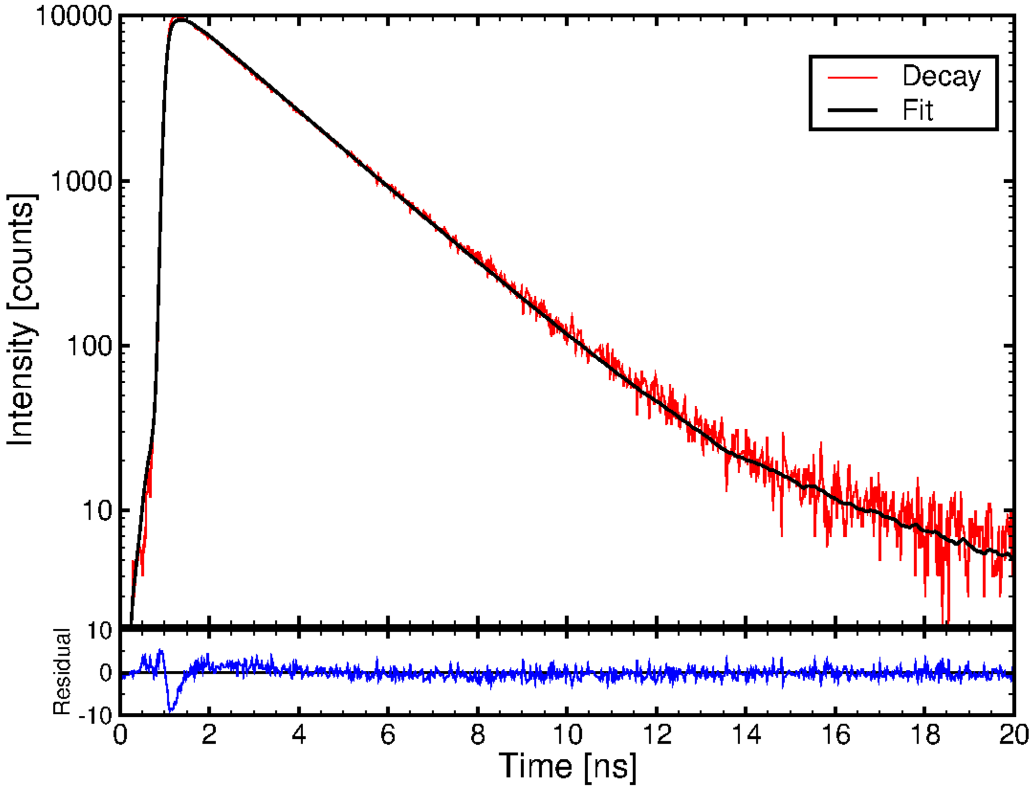

Figure S11 E: Raw decay data and 2 decay component fit for BODIPY-C10 in [C_4C_1im][NTf_2] at 282 K. Bottom graph shows residual values at each point.

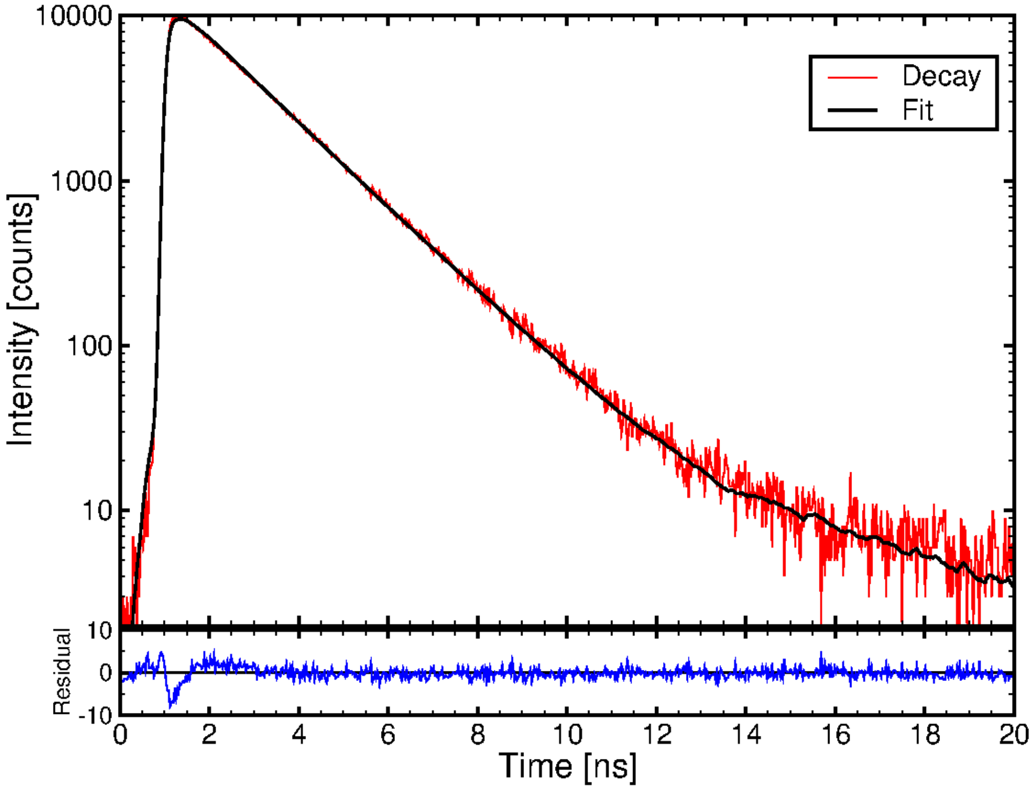

Figure S11 F: Raw decay data and 2 decay component fit for BODIPY-C10 in [C_4C_1im][NTf_2] at 286 K. Bottom graph shows residual values at each point.

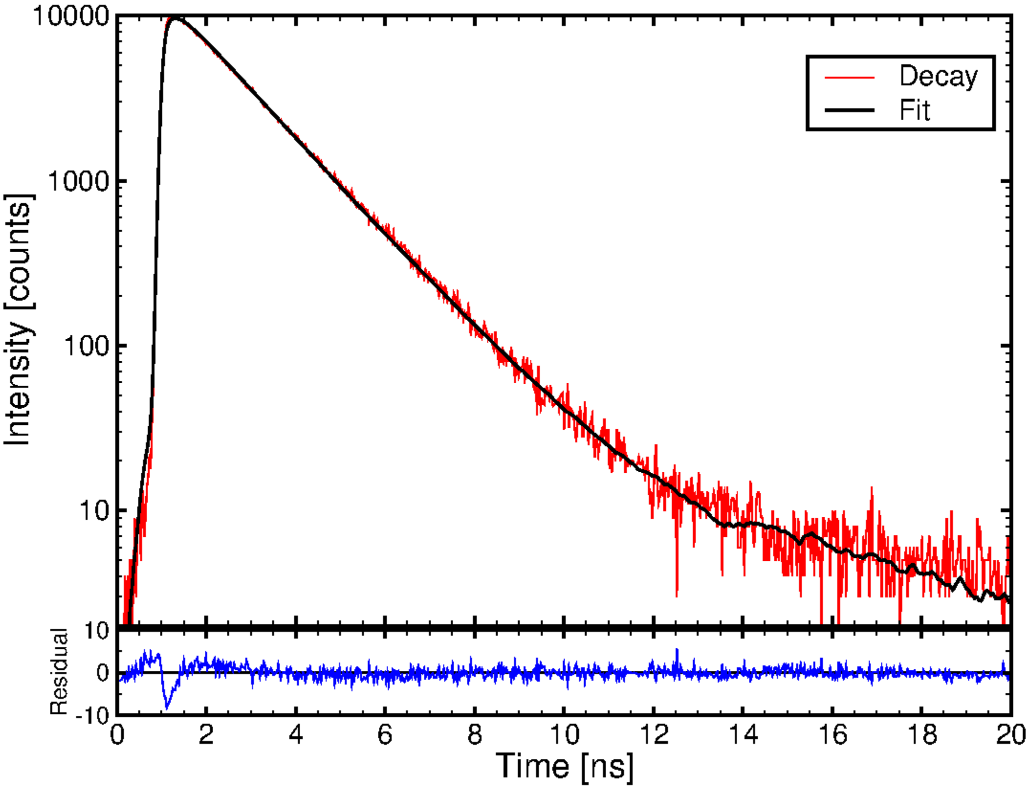

Figure S11 G: Raw decay data and 2 decay component fit for BODIPY-C10 in [C_4C_1im][NTf_2] at 290 K. Bottom graph shows residual values at each point.

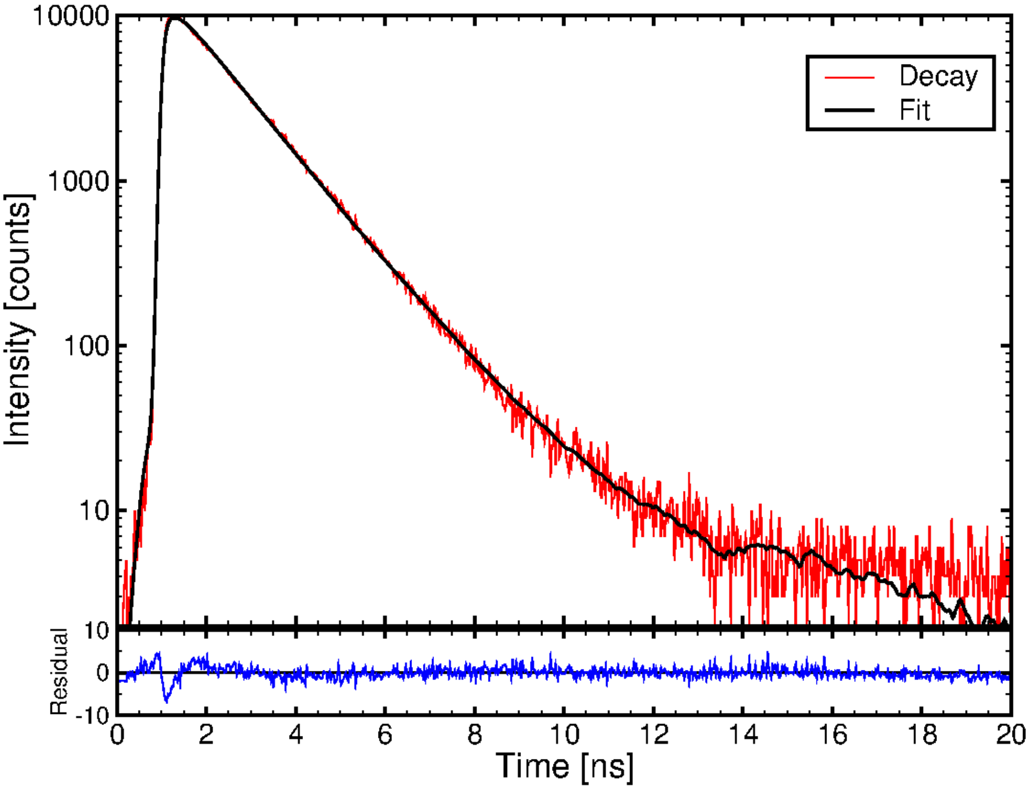

Figure S11 H: Raw decay data and 2 decay component fit for BODIPY-C10 in [C_4C_1im][NTf_2] at 294 K. Bottom graph shows residual values at each point.

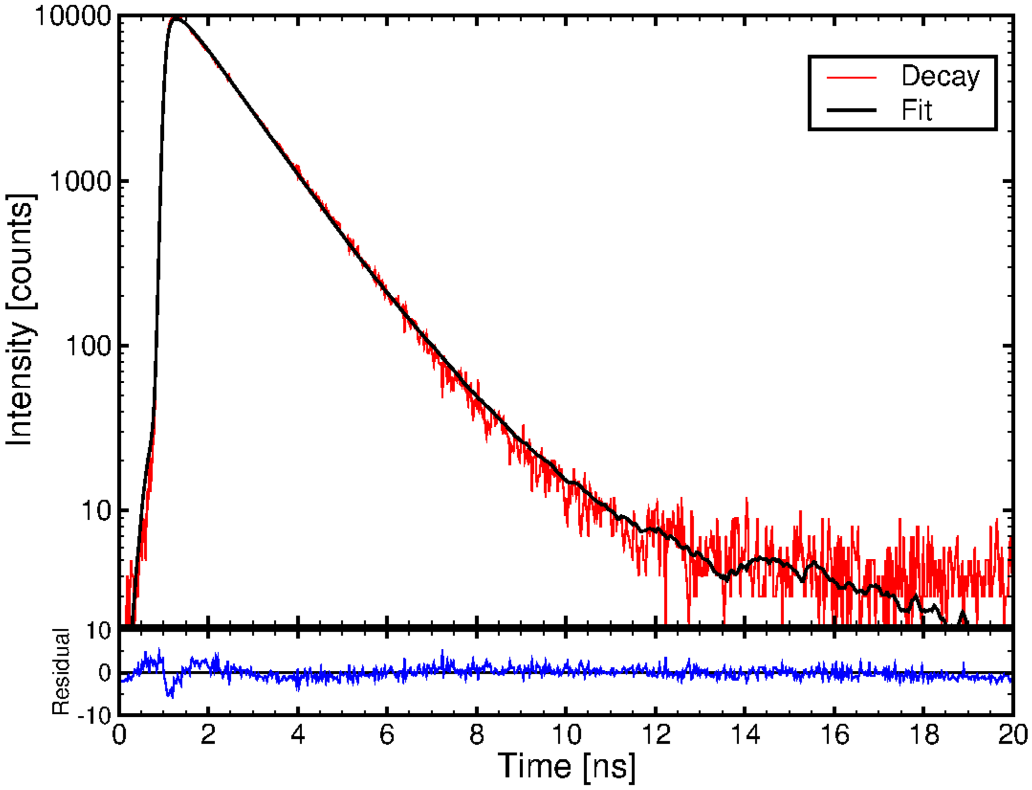

Figure S11 I: Raw decay data and 2 decay component fit for BODIPY-C10 in [C_4C_1im][NTf_2] at 298 K. Bottom graph shows residual values at each point.

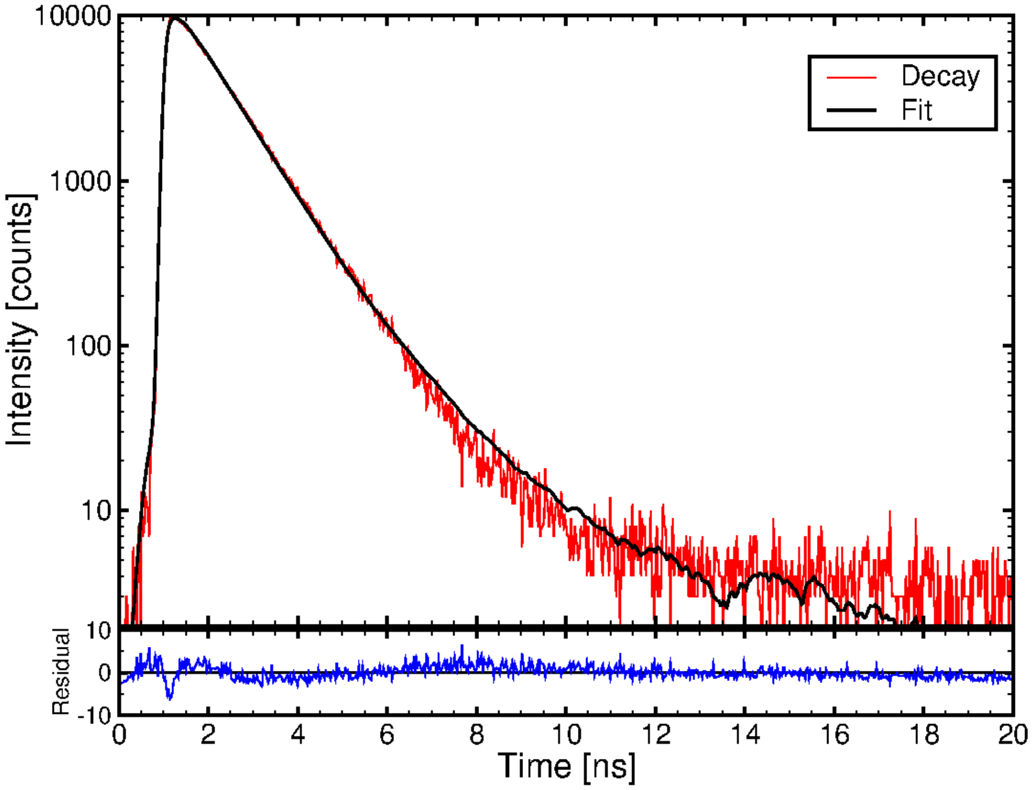

Figure S11 J: Raw decay data and 2 decay component fit for BODIPY-C10 in [C_4C_1im][NTf_2] at 302 K. Bottom graph shows residual values at each point.

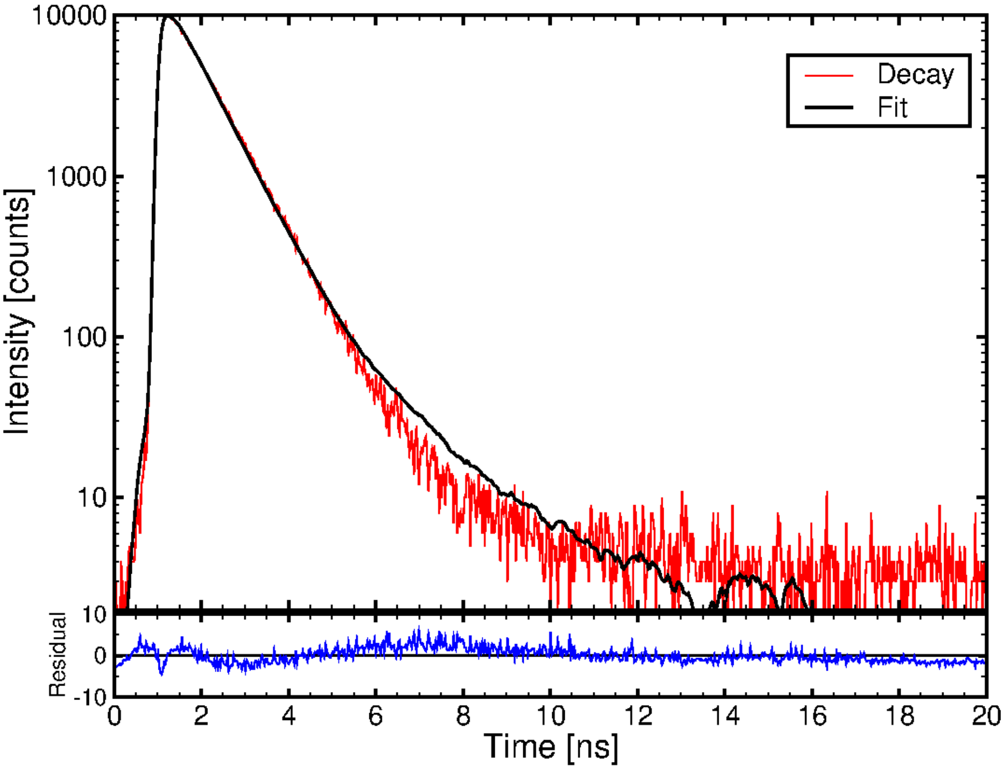

Figure S11 K: Raw decay data and 2 decay component fit for BODIPY-C10 in [C_4C_1im][NTf_2] at 311 K. Bottom graph shows residual values at each point.

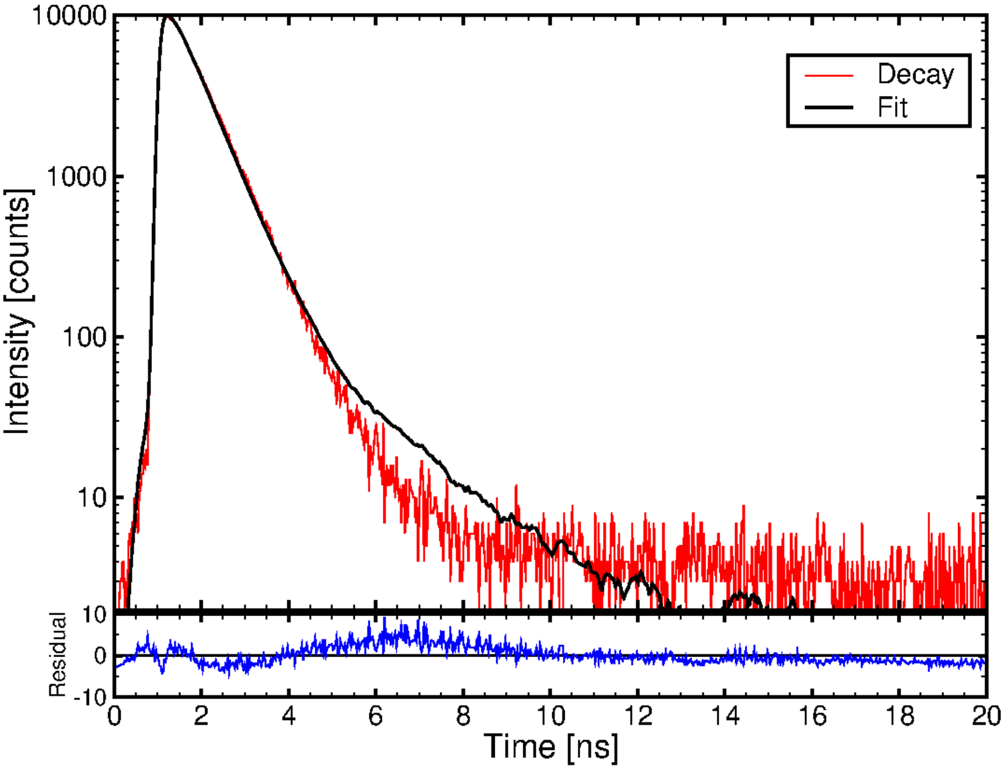

Figure S11 L: Raw decay data and 2 decay component fit for BODIPY-C10 in [C_4C_1im][NTf_2] at 320 K. Bottom graph shows residual values at each point.

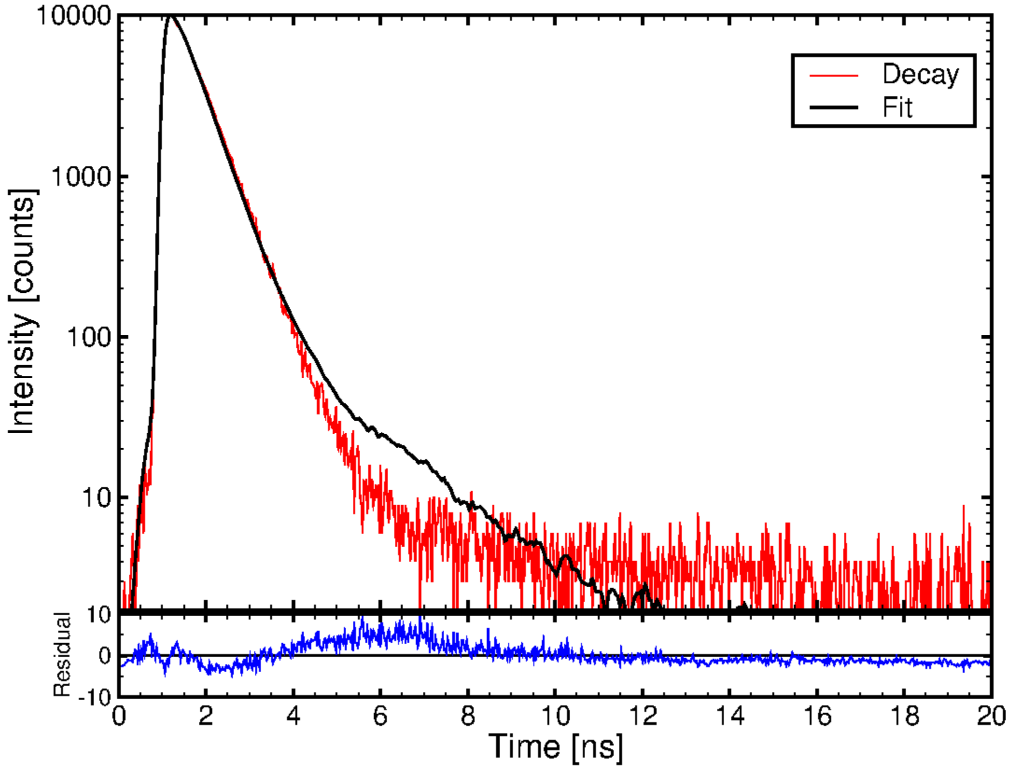

Figure S11 M: Raw decay data and 2 decay component fit for BODIPY-C10 in [C_4C_1im][NTf_2] at 329 K. Bottom graph shows residual values at each point.

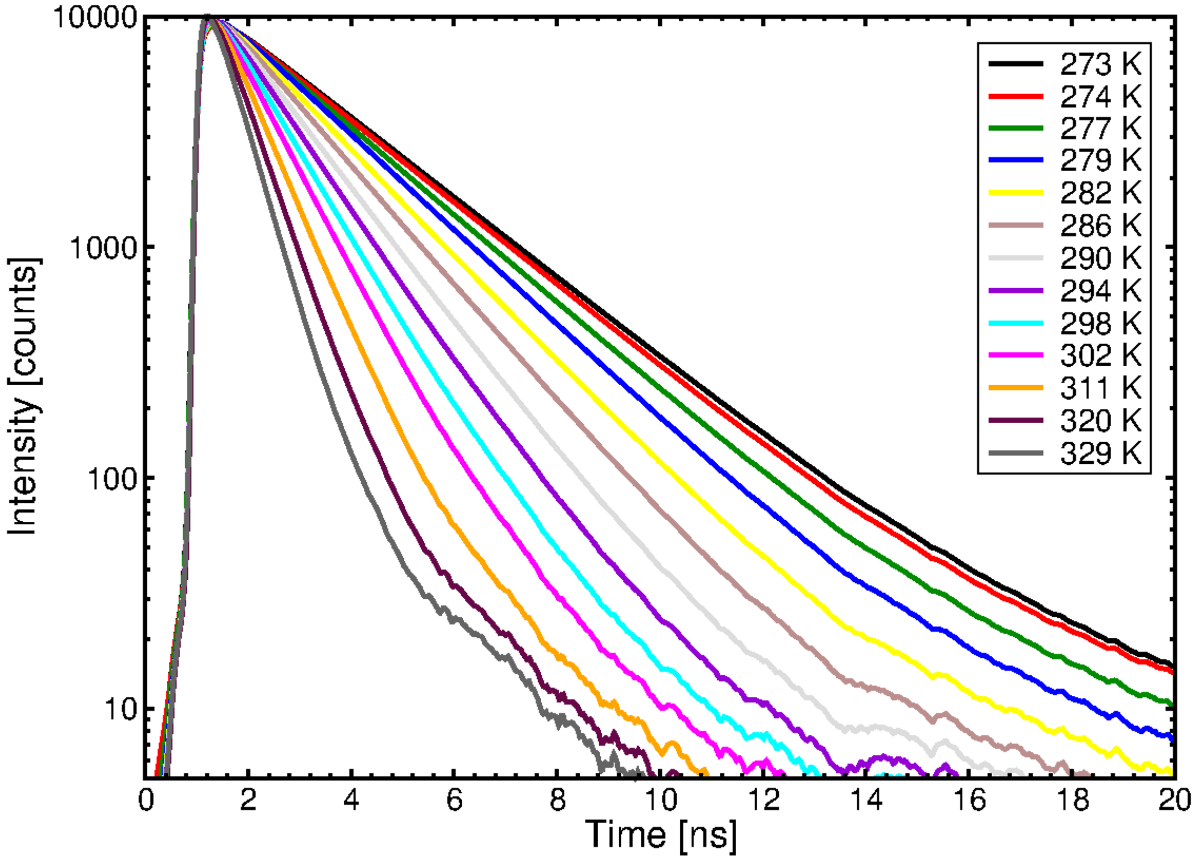

Figure S11 N: Decay data for BODIPY-C10 in [C_4C_1im][NTf_2] at various temperatures.

References

1 F. J. Waller, A. G. M. Barrett, D. C. Braddock, D. Ramprasad, R. M. McKinnell, A. J. P. White, D. J. Williams and R. Ducray, *J. Org. Chem.*, 1999, **64**, 2910–2913.

2 S. Plimpton, *J. Comput. Phys.*, 1995, **117**, 1–19.

3 A. Dequidt, J. Devémy and A. A. H. Pádua, *J. Chem. Inf. Model.*, 2016, **56**, 260–268.

4 R. Clark, M. von Domaros, A. J. S. McIntosh, A. Luzar, B. Kirchner and T. Welton, *J. Chem. Phys.*, 2019, **151**, 164503.

5 J. N. C. Lopes and A. A. H. Padua, CLP Force Field.

6 A. A. H. Pádua, 2015.

7 C. E. S. Bernardes, K. Shimizu, J. N. C. Lopes, P. Marquetand, E. Heid, O. Steinhauser and C. Schröder, *Phys. Chem. Chem. Phys.*, 2016, **18**, 1665–1670.

8 L. Martinez, R. Andrade, E. G. Birgin and J. M. Martínez, *J. Comput. Chem.*, 2009, **30**, 2157–2164.

9 Q. G. Zheng, H. Liu, Q. Xia, Q. S. Liu and L. Mou, *Acta Physico-Chimica Sin.*, 2017, **33**, 736–744.

10 M. Brehm and B. Kirchner, *J. Chem. Inf. Model.*, 2011, **51**, 2007–2023.

11 M. Brehm, H. Weber, M. Thomas, O. Hollõczki and B. Kirchner, *ChemPhysChem*, 2015, **16**, 3271–3277.

12 K. Bica, M. Deetlefs, C. Schröder and K. R. Seddon, *Phys. Chem. Chem. Phys.*, 2013, **15**, 2703.

13 Y. Marcus, *J. Mol. Liq.*, 2015, **209**, 289–293.

14 2014.

15 G. M. Sheldrick, *Acta Crystallogr. Sect. A Found. Crystallogr.*, 2008, **64**, 112–122.

16 O. V. Dolomanov, L. J. Bourhis, R. J. Gildea, J. A. K. Howard and H. Puschmann, *J. Appl. Crystallogr.*, 2009, **42**, 339–341.

17 L. J. Farrugia, *J. Appl. Crystallogr.*, 2012, **45**, 849–854.

18 C. F. Macrae, I. J. Bruno, J. A. Chisholm, P. R. Edgington, P. McCabe, E. Pidcock, L. Rodriguez-Monge, R. Taylor, J. van de Streek and P. A. Wood, *J. Appl. Crystallogr.*, 2008, **41**, 466–470.

19 P. J. Wheatley, *J. Chem. Soc.*, 1959, 3245.

20 P. J. Wheatley, *J. Chem. Soc.*, 1959, 4096–4100.

21 L. M. Jagupolskii, N. V. Kondratenko, O. I. Chernega, S. A. Buth, Y. G. Vlasenko and L. J. Yu, *CSD Commun.*, , DOI:10.5517/ccdc.csd.ccqgxrt.

22 W. Falkenberg, E. Höhne, J. Sieler and R. Wagener, *Krist. und Tech.*, 1973, **8**, 239–244.

23 B. Ziemer and S. Kulpe, *J. fur Prakt. Chemie*, 1975, **317**, 199–213.

24 V. F. Kaminskii, R. P. Shibaeva and L. O. Atovmyan, *Zhurnal Strukt. Khimii*, 1973, **14**, 700.

25 V. F. Kaminskii, R. P. Shibaeva and L. O. Atovmyan, *Zhurnal Strukt. Khimii*, 1973, **14**, 1082.

26 S. Alvarez, *Dalt. Trans.*, 2013, **42**, 8617.

27 G. Ponterini and F. Momicchioli, *Chem. Phys.*, 1991, **151**, 111–126.

28 I. Baraldi, A. Carnevali, F. Momicchioli and G. Ponterini, *Spectrochim. Acta Part A Mol. Spectrosc.*, 1993, **49**, 471–495.

29 K. G. Vladimirova, A. Y. Freidzon, A. A. Bagatur'yants, G. V. Zakharova, A. K. Chibisov and M. V. Alfimov, *High Energy Chem.*, 2008, **42**, 275–282.